

**Paul A. Harden**  
Site Vice President724-682-5234  
Fax: 724-643-8069September 28, 2010  
L-10-115

10 CFR 50.54(f)

ATTN: Document Control Desk  
U. S. Nuclear Regulatory Commission  
Washington, DC 20555-0001**SUBJECT:**Beaver Valley Power Station, Unit Nos. 1 and 2  
BVPS-1 Docket No. 50-334, License No. DPR-66  
BVPS-2 Docket No. 50-412, License No. NPF-73  
Response to Request for Additional Information Related to Generic Letter 2004-02  
(TAC Nos. MC4665 and MC4666)

By letters dated December 20, 2007, February 14, 2008, February 29, 2008, August 28, 2008, October 29, 2008, March 11, 2009, March 12, 2009, April 30, 2009, and June 30, 2009 (References 1 through 9, respectively), FirstEnergy Nuclear Operating Company (FENOC) submitted supplemental responses to Generic Letter (GL) 2004-02, "Potential Impact of Debris Blockage on Emergency Recirculation During Design Basis Accidents at Pressurized Water Reactors," for the Beaver Valley Power Station, Unit Nos. 1 and 2 (BVPS-1 and BVPS-2).

On February 18, 2010, the Nuclear Regulatory Commission (NRC) staff requested additional information regarding the FENOC response to Generic Letter 2004-02 (Reference 10). The FENOC response to the NRC staff request for information is provided in Attachment 1.

Attachment 2 provides a list of regulatory commitments made in this submittal. If there are any questions or if additional information is required, please contact Mr. Thomas A. Lentz, Manager—Fleet Licensing, at 330-761-6071.

I declare under penalty of perjury that the foregoing is true and correct. Executed on September 28, 2010.

Sincerely,



Paul A. Harden

A116  
NRR

Attachments:

1. Response to Request for Additional Information Regarding the Supplemental Responses to Generic Letter 2004-02 for Beaver Valley Power Station Unit No. 1 (BVPS-1) and Unit No. 2 (BVPS-2)
2. Regulatory Commitment List

References:

1. FENOC Letter L-07-519, Beaver Valley Power Station Unit Nos. 1 and 2, Generic Letter 04-02, "Potential Impact of Debris Blockage on Emergency Recirculation During Design Basis Accidents at Pressurized-Water Reactors" - Request for Extension of Completion Date for Corrective Actions, December 20, 2007, Agencywide Documents Access and Management System (ADAMS) Accession No. ML073620201.
2. FENOC Letter L-08-054, Beaver Valley Power Station, Unit Nos. 1 and 2, Generic Letter 2004-02, "Potential Impact of Debris Blockage on Emergency Recirculation During Design Basis Accidents at Pressurized-Water Reactors" - Request for Extension of Completion Date for Corrective Actions, February 14, 2008, ADAMS Accession No. ML080510246.
3. FENOC Letter L-08-035, Beaver Valley Power Station, Unit Nos. 1 and 2, Supplemental Response to Generic Letter 2004-02, "Potential Impact of Debris Blockage on Emergency Recirculation During Design Basis Accidents at Pressurized - Water Reactors," February 29, 2008, ADAMS Accession No. ML080660597.
4. FENOC Letter L-08-257, Beaver Valley Power Station, Unit Nos. 1 and 2, Generic Letter 2004-02, "Potential Impact of Debris Blockage on Emergency Recirculation During Design Basis Accidents at Pressurized-Water Reactors," Request for Extension of Completion Date for Corrective Actions, August 28, 2008, ADAMS Accession No. ML082480045.
5. FENOC Letter L-08-321, Beaver Valley Power Station, Unit Nos. 1 and 2, Supplemental Response to Generic Letter 2004-02, "Potential Impact of Debris Blockage on Emergency Recirculation During Design Basis Accidents at Pressurized Water Reactors," October 29, 2008, ADAMS Accession No. ML083080094.
6. FENOC Letter L-09-056, Beaver Valley Power Station, Unit No. 1, Downstream Effects for Recirculation Spray System Pumps and Low Head Safety Injection System Pumps, March 11, 2009, ADAMS Accession No. ML090750619.
7. FENOC Letter L-09-060, Beaver Valley Power Station, Unit No. 2, "Revised Commitment Date Relevant to FirstEnergy Nuclear Operating Company

Correspondence to the NRC, Dated August 28, 2008 (TAC No. MC4666)," March 12, 2009, ADAMS Accession No. ML090750618.

8. FENOC Letter L-09-131, Beaver Valley Power Station, Unit No. 1, Generic Letter 2004-02, "Potential Impact of Debris Blockage on Emergency Recirculation During Design Basis Accidents at Pressurized-Water Reactors" - Request for Extension of Completion Date for Additional Corrective Actions, April 30, 2009, ADAMS Accession No. ML091250180.
9. FENOC Letter L-09-152, Beaver Valley Power Station, Unit Nos. 1 and 2, Supplemental Response to Generic Letter 2004-02, June 30, 2009, ADAMS Accession No. ML091830390.
10. NRC staff Letter from N. S. Morgan, NRC Project Manager, to P. A. Harden, Site Vice President FENOC, Regarding Beaver Valley Power Station, Unit Nos. 1 and 2, "Request For Additional Information Re: Supplemental Response To Generic Letter 2004-02, 'Potential Impact of Debris Blockage on Emergency Recirculation During Design Basis Accidents at Pressurized Water Reactors,'" TAC Nos. MC4665 and MC4666, dated February 18, 2010, ADAMS Accession No. ML100290318.

cc: NRC Region I Administrator  
NRC Resident Inspector  
NRC Project Manager  
Director BRP/DEP  
Site BRP/DEP Representative

ATTACHMENT 1  
L-10-115

Response to Request for Additional Information Regarding the Supplemental Responses to Generic Letter 2004-02 for Beaver Valley Power Station Unit No. 1 (BVPS-1) and Unit No. 2 (BVPS-2)  
Page 1 of 132

By letters dated December 20, 2007, February 14, 2008, February 29, 2008, August 28, 2008, October 29, 2008, March 11, 2009, March 12, 2009, April 30, 2009, and June 30, 2009, FirstEnergy Nuclear Operating Company (FENOC) submitted supplemental responses to Generic Letter (GL) 2004-02, "Potential Impact of Debris Blockage on Emergency Recirculation During Design Basis Accidents at Pressurized Water Reactors," for BVPS-1 and BVPS-2. The Nuclear Regulatory Commission (NRC) staff requested additional information to complete its review of the BVPS response to GL 2004-02 in a letter dated February 18, 2010. Each request for additional information (RAI) in the February 18, 2010 letter is presented below in bold type and is followed by the FENOC response.

**Break selection**

**RAI 1**

**Please confirm that limiting break locations as defined in responses to date remain limiting after new evaluations based on planned replacement of problem insulation. Describe any differences in the break selection process from that previously used and verify that the new process maximizes each remaining debris source and the potential for debris combinations that could result in the most challenging head loss for the strainer.**

**FENOC Response**

As stated in Section 3.a of the June 30, 2009 supplemental response to Generic Letter 2004-02 (Reference 1), the process for break selection involved the selection of breaks that produce the maximum amount of debris and also the worst combination of debris mixes with the possibility of being transported to the sump screen. It further stated that the key to locating a break was less dependent on the location on the pipe but contingent on how other containment material was targeted.

The evaluation process and results for each break criterion, as presented in Section 3.a of the June 30, 2009 supplemental response, apply to the debris source resulting from the insulation modifications associated with the previously identified limiting break locations. In the cases of both BVPS-1 and BVPS-2, these insulation modifications were completed as planned, and the debris generation analyses were revised to account for these modifications. However, for BVPS-1 there remains an open commitment to address the additional Temp-Mat™ insulation discovered on the reactor coolant system (RCS) loop piping at the reactor vessel nozzles as described in FENOC letter dated April 30, 2009 (Reference 2), and the response to request for additional information (RAI) 2.

This RAI response addresses actions to date with respect to the discussions in the June 30, 2009 supplemental response. RAI 5 requested information relating to the debris generation analysis of calcium silicate (Cal-Sil) insulation materials. FirstEnergy Nuclear Operating Company's (FENOC's) response to RAI 5 includes a change in the percentage of Cal-Sil insulation debris generation and describes future removal of additional sources of Cal-Sil insulation associated with the limiting breaks. The response to RAI 5 contains additional information.

Considering the reduced debris loads resulting from the debris reduction efforts described above, FENOC has performed a re-evaluation of potential high energy line breaks not associated with the insulation replacement efforts. This evaluation determined whether the debris loads from other breaks that were previously bounded by the limiting breaks might exceed the reduced debris loads following the insulation reduction efforts. The re-evaluation was performed using break selection methodology consistent with the initial debris generation evaluation. RCS and connecting lines to the specified break isolation boundaries, consistent with the BVPS-1 and BVPS-2 licensing basis, were considered in the re-evaluation. Increased emphasis was placed on evaluating smaller RCS connecting lines located away from the limiting breaks to ensure that debris types and quantities could be accurately compared to the limiting breaks. Cal-Sil insulation debris loads were calculated in a manner consistent with FENOC's response to RAI 5.

The re-evaluation identified similar locations at BVPS-1 and BVPS-2 where the fibrous debris load, that had previously been bounded by the limiting breaks, could potentially exceed the fibrous debris load for the limiting breaks following insulation replacement efforts. The location for these breaks is the upper pressurizer cubicle that houses the pressurizer code safety relief valves (SRVs) and the power operated relief valves (PORVs). Specifically:

- At BVPS-1, the SRV insulation boxes contain a volume of Temp-Mat™ insulation that exceeds the fibrous debris quantity associated with the limiting RCS loop break, and
- At BVPS-2, the PORV piping insulation consists primarily of a volume of jacketed and unjacketed NUKON® that exceeds the fibrous debris quantity associated with the limiting RCS loop break.

To resolve these issues, FENOC is taking actions to ensure that the strainer head loss associated with these postulated breaks remains less than the head loss associated with the limiting breaks. These actions are summarized below.

#### BVPS-1

A calculation was performed to determine the bounding quantity of debris that would be generated from a break in a 6-inch line leading to one of the pressurizer SRVs. The calculation determined the quantity of Temp-Mat™ and coatings debris that would be

generated from the subject break. Based on existing insulation configuration plus the planned Cal-Sil reduction efforts discussed in RAI 5, Temp-Mat™ and qualified coatings are the only break-specific debris sources other than Reflective Metal Insulation (RMI) that must be considered. The calculation showed that the worst case Temp-Mat™ debris load at the sump strainer would be less than 9 cubic feet. Testing was then performed using the break specific debris load, combined with unqualified coatings and miscellaneous debris loads, and accounting for chemical effects. Appendix V of this RAI response attachment provides details of the analytical process used to determine the maximum debris quantities used in testing and the overall testing methodology. The results of the testing showed that the head loss associated with the SRV line break is bounded by the head loss from the RCS loop break. Thus, the RCS loop break remains the limiting break for strainer performance.

Based on results of this calculation, the pressurizer SRV line break is identified as the limiting break for fiber. However, the RCS loop break is still the limiting break with respect to Break Criterion 1- breaks in the RCS with the largest potential for debris. Thus, section 3.a of the June 30, 2009 supplemental response remains unchanged as a result of this evaluation.

Consideration was also given to the potential for debris generated as a result of the SRV line break to affect the holdup at upstream blockage points. An evaluation concluded that multiple drain paths exist for an SRV line break and that the debris size and quantity is not adequate to block all possible drainage paths. The evaluation also concluded that due to the drainage flow paths for this break, debris would not be washed down or transported to locations previously evaluated for upstream blockage as discussed in RAI 21.

Based on the evaluations described above, FENOC has concluded that the consequences of potential debris generated by the BVPS-1 pressurizer SRV line break are bounded by the limiting RCS loop break. Debris tabulation is being maintained by BVPS configuration control processes.

#### BVPS-2

Based on the current insulation installation configuration, that consists primarily of a combination of jacketed and unjacketed NUKON® insulation, the amount of fibrous debris generated by a break in the 6-inch common pressurizer PORV supply line was conservatively calculated using the zone of influence (ZOI) for unjacketed NUKON® insulation. This calculation shows that the volume of fibrous debris from this postulated break would be larger than the total volume of fibrous debris from the limiting RCS loop break. FENOC plans to remediate this condition by repairing and/or replacing the insulation on the 3-inch and 6-inch PORV supply piping with appropriately applied stainless steel jacketing and sure-hold bands to lower the ZOI radius for the NUKON® insulation to 2.4 pipe diameters (L/D) as allowed by section 3.4.2.2 of NEI 04-07, as modified by the Nuclear Regulatory Commission (NRC) Safety Evaluation (Reference 3). Plant modifications, repairing and/or replacing NUKON® insulation will be completed

on the 3-inch and 6-inch BVPS-2 PORV supply piping with appropriately applied stainless steel jacketing and sure-hold bands, prior to startup from the next refueling outage (2R15, Spring 2011).

Upon completion of these remedial activities, the debris load associated with the BVPS-2 pressurizer PORV line breaks will be bounded by the limiting breaks described in the June 30, 2009 supplemental response. Debris tabulation is being maintained by BVPS configuration control processes.

### **Debris Generation/Zone of Influence (ZOI)**

#### **RAI 2**

**In Reference 1, it is stated that additional Temp-Mat insulating material had been discovered on the reactor coolant system (RCS) piping at the BVPS-1 reactor vessel nozzles. Please provide details on how the revised strainer performance evaluations reflect this material or whether and how its impact has been otherwise mitigated.**

#### **FENOC Response**

The BVPS strainer testing did not include the Temp-Mat™ insulating material discovered on the BVPS-1 reactor coolant system at the reactor vessel nozzles. The testing assumed Reflective Metal Insulation (RMI) is installed at the reactor vessel nozzles. The June 30, 2009 supplemental response (Reference 1) defines the insulation debris load, and it does not include the Temp-Mat™ insulation discovered on the BVPS-1 reactor vessel nozzles. In accordance with a commitment in the April 30, 2009 FENOC letter (Reference 2), mitigation of the additional fibrous insulation will be accomplished through removal, replacement, analysis or design modification prior to startup from the next refueling outage (1R20), scheduled to be completed in the fourth quarter of 2010. The April 30, 2009 letter also included a commitment to provide a description of the proposed mitigation activities as a supplemental response to GL 2004-02 prior to the start of 1R20. The following response addresses RAI 2, and fulfills the commitment to provide a description of the proposed mitigation activities. An engineering change package has been prepared and approved to remove the Temp-Mat™ insulating material from the BVPS-1 hot and cold leg reactor vessel nozzles and replace it with RMI. The changes are scheduled to be completed during the fall 2010 BVPS-1 refueling outage (1R20).

#### **RAI 3:**

**Please provide additional details and assumptions on the alternate ZOI calculated for the Microtherm insulation installed on the RCS for BVPS-2, to describe how the ZOI was adjusted for the confined space within the reactor annulus. In Reference 1, it is stated that the alternate ZOI was calculated using the Boiling Water Reactor Owners Group Utility Resolution Guidance method 3 for restrained**

**breaks and was adjusted for the confined volume in the reactor annulus. Please provide details on the installation of the piping, insulation, and other structures or components that could affect the calculation, including how the axial and radial offsets were determined for the piping, the location of the insulation relative to the piping, pipe wall thickness, postulated break locations, whether longitudinal pipe breaks were considered, the destruction pressure used for the evaluation, etc. Please discuss whether a pancake-shaped jet as described in ANSI/ANS-58-2-1988 was evaluated, justify that a spherical ZOI is appropriate for the postulated restrained break, or describe how the jet was evaluated to behave within the confines of the reactor annulus. Provide information that describes how the amount of Microtherm debris would change with respect to the size of the ZOI. A non-conservative treatment of Microtherm would likely result in non-conservative head loss inputs. The Microtherm head loss is the bounding case for BVPS-2.**

### **FENOC Response**

The June 30, 2009 supplemental response (Reference 1) stated that the alternate ZOI was calculated using the Boiling-Water Reactor Owners Group Utility Resolution Guide (URG) Method 3 for restrained breaks and was adjusted for the confined volume in the reactor annulus. This alternate ZOI development method is being replaced by the American National Standards Institute ANSI/ANS 58.2-1988 standard methodology for assessing a jet profile impact on the Microtherm<sup>®</sup> insulation around the reactor pressure vessel and reactor coolant pipe nozzles. Therefore, the following information, as it pertains to the determination of an alternate ZOI, supersedes the determination of an alternate ZOI using Boiling-Water Reactor Owners Group URG Method 3.

Double ended guillotine breaks (DEGB) were considered at the reactor pressure vessel nozzle safe-end connection points to the hot and cold legs. These breaks were evaluated to be the worst case breaks for impact on the Microtherm<sup>®</sup> insulation. Longitudinal breaks were also assessed and because the jet profile from a longitudinal break is not directed toward the Microtherm<sup>®</sup> insulation, these breaks were determined to not cause limiting destruction of the insulation. For the double ended guillotine breaks, limited axial and radial displacements were evaluated to determine the ZOI.

The reactor coolant loop piping is fabricated from American Society of Mechanical Engineers (ASME) SA351 Grade CF8A material and is installed with full penetration circumferential butt welds. The cold leg is 27.5 inches nominal ID with a minimum fabricated wall thickness of 2.21 inches. The hot leg is 29 inches nominal ID with a minimum fabricated wall thickness of 2.33 inches. The hot and cold legs are routed through the reactor cavity wall penetration sleeves. The reactor cavity wall is constructed of reinforced concrete that is 4.5 feet thick. The reactor coolant loop piping is insulated with Diamond Power RMI.

The location of the Microtherm<sup>®</sup> insulation and the design configuration of the reactor coolant loop piping penetrating the reactor cavity wall are shown on Figure 3-1 and

Figure 3-2, respectively. Additional details on the configuration of the Microtherm<sup>®</sup> insulation and the supplemental neutron shield were presented on Attachment 1, page 20 of the June 30, 2009 supplemental response.

A destruction pressure of 40 pounds per square inch is used for the Microtherm<sup>®</sup> insulation based upon a 4D ZOI. The basis for this pressure is provided on Attachment 1, page 20 of the June 30, 2009 supplemental response.

The axial and radial displacements at the DEGB locations have been evaluated using a NUPIPE-SWPC computer model representing the reactor coolant loop piping, reactor coolant system components (reactor pressure vessel, reactor coolant pump, and steam generator), reactor coolant system component supports and the reactor coolant loop piping penetration sleeves through the reactor cavity wall. The break thrust force was applied at the decoupled reactor pressure vessel nozzle to pipe break points to ascertain the resulting pipe displacements. The hot leg break experiences limited axial displacement with the radial displacement being less than the pipe wall thickness; therefore, a cylindrical jet profile is developed similar to that depicted in Figure 7-2 (B) and Figure C-1 (B) of the ANSI/ANS 58.2 standard. The cold leg break experiences a limited axial and limited radial displacement. The limited radial displacement creates a crescent shaped jet profile that has been re-shaped to an equivalent diameter for developing the jet profile used in the analysis. These two cold leg breaks (axial and radial offsets) were developed and evaluated independently to conservatively capture the extent of the Microtherm<sup>®</sup> destruction ZOIs. The following pipe break displacements have been considered for use in projecting the jet profiles.

Table 3-1, Hot and Cold Leg Break Displacements Used in Determining ZOIs

Break / Direction	Analyzed Displacement	Displacement Used for Jet Profile	Comments
Hot Leg / Axial	1.47"	4.00"	
Hot Leg / Radial	0.82"	0"	Displacement less than wall thickness (1)
Cold Leg / Axial	9.86"	11.25"	Displacement limited by wall penetration
Cold Leg / Radial	5.10"	7.84"	Displacement limited by wall penetration.

(1) In accordance with ANSI/ANS 58.2 (Section 7.2 b), for a circumferential break that is physically restrained from significant separation, the jet centerline shall be assumed normal to the pipe centerline and extend 360° around the circumference of the pipe when the radial displacement is limited to less than the pipe wall thickness.

A spherical ZOI was used to represent a limited radial offset break, with the maximum axial distance (the centerline distance) that experiences the destruction pressure used

as the radius of the sphere. The Microtherm<sup>®</sup> destruction for a limited radial offset break was calculated using three different methods: 1) simple super-imposition, 2) spherical resizing (pancaking) using entire spherical volume, and 3) spherical resizing using half spherical volume. Method 3 assumes that the jet emanating from the nozzle side of the break exits out through the reactor cavity wall penetrations.

A cylindrical ZOI was created for any limited axial separation break, with the maximum radial and axial distances that experience the destruction pressure used as the cylinder radius and length. The Microtherm<sup>®</sup> destruction for this ZOI was calculated using two different methods: 1) simple ZOI super-imposition, and 2) cylindrical ZOI resizing keeping the ZOI volume constant with any solid volumes within the ZOI volume causing expansion of the ZOI such that the initial ratio of the cylinder length to cylinder diameter is constant. Resizing the cylinder enables the jet forces to be conserved within the confined space of the reactor cavity. The largest ZOI (spherical and cylindrical) determined from these methods has been used for assessment of the impact on the Microtherm<sup>®</sup> insulation.

Table 3-2 provides the Microtherm<sup>®</sup> destruction percentage for the analyzed hot and cold leg breaks. As more conservatism was integrated into the analysis, the amount of destroyed Microtherm<sup>®</sup> also increased. The table is structured in a manner to show the changes related to different considerations in the analysis. The maximum quantity of Microtherm<sup>®</sup> insulation debris, using the ANSI 58.2 jet profile method and the conservatisms discussed below, is approximately 33.1 percent of the total Microtherm<sup>®</sup> insulation on the reactor vessel. This amount equates to a volume of 20.2 cubic feet. The piping layout of the cold legs does not allow the maximum radial and axial displacements that were used for determination of the jet profiles to occur concurrently. The analysis considered that at the maximum axial displacement there is no radial displacement and at the maximum radial displacement there is no axial offset. Evaluation of various breaks concluded that the 11.25 inch axial offset cold leg break bounds all break scenarios, predicting destruction of approximately 33.1 percent of the total Microtherm<sup>®</sup> insulation on the reactor vessel. All Microtherm<sup>®</sup> panels predicted to be breached in the maximum limited radial offset break are enveloped by the maximum axial offset break.

Table 3-2, Microtherm<sup>®</sup> Destruction from Hot and Cold Leg Breaks

Break	ZOI	Microtherm <sup>®</sup> Destruction	Comments
Cold Leg Radial Offset	½ Sphere	7.4%	-ZOI destruction -1/2 sphere resizing
Cold Leg Radial Offset	Full Sphere	16.1%	-ZOI destruction -Spherical resizing
Cold Leg Radial Offset	Full Sphere	22.6%	-Full panel destruction -Spherical resizing
Cold Leg Axial Offset	11.25" Displacement Cylindrical ZOI	21.5%	-ZOI destruction -Simple super-imposition
Cold Leg Axial Offset	11.25" Displacement Cylindrical ZOI	27.5%	-ZOI destruction -Cylindrical resizing
Cold Leg Axial Offset	11.25" Displacement Cylindrical ZOI	33.1%	-Full panel destruction -Cylindrical resizing
Hot Leg Axial Offset	4" Displacement Cylindrical ZOI	3.3%	-Full panel destruction -Cylindrical resizing

The break generated Microtherm<sup>®</sup> insulation debris has been developed considering the following conservatisms:

1. A conservative Microtherm<sup>®</sup> insulation destruction pressure of 40 pounds per square inch has been used.
2. The break displacements used for development of the jet profiles are greater than those calculated in the reactor coolant loop pipe stress analysis (except the hot leg radial-displacement, see values in Table 3-1), resulting in larger and more destructive jets.
3. The Microtherm<sup>®</sup> insulation is located behind the reactor vessel supplemental neutron shielding. The shielding can be considered as a barrier to the direct impingement of the break jet and would reduce the amount of Microtherm<sup>®</sup> debris. However, the analysis assumes that the shield does not act as a robust barrier to maximize the extent of insulation destruction.
4. The spherical and cylindrical ZOI dimensions used in the analysis substantially increases the ZOI volume compared to the actual ZOI volumes predicted using ANSI 58.2.
5. The ZOI volumes were resized to account for confined space in the reactor cavity, and did not account for pressure losses due to jet impact and deflection.
6. The entire Microtherm<sup>®</sup> cassette has been considered to be destroyed if any portion of the cassette is contacted by the ZOI (referred to as full panel

destruction). A simple intersection method was also considered where only Microtherm<sup>®</sup> within the ZOI was destroyed (called ZOI destruction)

7. Although the Microtherm<sup>®</sup> insulation is located behind the supplemental neutron shield and the design configuration does not provide for a direct pathway from its location on the reactor vessel to the recirculation pool, the entire Microtherm<sup>®</sup> insulation destroyed by a reactor vessel nozzle break has been assumed to transport to the containment sump as particulate.
8. The destroyed Microtherm<sup>®</sup> insulation was considered as both particulate debris and as chemical effects load for prototypical sump screen testing, which is conservative since both phenomena cannot occur at the same time.

Additional sump screen prototypical testing has been performed for Microtherm<sup>®</sup> insulation debris loading. Information and test results relating to the testing has been provided as Appendix I to the RAI response attachment. The Microtherm<sup>®</sup> insulation debris determined by analysis has been shown to be less than the acceptable debris loading utilized with the prototypical testing. Conservatism was applied with the debris load analyses and with the prototypical sump screen testing. Margin remains under the worst case considerations; with 33.1 percent Microtherm<sup>®</sup> insulation debris determined by analysis versus 37.1 percent Microtherm<sup>®</sup> insulation debris determined acceptable by prototypical sump screen test.

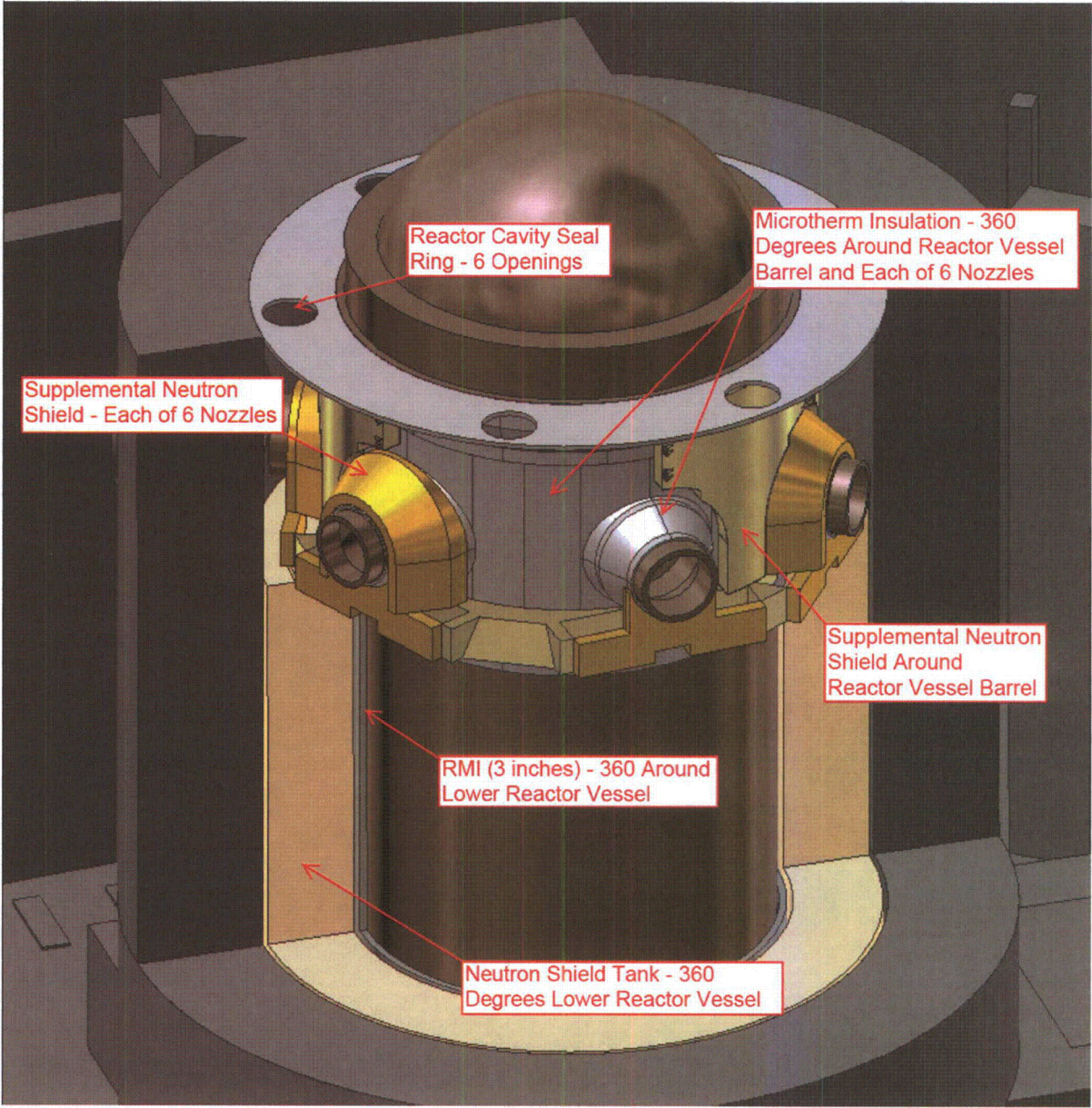


Figure 3-1, BVPS-2 Reactor Cavity Insulation and Neutron Shield Details

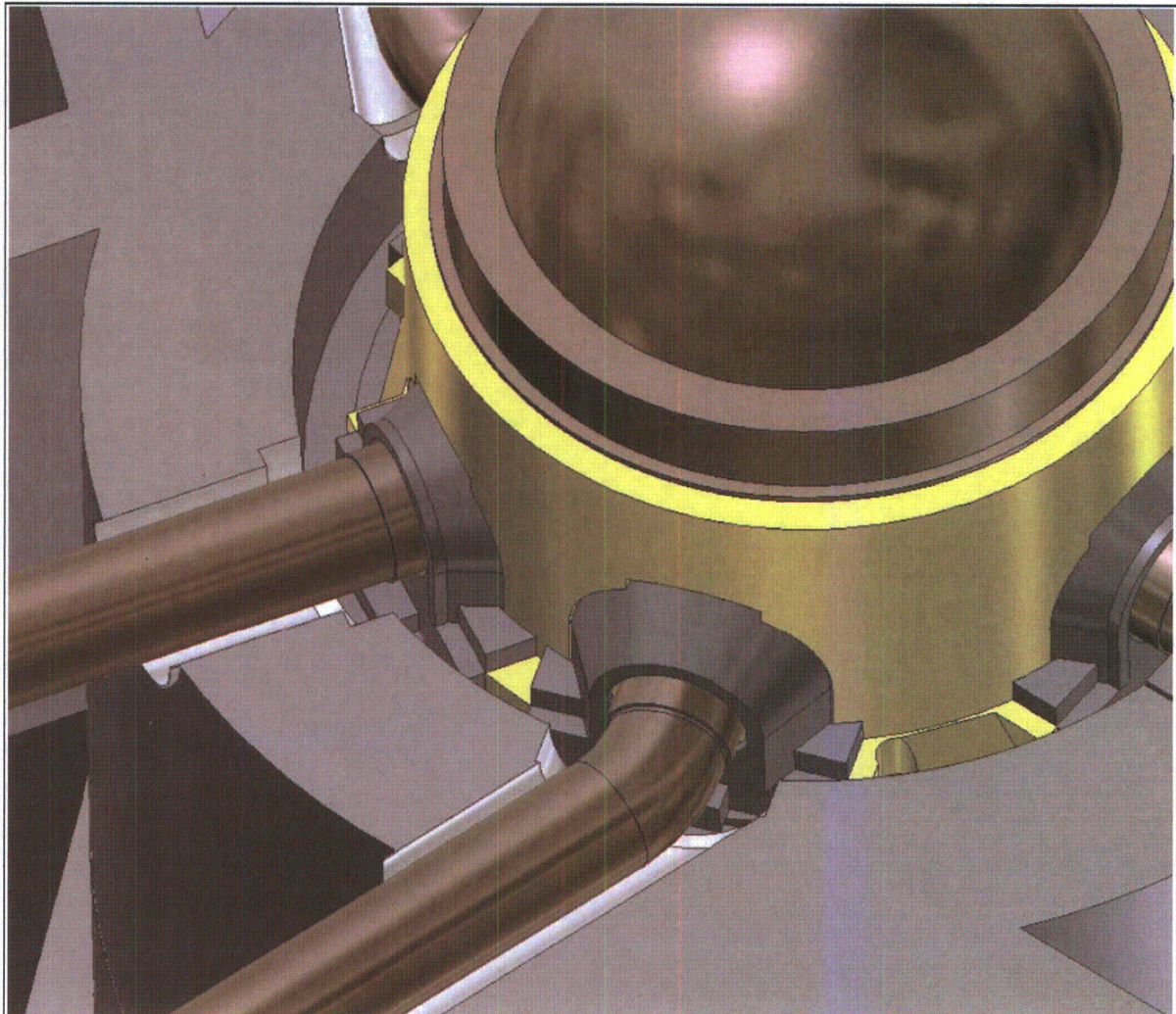


Figure 3-2, BVPS-2 Reactor Cavity Wall Penetration Details

#### **RAI 4**

**In Reference 1, it is stated that Benelex 401 is a high-density wood-based material composed of cellulose and lignin fibers. The response stated that the material was evaluated for seismic forces and loss-of-coolant accident (LOCA) pressure loading, but did not specify the assumptions for the evaluation. It was not clear that the evaluation considered all aspects of impingement from a LOCA steam jet. Please provide additional information for the evaluation that determined that the ZOI for Benelex 401 would be limited to 2 diameters (D). Please describe the methodology and assumptions for this evaluation. State whether any testing was performed to determine the appropriate destruction pressure for the material. If testing was conducted provide adequate information to justify that the testing was representative of, or bounded, the conditions that would be expected in the plant at the assumed ZOI. State whether the material is considered to be water soluble. If so, please provide information that justifies that the material would not fail due to the post-LOCA environment and potentially transport to the strainer.**

#### **FENOC Response**

This question is only applicable to BVPS-1. BVPS-2 containment does not contain any Benelex<sup>®</sup> shielding. FENOC has thoroughly evaluated Benelex<sup>®</sup> 401 and found it to be a hard, stable material that will withstand the initial impulse pressure of a reactor pressure vessel (RPV) Nozzle LOCA blowdown, as well as the mildly alkaline water spray/cascade of the post-LOCA environment at BVPS-1 without degradation over 30 days. No chemical compounds would be expected to form as a result of this exposure.

The following information is provided to support these findings. The response is divided into three parts: 'General Description', 'LOCA Impingement Evaluation Summary' and 'Post-LOCA Solubility Evaluation Summary'.

#### **General Description –**

Benelex<sup>®</sup> is used as a supplemental neutron shield near the bottom of the reactor vessel at BVPS-1, approximately 23 feet below the reactor vessel nozzles. The shield is comprised of four layers of two-inch thick Benelex<sup>®</sup> material shaped in the form of a large ring. The material is bolted together and supported by structural steel (as shown in Figure 4-1). The Benelex<sup>®</sup> shield ring does not perform any structural function. The material characteristics of Benelex<sup>®</sup> are described in detail in Section 3 of Appendix III to this RAI response attachment.

#### **LOCA Impingement Evaluation Summary –**

The reactor pressure vessel (RPV) nozzle breaks are postulated at the safe-end connections to the reactor coolant piping. It can be seen, as shown in Figure 4-2, that these break locations are above the top of the neutron shield tank, which is considered to be a robust barrier. The neutron shield tank will prevent direct jet impingement upon the Benelex<sup>®</sup> shield ring. Therefore, the only consideration for potential destruction of the Benelex<sup>®</sup> shield ring, as a result of a RPV nozzle break inside the reactor cavity,

would be the pressure that could occur as the expanding steam volume travels down the narrow gap between the neutron shield tank and the reactor vessel.

The Benelex<sup>®</sup> shield ring panels have been analyzed to show that the governing maximum normal stress is acceptable with a pressure loading of 120 pounds per square inch considering the support structure spans. The physical properties of the Benelex<sup>®</sup> provided in Table 1 of Appendix III to this RAI response attachment have been used for the analysis. Based on an acceptable pressure loading of 120 psi, 2D ZOI (destruction pressure of 114 pounds per square inch) has been established for Benelex<sup>®</sup>. The Benelex<sup>®</sup> shield ring support structure has been analyzed to show that it can withstand a pressure loading of 40 pounds per square inch upon the Benelex<sup>®</sup>. Standard structural analytical equations were used to evaluate the Benelex<sup>®</sup> support assembly. A destruction pressure of 40 psi is equivalent to a 4D ZOI. A 2D ZOI for the 29-inch hot leg nozzle break would result in a radius of approximately 5 feet and a 4D ZOI would result in a radius of approximately 10 feet, based conservatively on a fully offset DEGB. As discussed earlier, the distance from the reactor pressure vessel nozzles to the Benelex<sup>®</sup> shield ring is approximately 23 feet. Given the margin of distance from a 2D ZOI radius and a 4D ZOI radius to the Benelex<sup>®</sup> shield ring, and the presence of the neutron shield tank as a robust barrier to prevent direct jet impingement, it has been concluded that the pressure loading associated with the initial blowdown from a reactor vessel nozzle break would be well below the destruction pressure of the Benelex<sup>®</sup> shield ring and its support structure.

Considering that the RPV nozzle breaks direct the jet pressure within the reactor cavity, FENOC has also performed an evaluation to determine the pressure distribution of these breaks using the ANSI 58.2 steam jet pressure model. The analysis used spherical resizing of the ZOI volume within the confined space of the reactor cavity considering the actual offset resulting from a DEGB at the RPV nozzles for the hot and cold leg piping. The actual offsets were determined based on stress analysis of the piping. Using this methodology, the maximum pressure (less than 16 pounds per square inch) was found to be well below the destruction pressure of the Benelex<sup>®</sup> shield ring and the Benelex<sup>®</sup> shield ring support structure. The ANSI 58.2 steam jet pressure model used is similar to that described in the response to RAI 3 for the evaluation of the destruction pressure on the Microtherm<sup>®</sup> insulation around the reactor pressure vessel for BVPS-2. Based on this evaluation, FENOC has concluded that the Benelex<sup>®</sup> shield ring and its support structure will not be adversely impacted as a result of the RPV nozzle break jet pressure.

#### Post-LOCA Solubility Evaluation Summary –

The Benelex<sup>®</sup> shield ring is located above the maximum water level projected in the reactor cavity following a LOCA. However, containment spray water and/or LOCA break flow from a reactor pressure vessel nozzle break would drain to the reactor cavity floor via the annular gap between the reactor vessel and the neutron shield tank. A portion of this flow would cascade over the Benelex<sup>®</sup> shield rings (as shown in Figures 4-1 and 4-2).

FENOC commissioned a white paper on Benelex<sup>®</sup> properties by a polymer formulation consultant. The research findings discussed in this paper demonstrated that:

- Benelex<sup>®</sup> is not water soluble under LOCA conditions for the thirty day mission time,
- Benelex<sup>®</sup> will not erode under the water spray/cascade of mildly alkaline water that will exist in the post-LOCA containment, and
- Benelex<sup>®</sup> will not form particulate or fibrous debris under LOCA conditions for the thirty day mission time.

The white paper on Benelex<sup>®</sup> is provided as Appendix III to this RAI response attachment.

Additionally, in WCAP 16530-NP, "Evaluation of Post-Accident Chemical Effects in Containment Sump Fluids to Support GSI-191," Westinghouse researchers ruled out benchtop testing of Benelex<sup>®</sup> because it was "unlikely to breakdown to produce precipitate forming species." Therefore, no chemical effects are expected from the presence of Benelex<sup>®</sup> in containment.

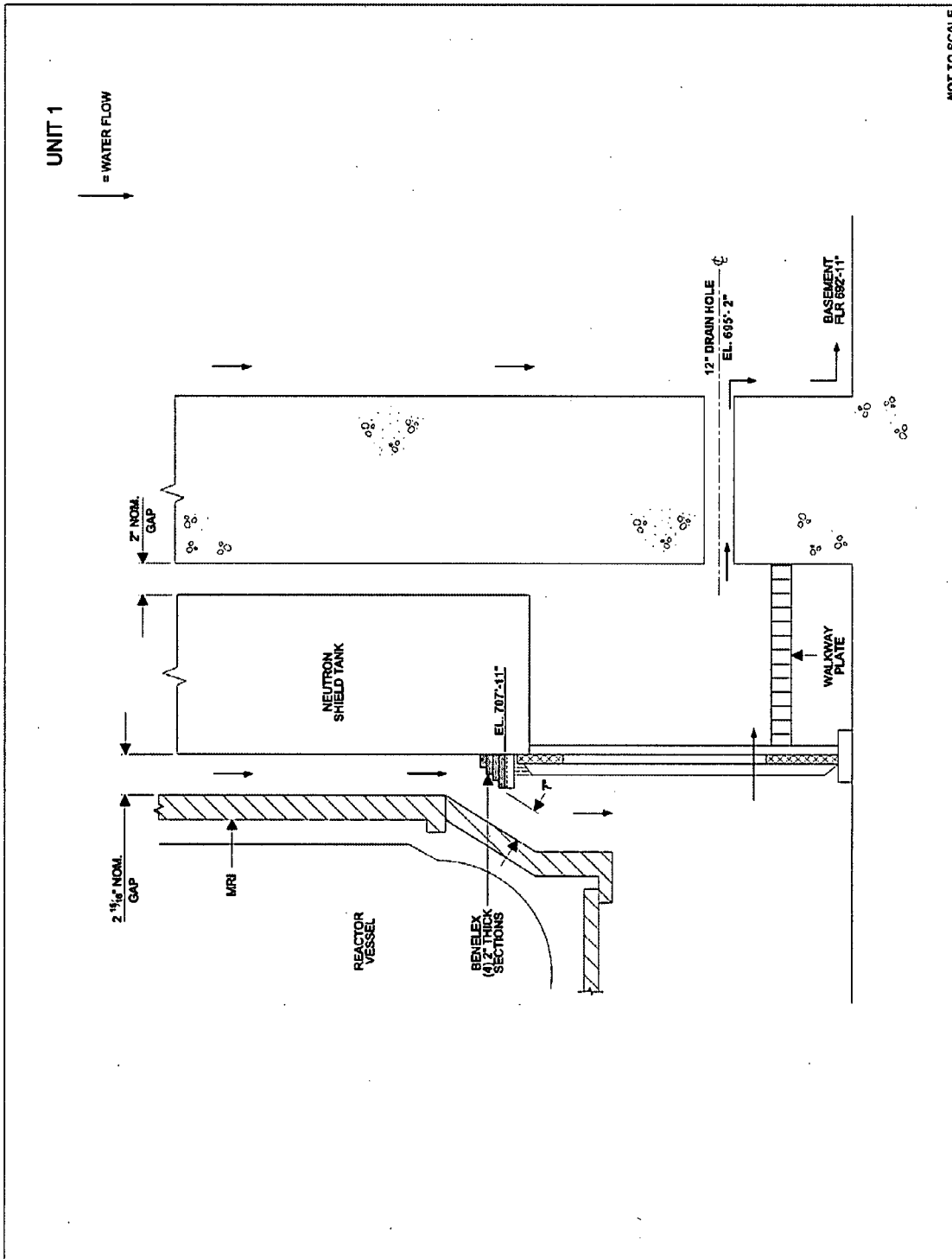


Figure 4-1, Benelex® Shield Ring Location



## **RAI 5**

**In Reference 1, it is stated that only 50% of the calcium silicate within the prescribed 5.45D ZOI was assumed to be destroyed into fines. The other 50% of the calcium silicate within this ZOI was not considered in the analysis (i.e., it was apparently assumed to remain intact following the impact of the LOCA jet). The stated basis for the 50% reduction in calcium silicate was Ontario Power Generation (OPG) testing for which less than 50% of the target calcium silicate was damaged by jet impingement. Please address the following items concerning the assumed calcium silicate debris distribution:**

- a. Significant portions of the target insulation in the OPG tests were not exposed to jet forces representative of the calculated ZOI. In other words, the insulation targets used for testing were so long (48 inches) that, due to the small size of the jet nozzle (2.86 inches), a significant portion of the insulation targets was not subjected to destruction pressures prototypical of a complete rupture of RCS piping. In addition, some OPG tests demonstrated the occurrence of insulation damage at distances in excess of that corresponding to a spherical 5.45D. Although a 5.45D ZOI was accepted for calcium silicate based on the OPG testing, the NRC staff's safety evaluation on Nuclear Energy Institute (NEI) 04-07 conservatively recommended that 100% of the calcium silicate within a spherical 5.45D ZOI be assumed to be destroyed into small fines, which compensated for these test setup issues. Thus, it is unclear that assuming a 5.45D ZOI with 50% intact pieces is justified based on the OPG test results.**
- b. Please identify the jacketing and banding, latching, etc., of the calcium silicate insulation at BVPS-1 and 2 and compare this insulation material to the material that was tested by OPG to support the assumed debris characterization of 50% intact pieces based on the application of the OPG test results. Please also compare the manufacturing process for the calcium silicate at BVPS-1 and 2 with that used for the OPG testing (i.e., hydraulically pressed or molded - see Section 3.3.3 of the NRC's Indian Point Audit Report).**
- c. The 50% of the calcium silicate considered to be undamaged was not considered for potential erosion and transport to the strainer. However, for some of the OPG tests, the insulation jacketing was removed, even when the base insulation material was not completely removed from the pipe. In light of the removal of the jacketing in a number of tests, please provide justification that erosion of the calcium silicate remaining on pipes need not be considered.**

### **FENOC Response**

Due to the NRC concerns regarding using the Ontario Power Generation (OPG) testing to justify that only 50 percent of the calcium silicate within the prescribed 5.45D ZOI was assumed to be destroyed into fines, FENOC has elected to revise its methodology to assume that 100 percent of the calcium silicate within a spherical 5.45D ZOI is destroyed into fines consistent with the NRC staff's safety evaluation on Nuclear Energy Institute (NEI) 04-07. Therefore, FENOC plans to make the necessary plant modifications such that for any potential break, the amount of destroyed calcium silicate based on a spherical 5.45D ZOI and 100 percent destruction to fines is less than the amount of calcium silicate used in the limiting head loss tests (BVPS-1 Test 6 and BVPS-2 Test 1A).

FENOC has completed the process of re-evaluating the break selection process to determine the scope of the additional insulation modifications. Plant modifications will be completed for BVPS-1 associated with Cal-Sil insulation removal that ensures that the requirements of FENOC's revised methodology of assuming 100 percent destruction of Cal-Sil to fines is met prior to startup from the next refueling outage (1R20, Fall 2010). Plant modifications will be completed for BVPS-2 associated with Cal-Sil insulation removal that ensures that the requirements of FENOC's revised methodology of assuming 100 percent destruction of Cal-Sil to fines is met prior to startup from the next refueling outage (2R15, Spring 2011).

Since FENOC has elected to revise its' methodology to be consistent with the NRC staff's safety evaluation on NEI 04-07, the concerns raised by the staff in sections a, b, and c of this RAI are no longer applicable due to the conservatism in using a spherical 5.45D ZOI and 100 percent destruction to fines.

### **RAI 6:**

**Please identify why Benelex is considered to be a particulate insulation in Table 3.c-6 of Reference 1, while page 19 of the same response identifies that this material is constructed from compressed cellulose and lignin fibers.**

### **FENOC Response**

This question is only applicable to BVPS-1. BVPS-2 containment does not contain any Benelex<sup>®</sup> shielding. As discussed in the FENOC response to RAI 4, it was determined that the Benelex<sup>®</sup> shield ring will not be destroyed, dissolved or eroded as the result of a LOCA.

### **Head Loss and Vortexing**

### **RAI 7:**

**In Reference 1, it is stated that deaeration of the fluid passing through the debris bed could occur, but that the majority of any gases would be absorbed by the**

**fluid prior to reaching the pump suction. The mechanism for the absorption of the gases was not understood by the NRC staff. It was not clear whether the gases could collect as bubbles in the strainer or piping and eventually transport to the pump suction. It was also not clear that the gases would absorb into the liquid prior to reaching the pump suction. Please provide the assumptions and methodology for the evaluation that predicted the final void fraction at the pump suction.**

### **FENOC Response**

The response to this RAI consists of two parts. First, an assessment is performed to determine the quantity of air evolved as well as its impact on NPSH required. Second, an assessment is performed to determine the ability of the evolved air to accumulate at the top of the waterbox.

#### Amount of Air Evolution

Deaeration occurs due to a decrease in the pressure of a fluid containing dissolved gases. The methodology for predicting deaeration is based on Henry's Law. Henry's Law is applied to the predominant gasses dissolved in the sump water: nitrogen and oxygen. The amount of gas that comes out of solution is directly proportional to the decrease in pressure as the water flows through the debris bed and strainer. Temperature can also impact the solubility of the gasses; however, the temperature is assumed to remain constant throughout the flow stream except near the BVPS-1 Recirculation Spray System (RSS) pumps that have colder water from the Refueling Water Storage Tank injected into the pump suction flow stream while the Quench Spray (QS) pumps are operating. Calculations are performed at various locations in the flow stream where pressure drops occur, for example, across the debris bed, through the strainer manifolds and waterboxes, through the pump suction piping and in the pump internal flow passages. As was discussed in FENOC letter dated June 30, 2009 (Agencywide Documents Access and Management System [ADAMS] Accession No. ML091830390), the analysis calculates the void fraction at four distinct points in time. These are the RSS pump start [minimum submergence], the point of minimum sub-cooling [highest potential for flashing], after transfer to safety injection recirculation, and when the containment pressure is at a minimum value [low containment sump temperature and pressure]. These points are selected based on the most sensitive analytical parameters (containment pressure, sump water temperature, and pump flow rates).

The static pressure at any point in the flow stream is impacted by the head loss through the debris bed and various components, the elevation relative to the water surface, and the local velocity. When the local static pressure is lower than the pressure at the water surface, gas may come out of solution since the gas is conservatively assumed to be saturated at the water surface. If the pressure in the flow stream increases above the pressure at the surface, Henry's Law predicts that gas would go back into solution. Since transient reabsorption is difficult to quantify, BVPS has taken the conservative approach that the maximum void fraction calculated anywhere in the flow stream is

assumed to arrive at the pump impeller. A void fraction acceptance criterion of 0.3 percent is used in order to limit the impact on the required pump NPSH to an increase of 15 Percent using the guidance of Reg. Guide 1.82, "Water Sources for Long-Term Recirculation Cooling Following a Loss-of-Coolant Accident," Revision 3, Appendix A.

The maximum void fractions have been re-evaluated since the values were reported in the June 30, 2009 supplemental response (ADAMS Accession No. ML091830390). A change in the application of the debris head loss was included in this re-evaluation. This change involves the temperature at the onset of chemical effects. Based on generic industry data and plant specific sump water chemistry, it was determined that chemical effects on the debris head loss will not occur until the sump water temperature drops below a specific value. For BVPS-1 a value of 150 °F is used and for BVPS-2 a value of 140 °F is used. Appendix II of this RAI response attachment has more discussion on the application of chemical effects.

Using these changes, as well as the results of the revised containment analyses reflected in the responses to RAIs 20, 21, and 24, the maximum calculated void fraction is 0.23 percent for BVPS-1 and 0.26 for BVPS-2. The maximum void fraction for BVPS-1 occurs at the Outside Recirculation Spray (ORS) pump suction for the minimum containment pressure case. No flashing of the liquid flowing to the pumps occurs at any point in time. These results meet the void fraction acceptance criterion of 0.3 percent that is used in the NPSH analyses to establish the NPSH required and the NPSH margins.

#### Air Accumulation

The voids calculated in the section above are expected to take the form of small air bubbles. Air bubbles can accumulate at the top of the BVPS-1 waterbox, or another flat surface, if the rise velocity of the bubbles due to buoyancy is greater than the velocity of the water moving through the waterbox to the suction piping. If the bubbles have a very low rise velocity, they will be swept along with the water flow and only exist as voids at the pump. As described above, these voids would increase the required NPSH of the pumps.

There are two factors in determining if air will accumulate: the bubble size and the velocity of the water in the waterbox. The size of bubbles is based on many different factors, including the pressure drop, the flow velocity, and the quantity of nucleation points (very fine particulate and fiber) in the water (based on "Bubble Size Distribution Formed by Depressurizing Air-Saturated Water" by A. Vlyssides et. al. from *Industrial & Chemical Engineering Research Journal*, 2004). A higher pressure drop leads to larger bubble sizes. In the Vlyssides article, water saturated with air at pressures of 2, 5, and 8 atmospheres (atm) was subjected to pressure drops of approximately 1, 4, and 7 atm, respectively. For an air saturation pressure of 8 atm, the bubbles ranged in size from 5 micrometers ( $\mu\text{m}$ ) to 195  $\mu\text{m}$  with roughly half of the total volume of air in bubbles that are 115  $\mu\text{m}$  or larger. For an air saturation pressure of 2 atm, the bubbles ranged in size from 5  $\mu\text{m}$  to 170  $\mu\text{m}$  with roughly half of the total volume of air in bubbles that are 95  $\mu\text{m}$  or larger. Because large bubbles contain much more air than small bubbles, at

an air saturation pressure of 2 atm, only 4 percent of all the bubbles were larger than 70  $\mu\text{m}$ . At BVPS-1, the maximum pressure drop is roughly 2 pounds per square inch, which is approximately 0.1-0.2 atm. With the lower pressure and the lower pressure drops at Beaver Valley, the bubble size is expected to be much smaller than the bubbles in the Vlyssides tests.

The nozzle used to create the pressure drop in the Vlyssides tests was designed to minimize the collisions between bubbles due to the turbulent (high Reynolds number) flow, thus minimizing the bubble size. The BVPS strainers have very low flow rates compared to the flow rates from the Vlyssides tests, meaning fewer bubble collisions would occur. This further supports the argument that the bubbles that form at BVPS will be much smaller than those measured in the tests.

A separate study examined the effects of fine particles and fibers on bubble size. In champagne, bubbles are formed at the small residual fibers in the fluid (from "Close-up on Bubble Nucleation in a Glass of Champagne" by Gerard Liger-Belair, 2002). The pressure drop for champagne in a bottle following the popping of the cork is 6 atm. In the Liger-Belair article, very fine photography was used to determine the location of bubble formation and the size of the bubbles that formed. Most of the particles that acted as nucleation sites were cellulose fibers roughly 100  $\mu\text{m}$  long and several micrometers (approximately 10  $\mu\text{m}$ ) in diameter. This is very comparable to the size and shape of the fine debris in the debris bed where nucleation would occur at BVPS. The initial bubble diameters found in the Liger-Belair tests were between 14 and 31  $\mu\text{m}$ . Because the debris bed will contain similar fibers to those expected in the champagne, the air bubbles at BVPS are expected to be similar sized.

By comparing the testing performed in the two studies referenced above to the BVPS conditions, the diameter of bubbles forming are expected to be in the range of 10  $\mu\text{m}$  to 100  $\mu\text{m}$ .

The maximum upward air bubble velocity in a fluid is called the terminal rise velocity. The terminal rise velocity is computed by performing a force balance on a spherical bubble where the buoyancy force is offset by the drag force (which is dependent on velocity). Per Stokes' Law, the terminal bubble velocity is calculated by the equation below.

$$V = \frac{2 \cdot g \cdot r^2 \cdot (\rho_w - \rho_a)}{9 \cdot \mu}$$

Where:

V = terminal rise velocity in feet per second (ft/s)

g = gravity (32.2 ft/s<sup>2</sup>)

r = bubble radius in feet

$\rho_w - \rho_a$  = difference in densities of the sump water and the air bubble in pound-mass per cubic foot (lbm/ft<sup>3</sup>)

$\mu$  = dynamic viscosity in pound-mass per foot-second (lbm/ft-s)

A bubble that is 100  $\mu\text{m}$  in diameter has a terminal rise velocity of roughly 0.3 to 1.0 inches per second (in/s) for sump temperatures of 100 °F to 260 °F, respectively. A bubble that is 10  $\mu\text{m}$  in diameter has a terminal rise velocity of roughly 0.003 to 0.01 in/s for sump temperatures of 100 °F to 260 °F, respectively.

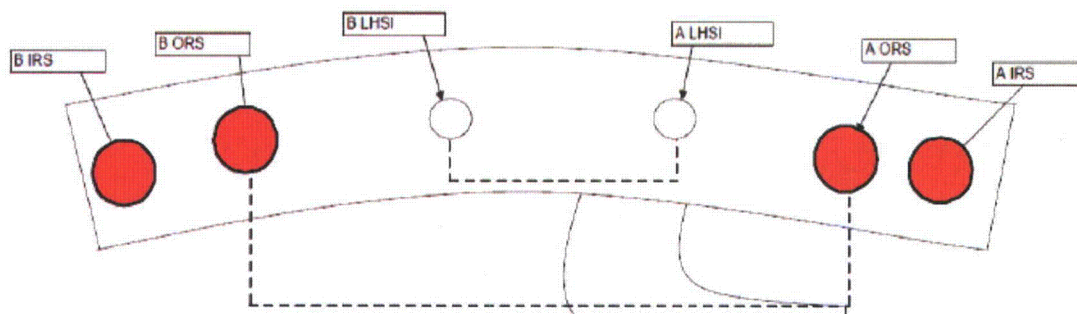
For BVPS-1, the flow rate to each pump from the waterbox is dependent on the assumed single failure and the mode of operation (before or after safety injection recirculation). Prior to transfer to safety injection recirculation, either two or four Recirculation Spray pumps will be taking suction from the waterbox depending on single failure assumptions. Following transfer to safety injection recirculation, one or two Low Head Safety Injection Pumps as well as two Recirculation Spray pumps will take suction from the waterbox. Based on the deaeration calculations performed as described above, the only flow cases that result in air evolution in the strainer or waterbox are those associated with maximum flow conditions. These cases result from the assumption of no single failures. Since all cases resulting in air evolution occur prior to safety injection recirculation, all four RSS pumps must be operating to achieve maximum flow conditions.

Air bubbles will be formed primarily in the debris bed and the strainer modules upstream of the duct connecting the modules to the waterbox. The velocities internal to the strainer modules are high enough to sweep the air bubbles into the waterbox. The ability of air bubbles to remain in the flow stream is addressed using streamlines produced as part of the computational fluid dynamics (CFD) analysis of the waterbox created for the strainer head loss computation. Figure 7-1 shows a layout of the BVPS-1 waterbox and the location of the suction piping to the pumps from the waterbox. The velocity distribution plots show the flow of water from the duct, which then splits in the waterbox to the pump suction inlet pipes. Figures 7-2 and 7-3 show the CFD results for the case that is representative of those cases where voids are generated. This case corresponds to operation prior to transfer to safety injection recirculation where four Recirculation Spray pumps are in operation. Based on the plots shown in Figures 7-2 and 7-3 below, there is a clear movement of water entering the waterbox from the duct to the emergency core cooling system (ECCS) pump suction pipes, with velocities in the top region of the waterbox of 1.5 in/s or more. Some small areas are slightly below this velocity. These areas are inconsequential since surrounding areas have higher velocities and will tend to sweep air bubbles into the flow stream.

As discussed above, calculations have been performed to determine the air evolution due to the pressure drop through the debris bed, the strainer modules, and ductwork. The results of these analyses show that air evolution is limited to a relatively short period of time prior to transfer to safety injection recirculation mode. Safety injection recirculation usually occurs less than one hour following the accident for the large break LOCA scenarios, and approximately one hour following the accident for the small break LOCA scenarios. In all cases analyzed, air evolution occurs for less than three hours, and the maximum void fraction is 0.11 percent in the BVPS-1 waterbox. However, as

stated above, high velocity areas at the top of the waterbox will sweep air bubbles to the pumps.

Thus, air bubbles are not expected to accumulate at the top of the BVPS-1 waterbox and in the unlikely event this occurs, the accumulation of air bubbles is limited by the small percentage of time air is evolved over the mission time of the pumps.



**Notes:**

1. Dashed lines denote that the suction inlet piping is cross connected under the floor
2. Solid red circles denote operating pumps prior to transfer to SI recirculation

**Designations:**

- 'A' and 'B' denotes 'A' and 'B' train  
IRS: - Inside Recirculation Spray pump  
ORS: - Outside Recirculation Spray pump  
LHSI: - Low Head Safety Injection pump

Figure 7-1 Pump Suction Piping Configuration for BVPS-1

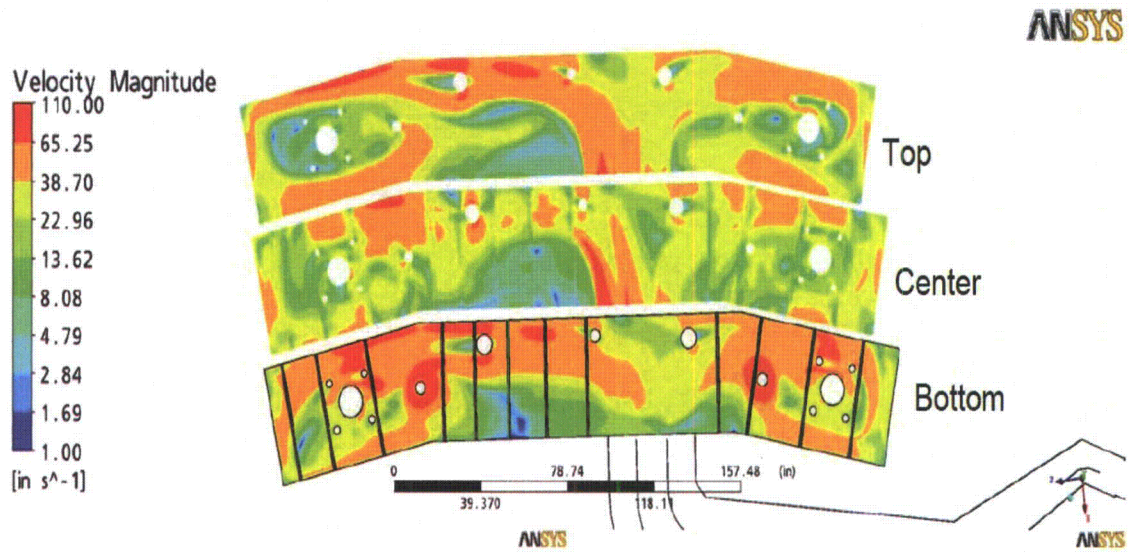


Figure 7-2 Waterbox Velocity Plot for BVPS-1

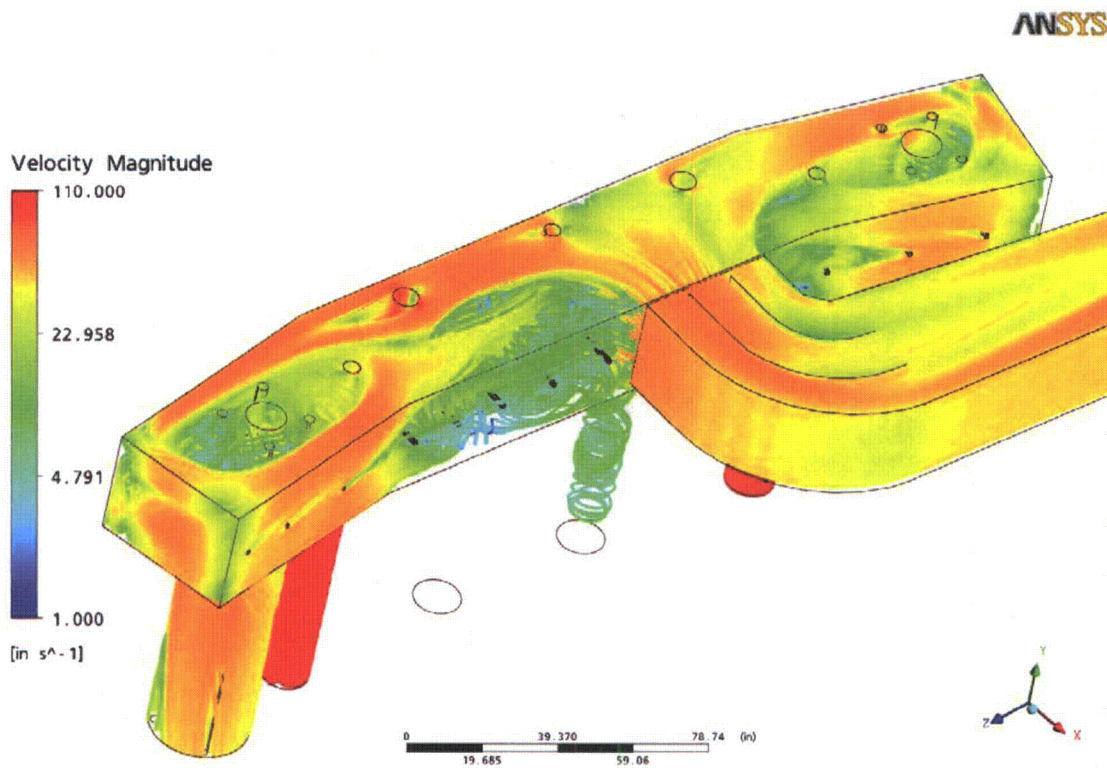


Figure 7-3 Waterbox Velocity Streamlines for BVPS-1

For BVPS-2, collection of air bubbles is not expected. The BVPS-2 strainer design consists of cylindrical "top hats" that are oriented vertically on top of a manifold which directs water to the pump suction inlet pipes. The "top hats" are made up of two concentric cylindrical sections with perforated plates on the inner and outer surfaces. Flow enters the perforated cylinders and flows down through an annulus to the manifold. The velocities in the annular space are high enough, approximately 2-3 inches per second at a minimum, to move small bubbles along with the flow such that no accumulation is expected. If gas were to collect in the top part of the "top hat" assemblies, a path through the perforated cylinders is available for the gas to vent back to the sump pool.

### RAI 8

**The NRC staff could not confirm that testing included properly scaled quantities of all debris types. For example, for BVPS-1, Test 6 was stated to bound all breaks. However, Table 3.f.4-3 indicates that only a small amount of Temp-Mat was included in the test. In the transport section, the transport chart for the bounding RCS break appears to indicate that the break would result in more Temp-Mat debris. Another example for BVPS-1 is that the reactor nozzle break test case (Test 2) contains significant Temp-Mat, but the transport charts show that there would be no Temp-Mat debris for this break. For BVPS-2, Case 1A, it appears that the amount of fibrous debris added to the testing was lower than would be required by the transport evaluation. Please provide the basis for the amount of each debris source added to each test which is considered a design basis test for each strainer.**

### FENOC Response

The June 30, 2009 supplemental response was intended to provide a description of the BVPS-1 and BVPS-2 test programs, which utilized a series of tests to establish acceptable debris loads for the strainers. As such, the description included the results of tests involving debris loads with differing quantities of the various debris bed constituents. Following the test program, the debris loads associated with Test 6 for BVPS-1 and Test 1A and the August 2009 Test 2 for BVPS-2 were identified as the limiting acceptable debris loads. Design modifications were then planned for BVPS-1 and BVPS-2 to ensure that the debris loads for all breaks were lower than or equal to the limiting loads established by the testing. With the exception of the BVPS-1 Reactor Vessel Nozzle Temp-Mat™ insulation (described in RAI 2) scheduled for removal during the fall 2010 refueling outage (1R20), the originally planned design modifications have been completed. When all planned insulation remediation is completed (refer to RAI 1 and RAI 5), Test 6 is the design basis test for BVPS-1, and Test 1A and the August 2009 Test 2 are the design basis tests for BVPS-2.

All of the BVPS-1 and BVPS-2 design basis tests included the properly scaled quantities of all debris types after planned insulation modifications. The apparent inconsistencies in Temp-Mat™ volume values are the result of density correction for

quantifying the amount of Temp-Mat™ fiber that is collected on the strainer after transport. The quantity of Temp-Mat™ fiber used in testing was determined using the mass of material destroyed by the subject break and transported to the strainer.

The NRC staff provided three specific examples where they could not confirm that the testing included the properly scaled quantities. The following three paragraphs provide a detailed response to the three RAI examples, and correspond to the sequence of issues presented in the RAI:

*Example 1 – BVPS-1 Test 6 Temp-Mat™ Load*

Table 3.e-6 of the June 30, 2009 supplemental response provides a total Temp-Mat™ volume at the sump of 4.0 ft<sup>3</sup> for BVPS-1 bounding RCS loop break. The 4.0 ft<sup>3</sup> is the density corrected volume of Temp-Mat™. Temp-Mat™ is a High Density Fiberglass (HDFG) product with an as-manufactured density of 11.8 lbm/ft<sup>3</sup>. However, HDFG fines and small pieces have been shown to be very similar to Low Density Fiberglass (LDFG) debris. The HDFG debris loses its "felt" type characteristics when it breaks down to individual fibers or clumps of fibers. As such, use of the HDFG as-manufactured density underestimates the volume of debris generated since the density of HDFG small pieces and fines is significantly less than the density of the original felted material. There are no large pieces of Temp Mat™ generated by the bounding RCS loop break. Therefore, in the BVPS-1 Debris Generation and Debris Transport analyses, the volume of transportable HDFG debris is determined by multiplying the volume of HDFG fines and small pieces generated within the ZOI by the ratio of HDFG as-manufactured density to LDFG as-manufactured density. The properties of NUKON® are commonly used as representative of LDFG. The volume of Temp-Mat™ debris stated in Table 3.e-6 of the June 30, 2009 supplemental response, therefore, is based on the calculated volume of fine and small piece Temp-Mat™ multiplied by the as-manufactured density ratio of Temp-Mat™ to NUKON®. Without density correction, the nominal Temp-Mat™ volume for the bounding RCS loop break is 0.8 ft<sup>3</sup>. As the testing used actual Temp-Mat™ to represent the HDFG Temp-Mat™ at BVPS-1, the scaling was done based on the nominal volume of Temp-Mat™, without density correction. Test 6 was conservatively performed using the scaled equivalent of 1.0 ft<sup>3</sup>, which bounds the plant design basis load of 0.8 ft<sup>3</sup>. The scaled equivalent of 0.3 pound-mass (lbm) was determined by multiplying the bounding plant load by the as-fabricated density of Temp-Mat™ and the scaling factor [(1.0 ft<sup>3</sup> x 11.8 lb/ft<sup>3</sup>) x (0.025 scaling factor)] as shown in Table 3.f.4-3 of the June 30, 2009 supplemental response. The following table summarizes these calculations:

Table 8-1, BVPS-1 Test 6

Plant Density Corrected Volume (ft <sup>3</sup> )	Plant Nominal Volume (ft <sup>3</sup> )	Tested Volume, Unscaled (ft <sup>3</sup> )	Test Load, Scaled (lbm)
4.0	0.8	1.0	0.3

*Example 2 – BVPS-1 Reactor Nozzle Break Case (Test 2) Temp-Mat™ Load*

Table 3.f.4-3 of the June 30, 2009 supplemental response provides a total scaled Temp-Mat™ load of 17.35 lbm for BVPS-1, Test 2. Table 3.e-8 of the June 30, 2009 supplemental response provides a Temp-Mat™ volume of 0 ft<sup>3</sup> for the BVPS-1 reactor nozzle break. The BVPS-1, Test 2 was representative of the BVPS-1 Reactor Nozzle Break prior to planned insulation modifications. After completion of all planned insulation modifications, no Temp-Mat™ is destroyed by a BVPS-1 Reactor Nozzle Break. As stated on page 88 (Section 3.f.4) of the June 30, 2009 supplemental response, Test 6 represents the final configuration for BVPS-1, and bounds the BVPS-1 loop break, BVPS-1 reactor nozzle break and surge line break. BVPS-1 Test 2 is not a design basis test.

*Example 3 – BVPS-2 Test 1A Temp-Mat™ Load*

Table 3.e-10 of the June 30, 2009 supplemental response provides a total Temp-Mat™ volume at the sump of 11.4 ft<sup>3</sup> for BVPS-2 bounding RCS loop break. The 11.4 ft<sup>3</sup> is the density corrected volume of Temp-Mat™. Consistent with the BVPS-1 analyses, the volume of Temp-Mat™ debris stated in Table 3.e-6 of the June 30, 2009 supplemental response, therefore, is based on the calculated volume of fine and small piece Temp-Mat™ multiplied by the as-manufactured density ratio of Temp-Mat™ to NUKON®. Without density correction, the nominal Temp-Mat™ volume for the bounding RCS loop break is 2.3 ft<sup>3</sup>. As the testing used actual Temp-Mat™ to represent the HDFG Temp-Mat™ at BVPS-2, the scaling was done based on the nominal volume of Temp-Mat™ without density correction. Test 1A was conservatively performed using the scaled equivalent of 2.8 ft<sup>3</sup>, which bounds the plant design basis load of 2.3 ft<sup>3</sup>. The scaled equivalent of 1.84 lbm was determined by multiplying the bounding plant load by the as-fabricated density of Temp-Mat™ and the scaling factor [(2.8 ft<sup>3</sup> x 11.8 lb/ft<sup>3</sup>) x (0.0556 scaling factor)] as shown in Table 3.f.4-4 of the June 30, 2009 supplemental response. The following table summarizes these calculations:

Table 8-2, BVPS-2 Test 1A

Plant Density Corrected Volume (ft <sup>3</sup> )	Plant Nominal Volume (ft <sup>3</sup> )	Tested Volume, Unscaled (ft <sup>3</sup> )	Test Load, Scaled (lbm)
11.4	2.3	2.8	1.84

The following table summarizes the Temp-Mat™ design basis test loads for BVPS-1 and BVPS-2 testing:

Table 8-3, Summary of Design Basis Testing Temp-Mat™ Loads

	DESIGN TEST	NOMINAL VOLUME at STRAINER (ft <sup>3</sup> )	TESTED VOLUME (UNSCALED) (ft <sup>3</sup> )	TEST LOAD (SCALED) (lbm)
BVPS-1	6 (for loop, surge line, and nozzle breaks)	0.9	1.0	0.3
BVPS-2	1A (for loop and surge line breaks)	1.2	2.8	1.84
BVPS-2	August 2009 Test 2 (for nozzle break)	0	0	0

Note that the Tested Volume was greater than the Nominal Volume to create margin for Test 6 and 1A. The nominal Temp-Mat™ volumes provided in Table 8-3 vary slightly from the values provided in Table 8-1 and Table 8-2. The values presented in Table 8-1 and Table 8-2 are based on the values presented in the June 30, 2009 supplemental response which were pre insulation replacement. The values provided in Table 8-3 are based on the latest debris generation and debris transport analyses, which reflect the final values post insulation replacement. As shown in Table 8-3, the tested loads are still bounding.

#### RAI 9

**According to Reference 1, for BVPS-1, 0.25 cubic feet (ft<sup>3</sup>) of latent fiber is generated and that there would be about 24 pounds (lbs) of latent fiber. Generally, this would be considered to be about 10 ft<sup>3</sup> of fiber. Apparently, a latent fiber density of 94 lb/ft<sup>3</sup> was used to calculate the amount of fiber. It appears that the correct mass of Nukon fiber was added to the head loss testing to represent the latent fibrous debris. Please provide information that specifies the characteristics and amount of latent fibrous debris that was used in head loss testing for BVPS-1. The BVPS-2 evaluation lists a volume of 11.3 ft<sup>3</sup> of latent fiber, an apparently more reasonable value.**

#### FENOC Response

For BVPS-1 and BVPS-2, the quantity of latent fiber in containment was established using an assumed 15 percent of the mass of total latent debris in the containment, consistent with Section 3.5.2.3 of the NRC safety evaluation (SE) (Reference 3). Thus, the quantity of latent fiber was initially established as a mass value of 23.8 pounds (lbs) for BVPS-1 and 27.6 lbs for BVPS-2. To establish the latent fiber volume at BVPS-1, the latent fiber mass was divided by the microscopic density of 94 lb/ft<sup>3</sup> as defined in

Section 3.5.2.3 of the NRC SE, resulting in a latent fiber volume of 0.25 ft<sup>3</sup>. Conversely, to establish the latent fiber volume at BVPS-2, the latent fiber mass was divided by the “as-manufactured” density of 2.4 lb/ ft<sup>3</sup> as defined in Section 3.5.2.3 of the NRC SE, resulting in a latent fiber volume of 11.5 ft<sup>3</sup>.

Table 9-1, Latent Fiber

	Latent Fiber Weight (lb)	Latent Fiber Density (lb/ft <sup>3</sup> )	Latent Fiber Volume (ft <sup>3</sup> )
BVPS-1	23.8	94	0.25
BVPS-2	27.6	2.4	11.5

NUKON<sup>®</sup> was used as the surrogate for latent fiber in the head loss testing for BVPS-1. The characteristics of NUKON<sup>®</sup> are an “as-manufactured” density of 2.4 lb/ft<sup>3</sup> and a fiber diameter of 7 microns. The latent fiber load used in BVPS-1, Test 6, was 30 lbs, before scaling, which bounds the plant load of 23.8 lbs. The scaled load was 0.75 lbs [30 lbs x 0.025 scaling factor]. Therefore, the correct mass of NUKON<sup>®</sup> was added to the head loss testing for BVPS-1.

The scaled loads used for BVPS-2 testing were as follows:

1.67 lbs for the BVPS-2 Test 1A [30 lbs x 0.0556 scaling factor]

1.57 lbs for the BVPS-2 August 2009 Test 2 [30 lbs x 0.0521 scaling factor]

Summarizing, BVPS-1 and BVPS-2 were both tested with a conservative latent fiber load (before scaling) of 30 lbs. This bounding value was based upon an assumed 15 percent latent fiber content with a latent debris load of 200 lbs. NUKON<sup>®</sup> was used as the surrogate for latent fiber in both the BVPS-1 and BVPS-2 cases. The latent fiber volume used for testing at each unit is the same when the same densities are applied in the pound mass to volume conversion. (Refer to Tables 9-2 and 9-3.)

Table: 9-2, Plant Latent Debris Load

	Latent Fiber Weight (lbs.)	Microscopic Density (lbs/ft <sup>3</sup> )	As-Manufactured Density * (lbs/ft <sup>3</sup> )	Latent Fiber Volume (ft <sup>3</sup> ) **
BVPS-1	23.8	94	2.4	9.92
BVPS-2	27.6	Not reported	2.4	11.5

Notes: \* based upon NUKON<sup>®</sup> fiber as the surrogate material.  
 \*\* volume calculated using the as-manufactured density.

Table: 9-3, Latent Fiber Testing Quantities

Unit – Test	Bounding Fiber Load (lbs.) ***	Scaling Factor	Scaled Load (lbs.)
BVPS-1 Test 6	30	0.025	0.75
BVPS-2 Test 1A	30	0.0556	1.67
BVPS-2 August 2009 Test 2	30	0.0521	1.57

Note: \*\*\* based upon a bounding latent fiber weight of 30 lbs. [0.15 x 200 lbs.]

### RAI 10

**The flow rates used during BVPS-1 vortex testing were not compared against the maximum potential strainer module flow rates. The maximum flow stated to be used during testing was 600 gallons per minute (gpm) at 1 inch submergence, with a repeated test at zero submergence. The design scaled flow rate was 360 gpm. The design minimum submergence is 2.2 inches. Because the strainer consists of a long train of strainer modules, when the strainer is clean, the module closest to the pump suction will have a significantly higher flow rate than those further from the pump. Please provide the flow rate through the limiting module and verify that this flow rate was considered in the vortex evaluation.**

### FENOC Response

The maximum potential flow rates through the BVPS-1 strainers are within the range of velocities used in the CCI Generic Vortex Tests. The BVPS-1 maximum pocket entrance velocity to the worst case clean screen strainer is 0.414 meters per second (m/s) for String 1 and 0.493 m/s for String 2. These values are derived from the maximum flow case with 14,500 gpm through the strainers. The pocket entrance velocity used in the limiting test case, used for the comparison below, is 0.310 m/s and the maximum pocket entrance velocity in the vortex tests is 1.03 m/s.

The vortex analysis is based on a video that was taken during the CCI Generic Vortex Tests conducted in January 2008.

The video was used to determine the size of potential vortices which could occur for the clean strainer condition. The size of the vortex relative to the pocket was estimated based on the image below. Figure 10-1 was taken from the video of a clean strainer vortex test where the Froude number (0.218 using  $Fr = v^2 / g \times h$ ) and submergence (1.8 in) bound the worst case Froude number and submergence (4.17 inches for the modules closest to the pump suction) at BVPS-1.

The CCI Generic Vortex Tests were used to develop Figure 10-2 below. Figure 10-2 shows strainer operating regions with respect to vortex formation based on strainer submergence level and Froude number. The data point (the test shown in Figure 10-1) selected for the vortex analysis is marked in Figure 10-2 as a black 'X' on the red "Limit\_C" line used to delineate the unsafe operating region from the operating region

with limited air intake. Vortices such as the one shown in Figure 10-1 occurred less than 20 percent of the time for the given Froude number and submergence, but are conservatively assumed to occur 100 percent of the time in the vortex analysis.

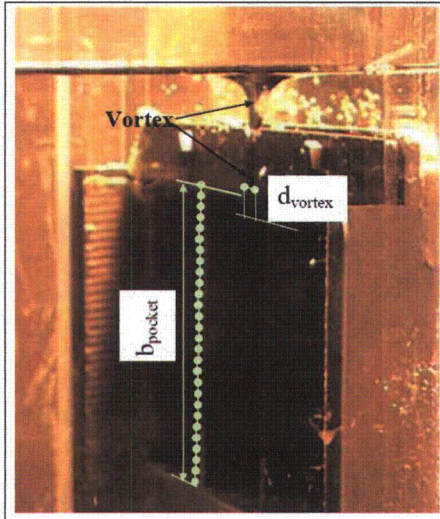


**Figure 10-1, Screen Shot from Vortex Test Video**

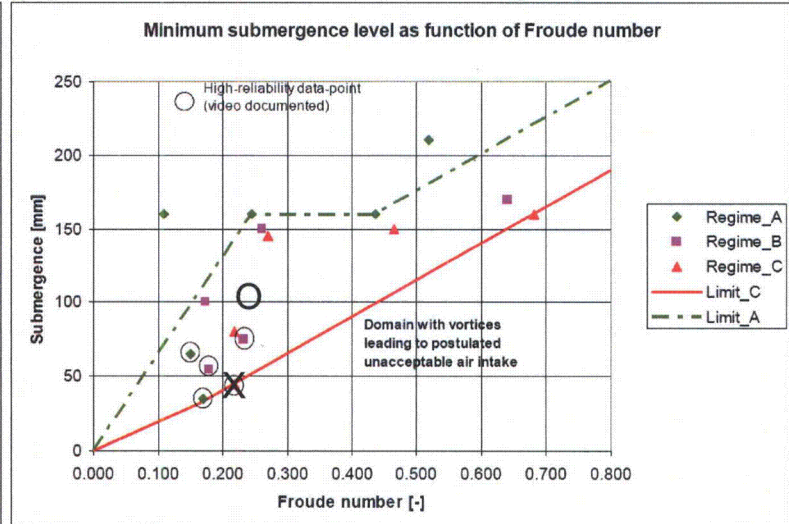


**Figure 10-2, Clean Strainer Vortex Test Results**

The BVPS-1 maximum pocket entrance velocity to the worst case clean strainer is 0.493 m/s. This corresponds to a maximum flow rate of 14,500 gpm. The minimum submergence of the modules closest to the sump is 4.17 inches (106 millimeters [mm]). Thus, the Froude number for the worst BVPS-1 case is:

$$Fr = \frac{v^2}{g \times h} = \frac{(0.493 \frac{m}{s})^2}{9.81 \frac{m}{s^2} \times 0.106 \text{ m}} = 0.234 \quad (\text{This case is marked with an "O" on Figure 10-2})$$

The Froude number for the worst case is comparable to the test that resulted in the vortex shown in Figure 10-1, but the BVPS-1 submergence is more than twice the value in the test, thus significantly decreasing the amount and size of vortices. Based on Figure 10-2, the worst BVPS-1 case will be between the Limit\_A line and the Limit\_C line, where some unsteady vortices may occur, however, substantially less air will be ingested than in the case shown in Figure 10-1.

The effect on pump NPSH of a vortex similar to the one shown in Figure 10-1 is minimal since the ingested air results in a very small void fraction at the pump, as calculated below. As stated above, the vortex is conservatively considered to occur 100 percent of the time. Based on scaling of the screen shot in Figure 10-1, the vortex diameter is approximately 1/27<sup>th</sup> of the height of the pocket. Since the pocket opening is 120 mm tall, the diameter of the vortex is 4.44 mm [=120 mm/27], and the cross sectional area of the vortex is 1.55 x 10<sup>-5</sup> m<sup>2</sup> [=πd<sup>2</sup>/4].

The air ingested due to vortexing is modeled as reaching the velocity of water once it is inside the pocket. Thus, the proportion of air ingested ( $\alpha_p$ ) is the ratio of the cross section of the vortex to the cross section of the four pockets, which were used during the tests. The inside of the pocket is 70 mm wide and 109 mm tall. Thus, 0.05 percent [ $=1.55 \times 10^{-5} \text{ m}^2 / (4 \times 0.070 \text{ m} \times 0.109 \text{ m})$ ] air ingestion by volume is computed for the test condition. The pockets used in the BVPS-1 strainers are 70.5 mm wide and 79.4 mm tall. Because the tested and installed pocket sizes are comparable, the results of the generic vortex test are considered to apply to the BVPS-1 strainers.

To assess the total effective air ingestion, the test cross section area ( $4 \times 0.070 \times 0.109 = 0.031 \text{ m}^2$ ) is compared to the entrance cross section area of the module section closest to the wye connecting the installed strainer strings (as shown in Figure 16-1 in the response to RAI 16). The maximum velocities will occur in the closest third of the strainer module closest to the wye between the two strings. One third of Module 1/4 has an area of  $0.336 \text{ m}^2$  and one third of Module 2/9 has an area of  $0.295 \text{ m}^2$ . Note that Module 1/4 is the fourth module in String 1 and Module 2/9 is the ninth module in String 2. These are the modules in each string that are closest to the sump. Therefore, these modules experience the maximum flow rate and are the most susceptible to vortex formation. If the Froude number and submergence is on the Limit\_C line in Figure 10-2, the air ingested across the closest third of a strainer module is:

- String 1 - Module 1/4:  $0.336 \text{ m}^2 \Rightarrow \alpha_{pC,M1/4} = \frac{0.031}{0.336} \cdot 0.05\% = 0.0046\%$
- String 2 - Module 2/9:  $0.295 \text{ m}^2 \Rightarrow \alpha_{pC,M2/9} = \frac{0.031}{0.295} \cdot 0.05\% = 0.0053\%$

The actual amount of air ingested will be less than the value calculated above because the actual BVPS-1 conditions provide more submergence. Figure 10-3 shows the Froude number as a function of submergence for Module 1/4 (the M\_1/4 line) and for Module 2/9 (the M\_2/9 line). Because, the velocity is dependent on the flow rate and total pocket area, as opposed to the submergence, the Froude number is directly proportional to the inverse of the submergence. The worst case at BVPS-1 has a submergence of 4.17 inches, and is marked as "O" on both the M\_1/4 and M\_2/9 lines in Figure 10-3. The actual air ingestion is taken to be the linear interpolation along the M\_1/4 or M\_2/9 lines between the Limit\_A line (0 percent air ingestion) and the Limit\_C line (maximum air ingestion calculated above).

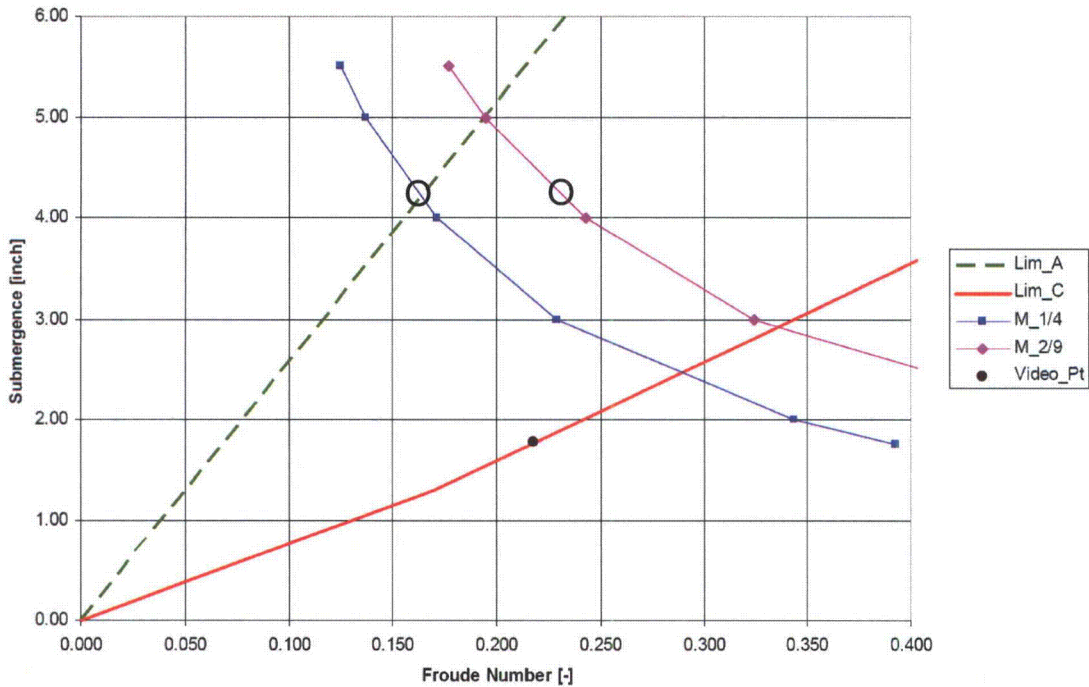


**Figure 10-3, Vortex formation risk in Modules 1/4 and 2/9**

Based on a linear interpolation of the data used in Figure 10-3 (from the results of the BVPS-1 vortexing calculation), the air ingestion due to vortexing will be 0.0001 percent through Module 1/4 and 0.00213 percent through Module 2/9. The total air ingestion due to vortexing takes into account the flow split between the strings. From the BVPS-1 vortex calculation, 46.5 percent of the flow goes through String 1 and 53.5 percent of the flow goes through String 2. The total air ingestion due to vortexing is calculated below.

- $0.0001\% \times 46.5\% + 0.00213\% \times 53.5\% = 0.00119\%$

Thus, the void fraction at the pump due to vortexing is 0.0012 percent (not accounting for the impact of static head). An average void fraction of 0.0012 percent results in a net positive suction head required (NPSHR) multiplier of 1.00056 (based on Appendix A of Regulatory Guide 1.82), which does not significantly impact the NPSHR.

**RAI 11:**

**The accumulators were credited for strainer submergence for the small-break LOCA. Please provide justification for this assumption or justify that the calculated levels are conservative.**

### **FENOC Response**

The MAAP-DBA code is used to determine the amount of water hold up in the containment nodes and also for the RCS inventory released for small and intermediate break sizes which are limiting for sump strainer submergence. An integrated primary system and containment model is used. This model tracks the amount of water contained and released from the RCS including the pressurizer. The accumulators will inject automatically in response to the RCS pressure which is calculated by the MAAP-DBA code. If partial or full injection occurs, this water will be available in the RCS and ultimately to the sump. For the limiting case for sump level and sump strainer submergence, a 2-inch break at the top of the pressurizer, the accumulators do not inject at BVPS-1 prior to the point at which minimum submergence occurs. For the same limiting case at BVPS-2, a small injection (approximately 2,100 gallons) occurs from the accumulators prior to the point of minimum submergence. This volume is not credited directly to increase the sump volume although it does add to the RCS inventory available for release from the break. The small volume represents less than one-half inch of level change in the sump.

### **RAI 12:**

**It was unclear that the debris preparation for the fibrous material resulted in prototypical fine fiber. In Reference 1, it is stated that the fibrous debris was prepared in a blender. The NRC staff has observed varying debris characteristics for fibrous debris prepared in a blender. In this case, if the fibers are blended for too long a time period, they could become particulate like instead of fibrous. On the other hand, if too much fiber is placed in the blender only a small amount may be affected. Alternately, the NRC staff has observed blended fiber to become compact balls, which is non-prototypical. In general, the NRC staff has stated that fine fiber should represent classes 1 through 3 as defined in NUREG/CR-6808, Table 3-2, with the majority being classes 2 and 3. The supplemental response dated June 30, 2009, stated that the fibers were inspected to ensure that they met the distribution requirements defined in the NUREG, but the NUREG does not define the size distribution. Please provide information that verifies that the fibrous debris used for testing was prototypical of that predicted to reach the strainer by the debris generation and transport evaluation.**

### **FENOC Response**

In order to properly prepare prototypical fibrous debris for testing, Section 6.2.2 of the *NRC Staff Review Guidance Regarding Generic Letter 2004-02 Closure in the Area of Strainer Head Loss and Vortexing, March 2008*, Accession Number ML080230038 (March 2008 NRC staff guidance) was followed. The guidance recommends that a licensee should "prepare the surrogate fibrous materials as very fine debris that will tend to remain suspended with relatively little pool turbulence. It has been demonstrated that a food processor can effectively break up shredded debris."

Using this guidance, the fibrous debris preparation step outlined in the test specific procedure indicates that in order to obtain fiber fines, one must start with standard prepared "smalls" ("smalls" are prepared by first cutting fiber blankets into 4-inch wide strips and then feeding the strips through the leaf shredder). Then to obtain fiber fines, the fiber "smalls" will be placed in a blender with water and blended. This step and similar controlling procedures were followed for each of the BVPS tests.

Additionally, the fine fibrous debris type has a specific concentration when it is mixed prior to adding to the test. The Test Plan states: "The Alion debris preparation procedure will be used to complete the fiber fines processing. Each ¼ lb batch of fiber fines will be added to approximately 4 gallons of water beat with a paint stirrer for 4 minutes. The fiber slurry resulting from the above process will be visually examined by the test engineer to verify that the fiber in slurry meets the required size distribution and photographs taken." The slurry is maintained at a low enough debris concentration to ensure proper mixing of all the materials in the bucket. Similar protocols were followed for each of the Beaver Valley tests.

The photograph in Figure 12-1 displays the results of the blended fiber debris preparation methodology and the photograph in Figure 12-2 shows a close up detail of the prepared fibers. Note that the fibers still have fiber like qualities and are quite dissimilar from particulate debris (a particulate example is shown in the photograph in Figure 12-3 for comparison purposes); they are also not showing any of the characteristics of an over-blended debris slurry resulting in too fine of fibers. Additionally, it is clear that there was sufficient blending affecting the majority of the fibers and adequate dilution of the debris slurry to prevent the accumulation of fiber clumps or balls in the blender.

The June 30, 2009 supplemental response did state that the fibers were inspected to ensure that they met the size distribution requirements that are defined in the NUREG/CR-6808. However, it would have been more appropriate to state that the fibers were inspected to ensure that they met the size classification description that are defined in the NUREG/CR-6808 Table 3-2 (see Figure 12-4). Consistent with staff guidance, fiber fines are defined as Classes 1-3 in the debris preparation procedure , and inspected to ensure that they are representative as Classes 1-3.

After the preparation, the fiber is mixed thoroughly with a paint mixer attached to an electric drill until a homogeneous slurry is formed. Then the debris is introduced at the top of the test tank near the return line and transported towards the strainer array by the water flow drawn through the strainers. This methodology ensures the fibrous debris used in testing is prototypically and conservatively representative of the fibrous debris predicated to reach the strainer as determined in the debris generation and transport evaluation.

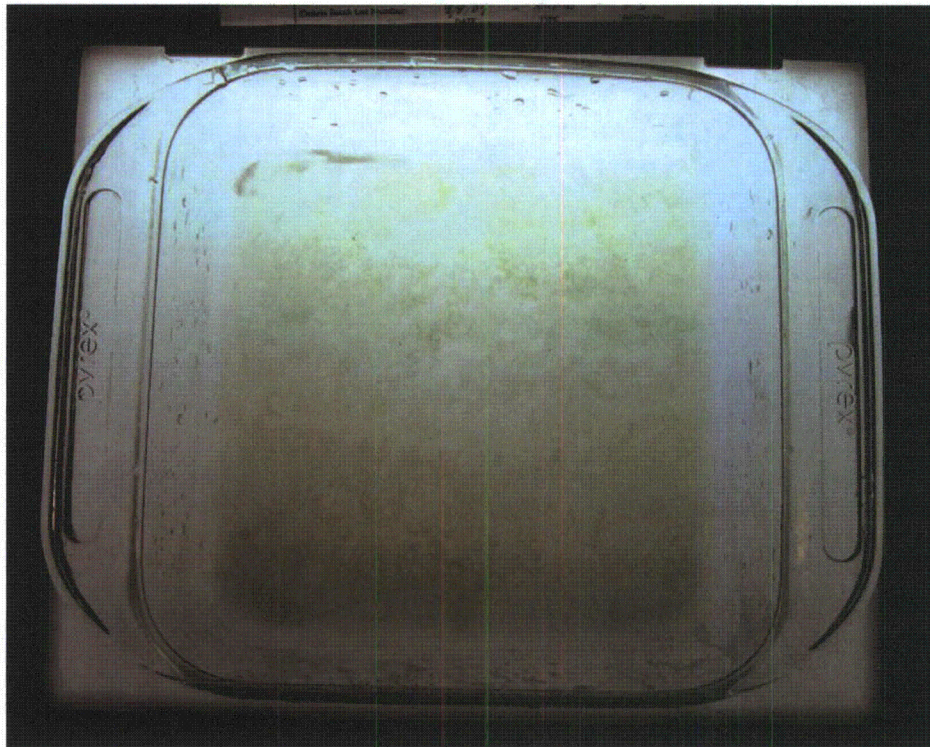


Figure 12-1, Blended Fiber Debris



Figure 12-2, Blended Fiber Debris Close Up Detail



Figure 12-3, Ground Silica Particulate Debris

No.	Description	
1		Very small pieces of fiberglass material; "microscopic" fines that appear to be cylinders of varying L/D.
2		Single, flexible strands of fiberglass; essentially acts as a suspending strand.
3		Multiple attached or interwoven strands that exhibit considerable flexibility and that, because of random orientations induced by turbulent drag, can exhibit low settling velocities.
4		Fiber clusters that have more rigidity than Class 3 debris and that react to drag forces as a semi-rigid body.
5		Clumps of fibrous debris that have been noted to sink when saturated with water. Generated by different methods by various researchers but easily created by manual shredding of fiber matting.
6		Larger clumps of fibers lying between Classes 5 and 7.
7		Fragments of fiber that retain some aspects of the original rectangular construction of the fiber matting. Typically pre-cut pieces of a large blanket to simulate moderate-size segments of original blanket.

Figure 12-4, Fibrous Debris Class Descriptions from Table 3-2 of NUREG/CR-6808

**RAI 13:**

**Reference 1 did not provide information regarding the debris introduction procedures, including the debris introduction locations with respect to the strainer and the potential for agglomeration of debris. Please provide information that shows that the debris was diluted and introduced, such that agglomeration of the debris did not occur and that the debris was allowed to transport to the strainer with the bulk flow in the test tank.**

**FENOC Response**

The credited testing for BVPS-1 and BVPS-2 was performed after the March 2008 NRC staff guidance was issued. Prior to the start of the BVPS-1 re-test and in order to ensure the March 2008 NRC staff guidance was followed, a NRC Reviewer's Guide Checklist was implemented. The test specific plans and procedures were specifically written to satisfy the recommendations in the guidance. The checklist specifically addressed agglomeration in the surrogate step:

Debris will be prepared for addition to the test tank by placing small quantities of each debris in 5-gallon buckets, and adding enough water to each bucket to ensure that debris is properly suspended, and diluted enough to prevent agglomeration. Debris will be added slowly and directly above the return line sparger, to further ensure that agglomeration does not occur.

Figure 13-1 shows the debris addition. As well as in the agitation step:

“Agitation was used in the form of a sparger on the return line in the tank, as well as two mechanical mixers, positioned to produce enough turbulence to help prevent particulate debris from settling on the bottom of the test tank. If any significant amount of particulate debris does settle on the bottom of the test tank, the particulate will be agitated by stirring manually. Shakedown testing was performed to verify that the agitation of the water did not prevent the debris bed from forming prototypically.” Finally, agglomeration is addressed in the thin bed step: “All debris will be prepared as described above to ensure that it is properly suspended, and diluted sufficiently to avoid agglomeration.”

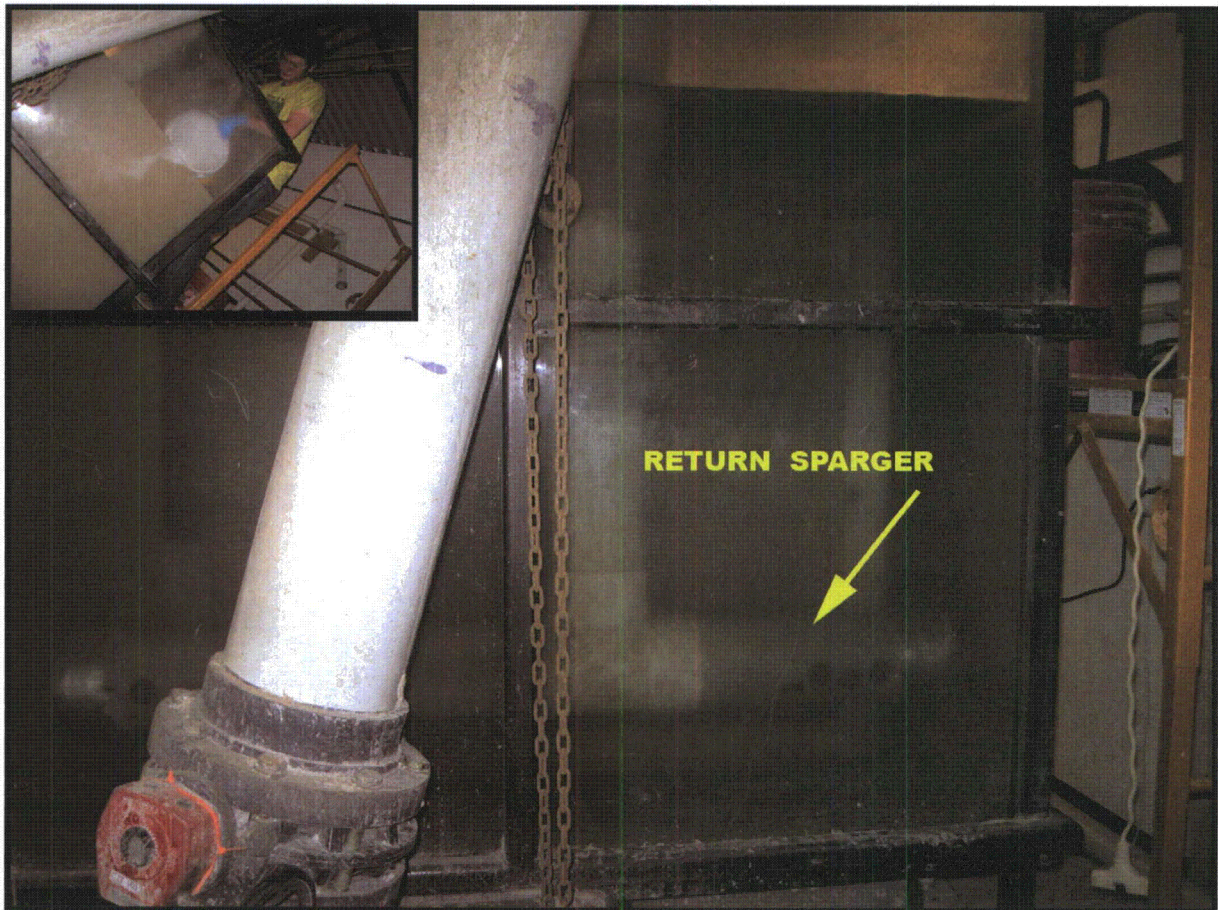


Figure 13-1, Debris Addition Over Return Sparger

Each debris type has a specific concentration when it is mixed prior to adding to the test. The Test Plan specifically addressed fibrous debris mixing in section 4.3.3: "The Alion debris preparation procedure will be used to complete the fiber fines processing. Each ¼ lb batch of fiber fines will be added to approximately 4 gallons of water beat with a paint stirrer for 4 minutes. The fiber slurry resulting from the above process will be visually examined by the test engineer to verify that the fiber in slurry meets the required size distribution and photographs taken. The slurry is maintained at a low enough debris concentration to ensure proper mixing of all the materials in the bucket, as shown in Figures 13-4 through 13-9. The debris is then added into the tank at the return line discharge (debris addition locations are shown in Figures 13-2 and 13-3) to ensure full entrainment of the debris into the flow stream.

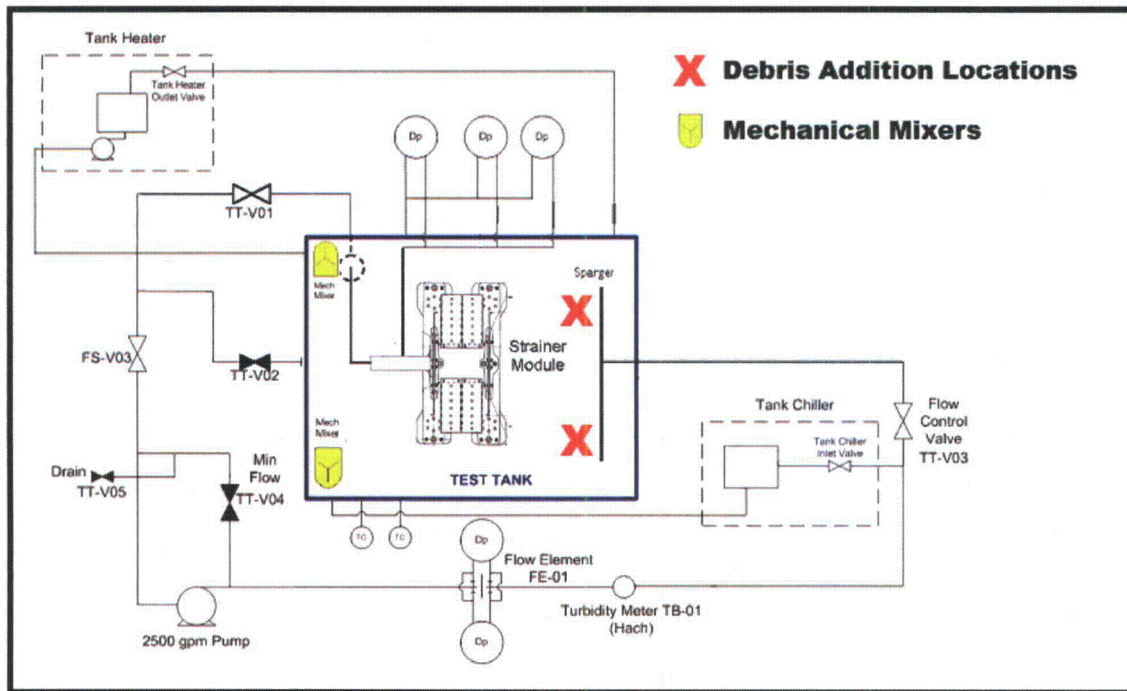


Figure 13-2, Debris Addition Locations for BVPS-1

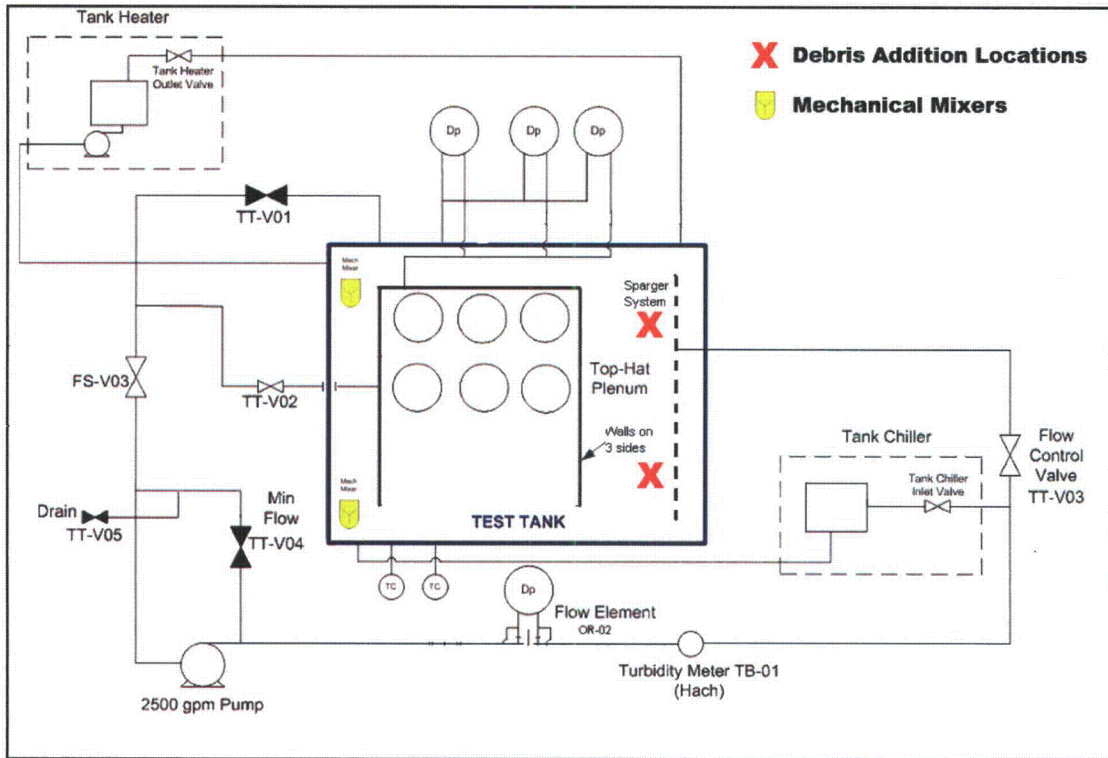


Figure 13-3, Debris Addition Locations for BVPS-2

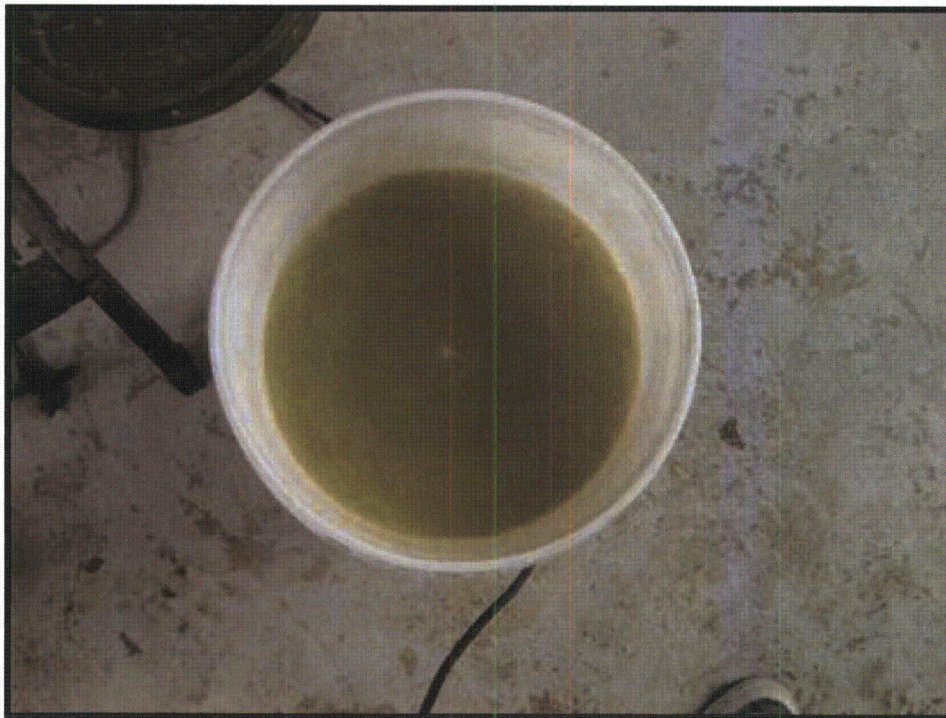


Figure 13-4, Fiber Slurry

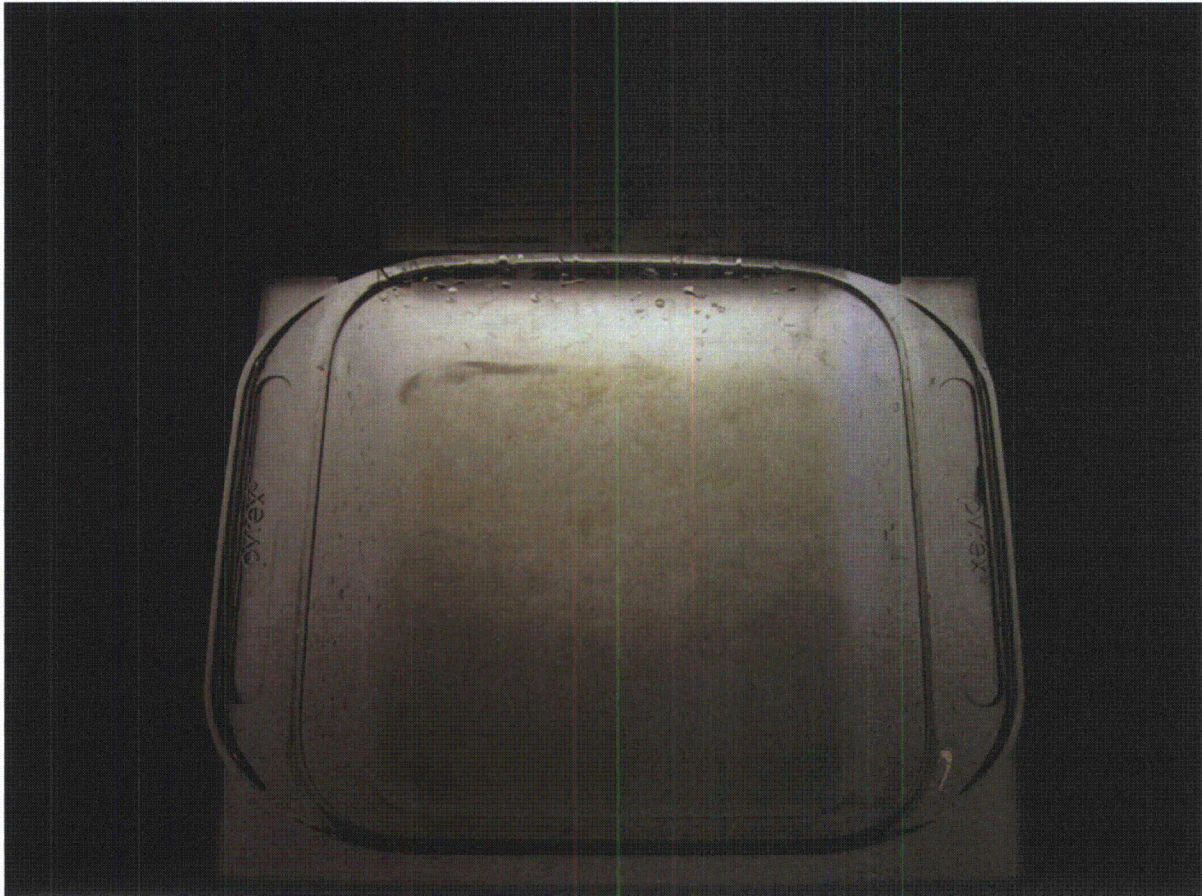


Figure 13-5, Fiber Detail

The Test Plan specifically addressed particulate debris, including dirt and coatings, mixing in section 4.3.4: "Particulates will be placed in a bucket with sufficient water to create a thin slurry. Particulate with water will be mixed using a paint stirrer until no agglomeration or clumping is observed. Before addition into the test, all particulate batches will be mixed once again with an electric paint stirrer to break up clumps and create a thin slurry consisting of approximately 10 lbs of particulate per 3 gallons of water taken from the tank." The Microtherm<sup>®</sup> particulate debris had a much lower concentration than 10 lbs/bucket, on the order of 1 to 3 lbs/bucket limited by the material bulk density. As shown in Figures 13-8 and 13-9.



Figure 13-6, Particulate Slurry

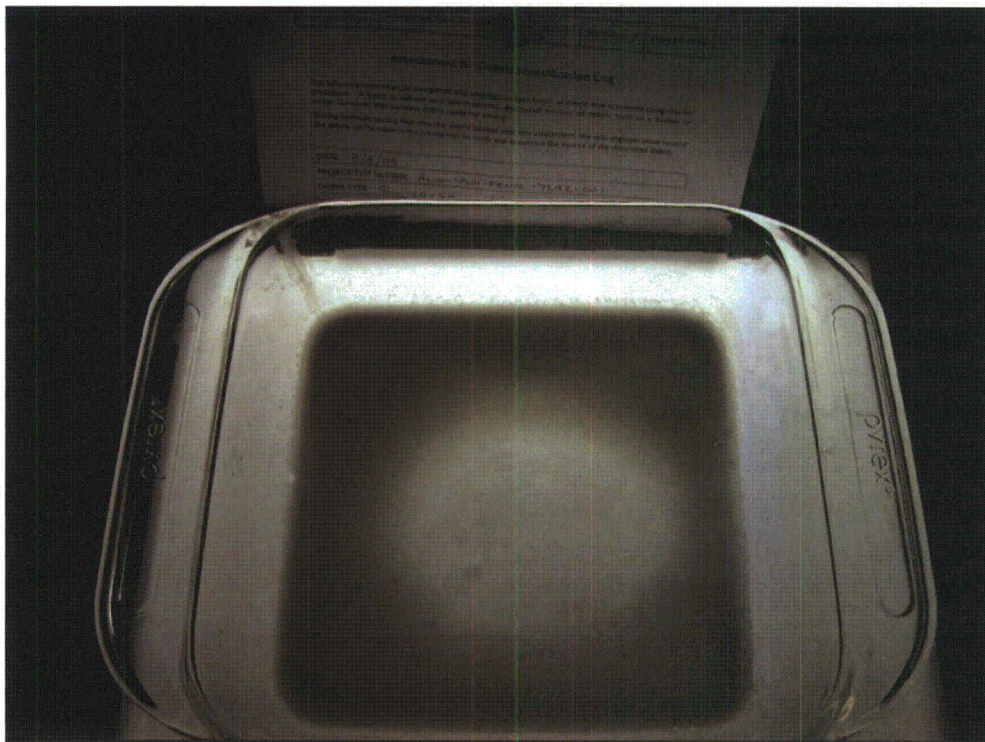


Figure 13-7, Particulate Detail

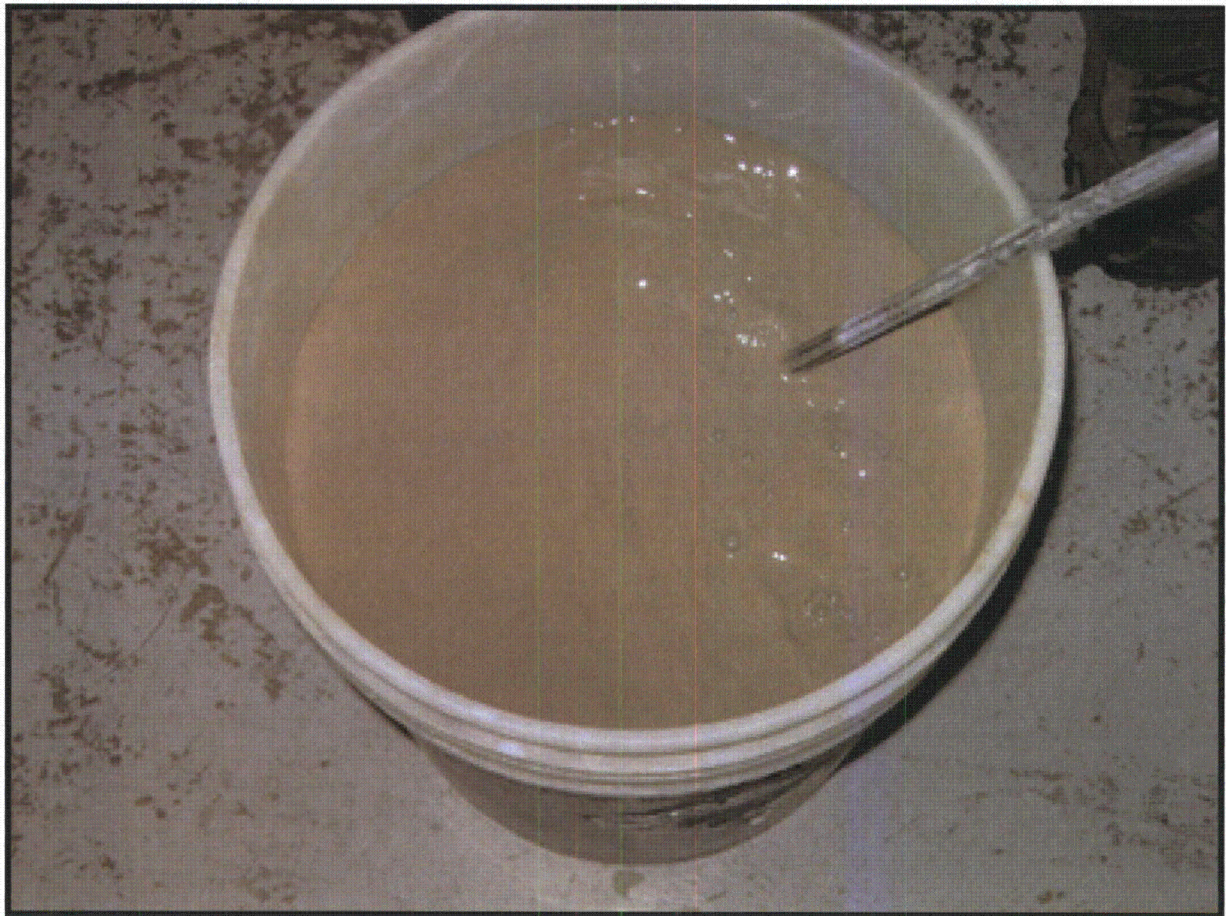


Figure 13-8, Microtherm<sup>®</sup> Slurry

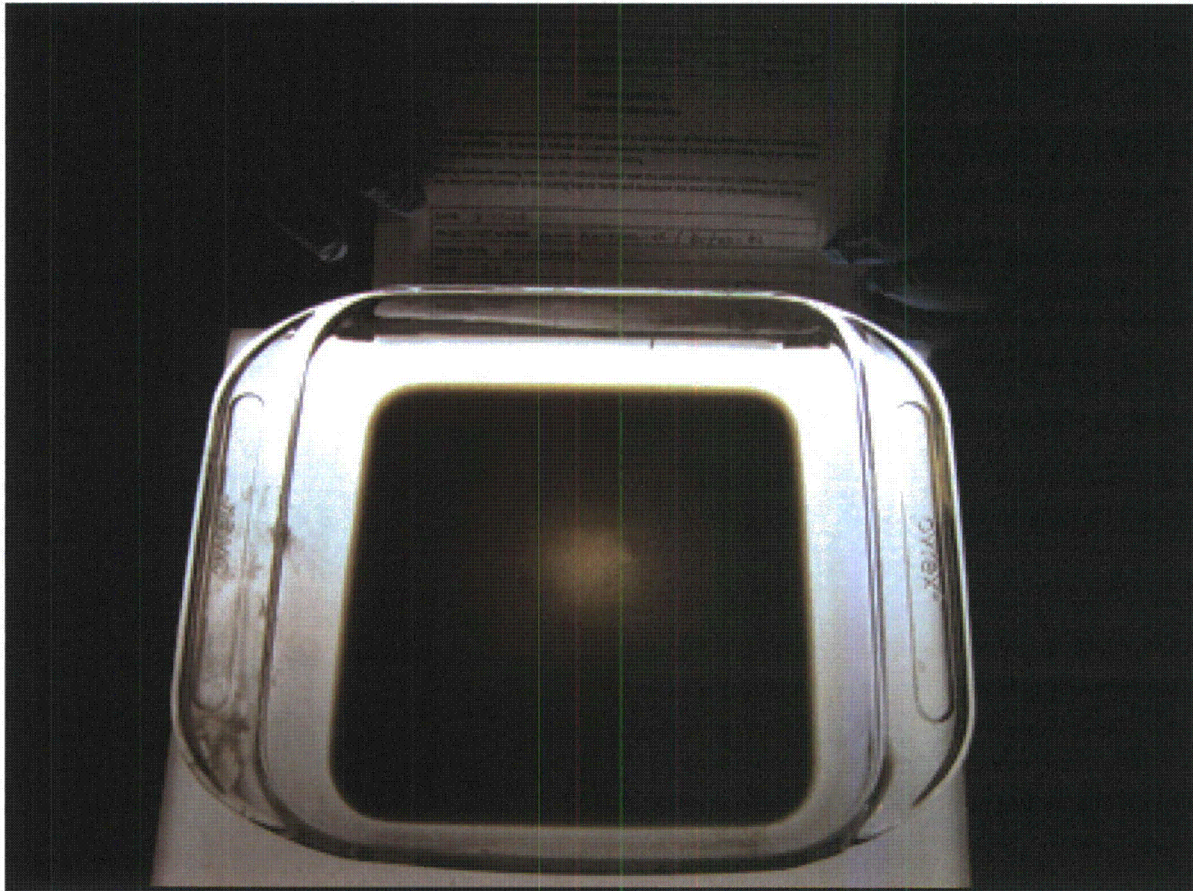


Figure 13-9, Microtherm® Detail

For the BVPS-1 and BVPS-2 prototype testing, a sparger system was installed on the return line to aid in the suspension of the debris within the water. All debris loads were added over the sparger. All debris loads (particulate debris, fibrous debris, and chemical precipitates) were added in two locations to maximize uniformity in debris distribution between the two sides of the strainer assembly (as shown in Figures 13-1 and 13-2). These methods of debris agitation were sufficient in keeping the debris suspended in the water; therefore, manual stirring was not conducted.

Section 3.o.2.15.i of the June 30, 2009 supplemental response notes that, "There was no insulation or chemical precipitate observed to have settled on the tank/flume floor for the BVPS-1 and BVPS-2 prototype testing. The only materials evidenced to have settled to the floor were some paint chips and dirt/dust. Due to the high average approach velocity utilized in the testing, and the sparger systems, the insulation and chemical debris remained suspended and deposited on the strainer array based on reported observations." Figures 13-10 through 13-14 show these results.



Figure 13-10, BVPS-1 Typical Debris After Draindown

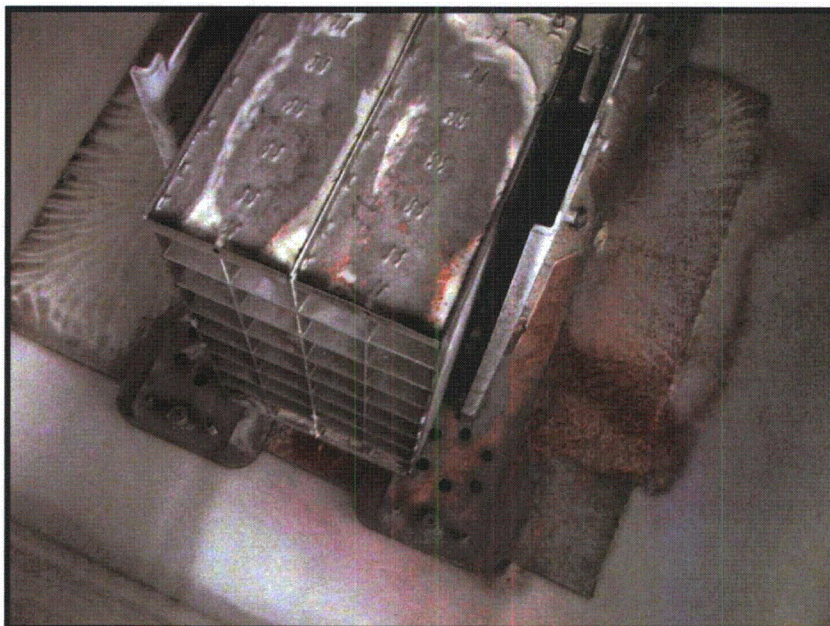


Figure 13-11, BVPS-1 Typical Debris After Draindown



Figure 13-12, BVPS-2 Typical Debris After Draindown (Test 1A)



Figure 13-13, BVPS-2 Typical Debris After Draindown (August 2009 Test 2)

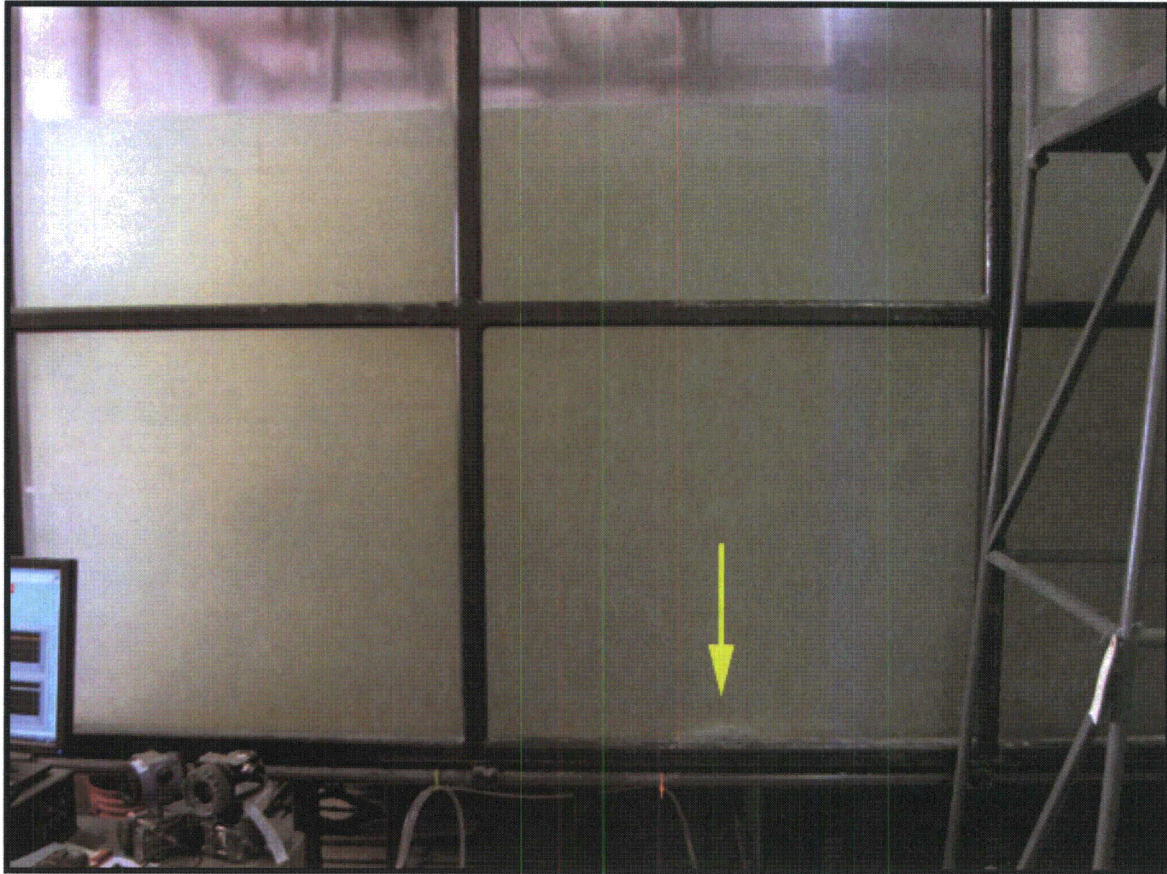


Figure 13-14, Example of Settled Debris (Paint Chips) During BVPS-2 Testing

All of the debris was prepared for testing using the same procedures and methodology as that for other Alion testing. Specifically, the Indian Point testing observed by the staff used the same debris preparation methodology. For that visit the staff noted in its trip report (Accession Number ML090500230) that:

The particulate surrogates, Temp-Mat™, and NUKON® were placed into 5-gallon buckets with water. There was sufficient water added to the debris to provide adequate dilution to prevent agglomeration...Each bucket of debris was then stirred with a drill driven paint mixer to mix the debris with the water. The debris water mixtures resulted in dilute heterogeneous slurries. The buckets were then poured into the test tank at two separate locations. The slurries were added to the test tank in an order such that a relatively homogeneous mixture resulted within the tank...When the debris was added to the large test tank it was apparent that it was well dispersed in the water and had not agglomerated in the bucket or when added to the tank...The silicon carbide and calcium-silicate were powdered and the dirt-dust mixture appeared to be reasonable. The debris preparation and addition appeared to meet the criteria established in the staff review guidance.

The debris settling is also affected by the approach velocity, a function of flow rate. The staff noted in a previous visit to the test lab to witness testing that "previous testing observed by NRC staff in the large test tank at Alion did not exhibit excessive settling of debris." (Reference ADAMS Accession No. ML071230203). As stated earlier in the response, for both the BVPS-1 and BVPS-2 prototype testing, the combination of the increased approach velocity and the sparger/mixer agitation performed well in order to keep the debris suspended in the fluid and prevent non-prototypical settling on the tank floor.

**RAI 14:**

**The particulate debris load added to the test included paint chips. The paint chips were added prior to the fine fibrous debris. This is not consistent with the March 2008 NRC staff guidance for head loss testing. Please provide information that justifies that the head loss test results were not affected non-conservatively by the debris addition sequence.**

**FENOC Response**

All of the head loss testing for BVPS-1 and BVPS-2 was performed after the March 2008 NRC staff guidance was issued. In accordance with the March 2008 NRC staff guidance, paint chips were used as a surrogate for unqualified coatings debris load because of the low fiber debris load and open screen area.

Section 6.1.2 of the March 2008 NRC staff guidance states the following: "The one consideration for plants that cannot generate a fibrous thin bed is that it may be more conservative to add coating debris as chips rather than particulate. For low-fiber plants, in the absence of a plant-specific evaluation on the characteristics of coating debris it may be necessary to test with paint chips. It may also be possible for plants to show that paint chips will not transport to their strainers, in which case it would be conservative to test with coatings as particulate. In general, the staff believes that testing with coatings as particulate will yield conservative head loss results. Unless there is significant bare screen, the staff will accept the treatment of coatings as particulate as conservative."

In accordance with the March 2008 NRC staff guidance, for additional conservatism, the unqualified coatings debris load was tested as fine particulate. For BVPS-1 Test 6, and BVPS-2 Test 1A, coatings were added as ground silica. The unqualified/chips were also added as paint chips for conservatism, because full fibrous debris screen coverage was not predicted.

The paint chips represented the unqualified coatings and, as such, were treated as a particulate with respect to the testing. Therefore, they were added prior to the fine fibrous debris similar to the other particulate debris loads. This methodology is in accordance with the March 2008 NRC staff guidance page 6, "Sequencing the debris for thin bed testing by adding 100 percent of the plant particulate load to the test flume and subsequently adding fibrous debris in incremental batches of an appropriate size is

an acceptable method for performing thin bed testing.” The paint chips are added for conservatism, to block any open screen area. For example, Figure 14-1 demonstrates the amount of potential open screen area for BVPS-2.

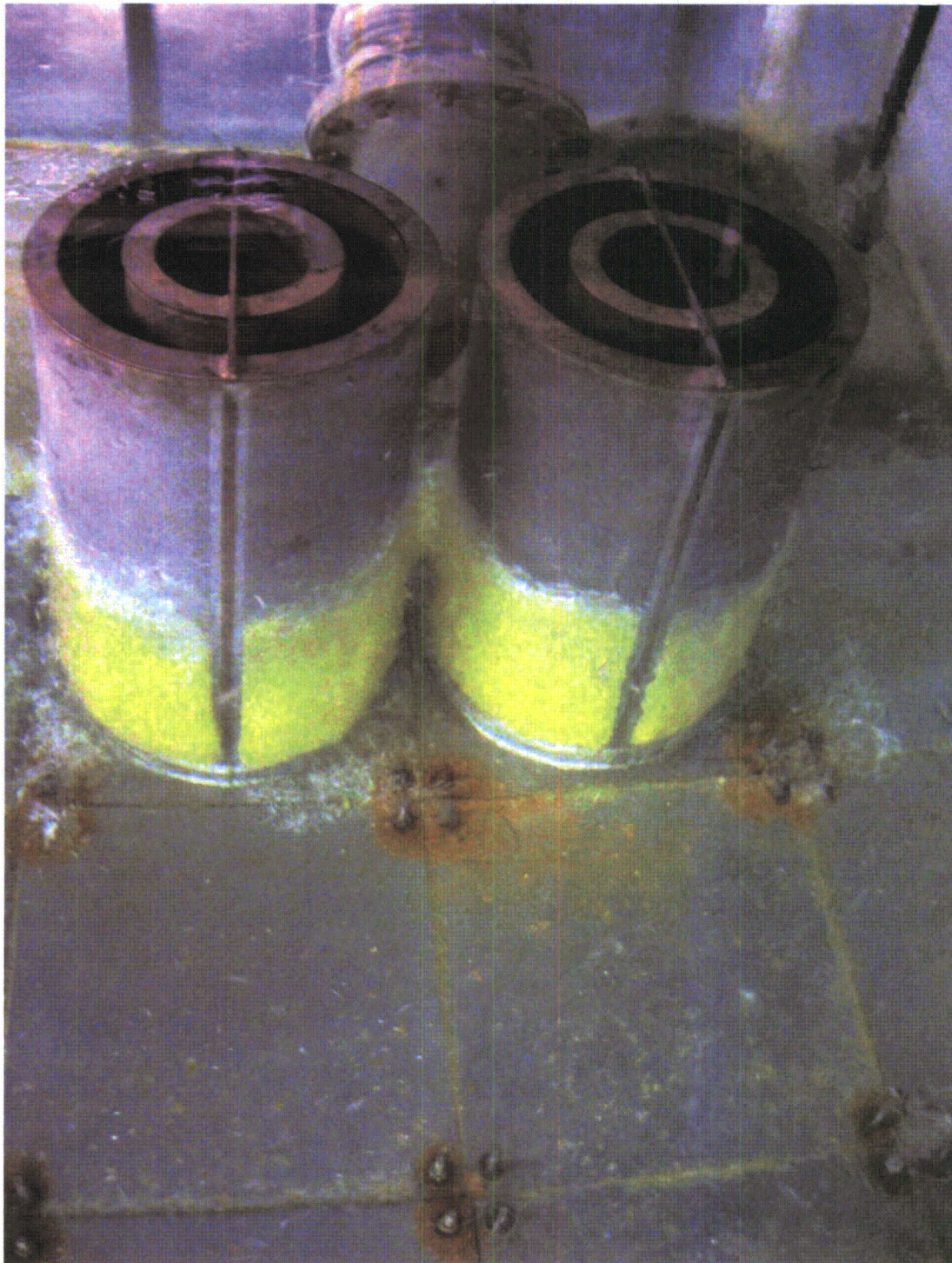


Figure 14-1, BVPS-2 Open Screen Area Example

To ensure the head loss test results were not affected non-conservatively by the debris addition sequence, several steps were taken for each test to ensure that all of the debris was properly diluted and suspended to prevent settling on the bottom of the tank.

Prior to the start of testing and in order to ensure the March 2008 NRC staff guidance was followed, a NRC Reviewer's Guide Checklist was implemented. The test specific plans and procedures were specifically written to satisfy the recommendations in the guidance. Some of the checklist highlights include:

The checklist specifically addressed debris settling in the agitation step:

Agitation was used in the form of a sparger on the return line in the tank, as well as two mechanical mixers, positioned to produce enough turbulence to help prevent particulate debris from settling on the bottom of the test tank. If any significant amount of particulate debris does settle on the bottom of the test tank, the particulate will be agitated by stirring manually. Shakedown testing was performed to verify that the agitation of the water did not prevent the debris bed from forming prototypically.

The particulate debris described in the step above specifically included paint chips.

For the BVPS-1 and BVPS-2 prototype testing, a sparger system was installed on the return line to aid in the suspension of the debris within the water. All debris loads were added over the sparger. All debris loads (particulate debris, paint chips, fibrous debris, and chemical precipitates) were added in two locations to maximize uniformity in debris distribution. These methods of debris agitation were sufficient in keeping the debris suspended in the water; therefore, manual stirring was not conducted.

Section 3.o.2.15.i of the June 30, 2009 supplemental response notes that:

There was no insulation or chemical precipitate observed to have settled on the tank/flume floor for the BVPS-1 and BVPS-2 prototype testing. The only materials evidenced to have settled to the floor were some paint chips and dirt/dust. Due to the high average approach velocity utilized in the testing, and the sparger systems, the insulation and chemical debris remained suspended and deposited on the strainer array based on reported observations.

Figure 14-2 is an example of the size of the settled debris pile described above.

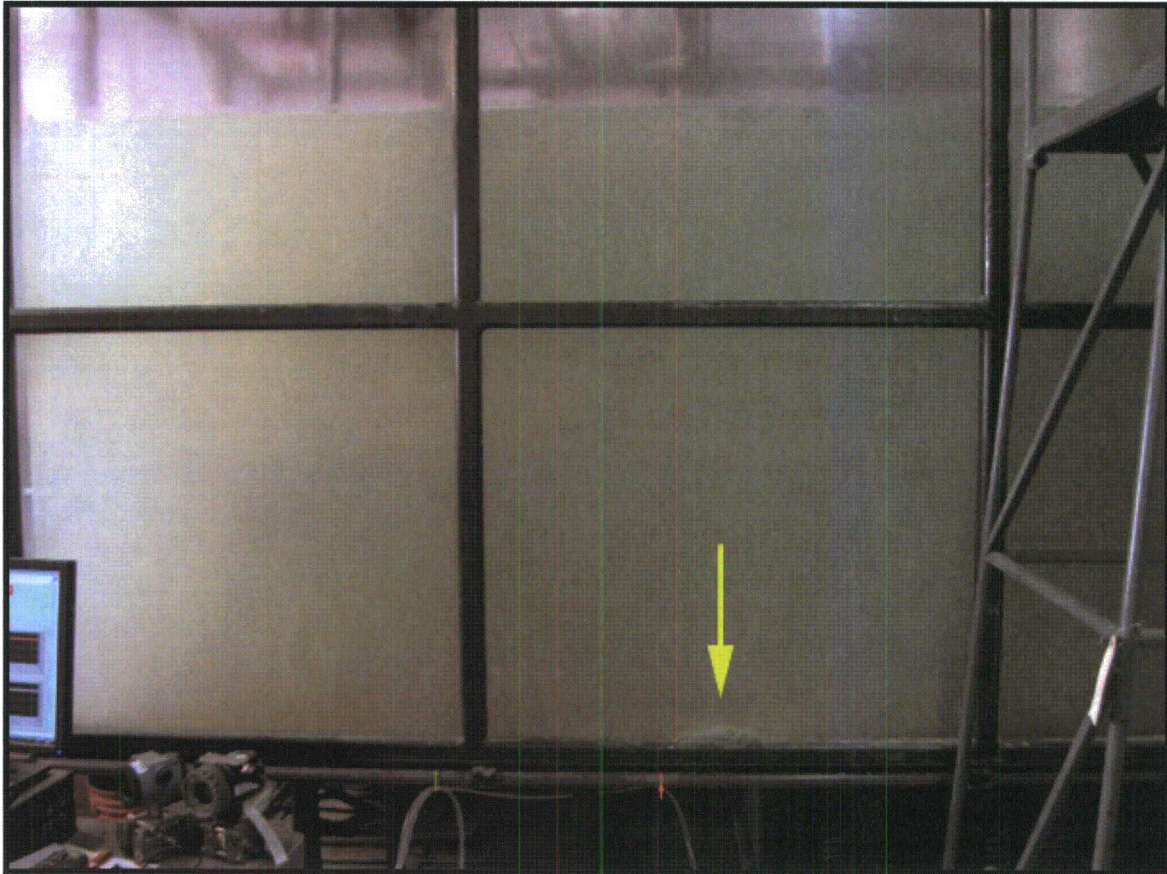


Figure 14-2, Example of Settled Debris (Paint Chips) During BVPS-2 Testing

**RAI 15:**

**The methodology for extrapolation of test results to higher temperatures was not understood by the NRC staff. Please provide the methodology and basis for extrapolation of the head loss test results to higher temperatures. Please state whether flow sweeps were conducted during testing to provide a basis for the extrapolations. Provide the relationship used to perform the extrapolations including the laminar and turbulent terms as appropriate.**

**FENOC Response**

During testing, flow sweeps were conducted after the addition of the total design basis debris load (for both non-chemical and chemical debris loads) and the stabilization criteria had been met.

The test temperature is not representative of the temperature that would be expected in containment; therefore, it is necessary to correct the test data for temperature.

The NUREG/CR-6224, "Parametric Study of the Potential for BWR ECCS Strainer Blockage Due to LOCA Generated Debris," correlation used to estimate the head loss through debris beds composed of fibrous and particulate debris, is given by the following equation:

$$\Delta H = \Lambda \left[ \underbrace{3.5 S_v^2 \alpha_m^{1.5} (1 + 57 \alpha_m^3) \mu U}_{\text{Laminar Term}} + \underbrace{0.66 S_v \frac{\alpha_m}{(1 - \alpha_m)} \rho U^2}_{\text{Turbulent Term}} \right] \Delta L_m \quad \text{Equation 1}$$

Where:

- $\Delta H$  = head loss (ft-water)
- $S_v$  = surface-to-volume ratio of the debris (ft<sup>2</sup>/ft<sup>3</sup>)
- $\mu$  = dynamic viscosity of water (lbm/ft/sec)
- $U$  = fluid approach velocity (ft/sec)
- $\rho$  = density of water (lbm/ft<sup>3</sup>)
- $\alpha_m$  = mixed debris bed solidity (one minus the porosity)
- $\Delta L_m$  = actual mixed debris bed thickness (in.)
- $\Lambda = 4.1528 \times 10^{-5}$  (ft-water/in.)/(lbm/ft<sup>2</sup>/sec<sup>2</sup>); conversion factor for English units.

The HLOSS computer code uses this equation and other inputs and iterations to estimate the head loss across perforated plates of flat screen and stacked-disks assemblies. Complex geometry screens cannot be directly modeled, because the debris bed thickness and fluid approach velocity vary for different parts of the strainer. Nonetheless, the correlation provides insights into how flow and temperature changes impact head loss even for these strainer designs.

The first part of this equation (proportional to viscosity and approach velocity) is the laminar head loss term, and the second part (proportional to density and approach velocity squared) is the turbulent head loss term. Knowing the relative proportion of the laminar and turbulent terms is important when making corrections for flow and temperature. The turbulent and laminar proportion can be determined in experimental measurements of head loss using flow sweep data, which involves measuring the head loss as a function of velocity.

Using the equation below, the measured head loss was corrected for changes in temperature.

$$\Delta H_2 = \Delta H_1 \left[ R_L \frac{\mu_2}{\mu_1} + R_T \frac{\rho_2}{\rho_1} \right]$$

Equation 2

Where:

- $R_L$  = ratio of laminar flow
- $\mu$  = dynamic viscosity at temperature (lbm/ft/sec)
- $R_T$  = ratio of turbulent flow
- $\rho$  = density at temperature (lbm/ft<sup>3</sup>)

The final flow sweep performed in each of the tests provides data relative to the flow regime through the debris bed, which is an important factor in correcting for temperature.

To calculate the corrected head loss at the desired temperatures, the viscosity and density of water at the desired temperature and test temperature of the particular test must be used. Furthermore, the head losses at temperatures higher than prescribed in the test plan may be adjusted to represent what the head losses would have been at the target temperatures. All adjustments can be used for comparison to NPSH requirements at those containment pool temperatures.

The measured head loss was corrected for changes in temperature using the laminar and turbulent ratios provided below.

Table 15-1, Laminar and Turbulent Ratios for BVPS-1 Test 6

Velocity	Laminar	Turbulent	Laminar Ratio	Turbulent Ratio
0.0105	0.6798	2.1786	23.8%	76.2%
0.0092	0.5992	1.6929	26.1%	73.9%
0.0079	0.5112	1.2322	29.3%	70.7%
0.0066	0.4291	0.8681	33.1%	66.9%
0.0052	0.3396	0.5437	38.4%	61.6%

Table 15-2, Laminar and Turbulent Ratios for BVPS-2 Test 1A

Velocity	Laminar	Turbulent	Laminar Ratio	Turbulent Ratio
0.0108	2.6650	3.9904	40.0%	60.0%
0.0094	2.3337	3.0600	43.3%	56.7%
0.0081	2.0149	2.2811	46.9%	53.1%
0.0069	1.7029	1.6294	51.1%	48.9%
0.0056	1.3867	1.0804	56.2%	43.8%

Table 15-3, Laminar and Turbulent Ratios for BVPS-2 August 2009 Test 2

Velocity	Laminar	Turbulent	Laminar Ratio	Turbulent Ratio
0.009813	3.1253	5.1890	37.6%	62.4%
0.009155	2.9157	4.5163	39.2%	60.8%
0.008200	2.6118	3.6239	41.9%	58.1%
0.007147	2.2762	2.7524	45.3%	54.7%
0.006123	1.9501	2.0203	49.1%	50.9%

The ratios are determined by plotting the flow sweep data, similar to the plot shown below in Figure 15-1. A curve is then fitted to the data points using Microsoft Excel. In this example, the curve fit yields the following equation:  $y = 34481x^2 + 247.73x - 0.1456$ .

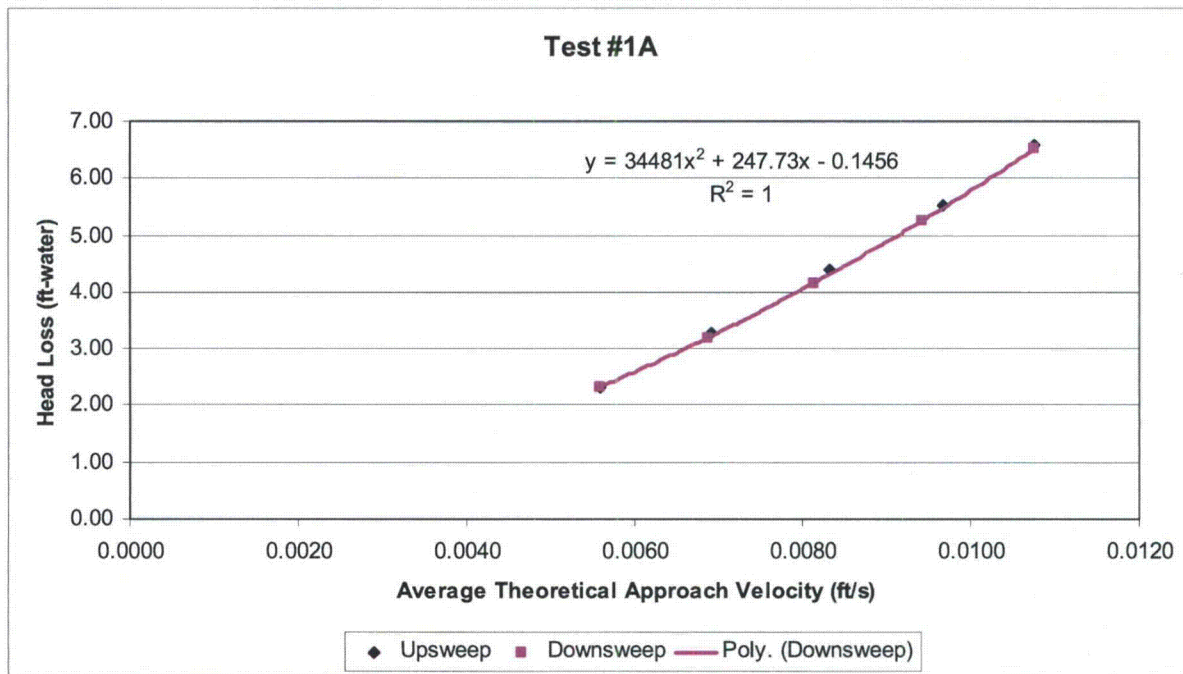


Figure 15-1, BVPS-2 Test 1A Final Flow Sweep Values, With Debris

**KEY**

Sweep Curve Fit Equation:  $y = Ax^2 + Bx - C$

Velocity	Laminar	Turbulent	Laminar Ratio	Turbulent Ratio
V	$L=B*V$	$T=V^2*A$	$=L/(L+T)$	$=T/(L+T)$

Once the laminar and turbulent ratios are determined using the above methodology, the head loss data is then adjusted. The temperature is adjusted from the maximum average test tank temperature at the end of the flow sweep to 65°F, 100°F, 150°F, 180°F, and 212°F for comparison to NPSH requirements at those containment pool temperatures. The viscosity and density water data is taken from standard engineering steam tables at the above temperatures.

The head loss test results for BVPS-1 Test 6 at an approach velocity of 0.0105 ft/sec, corrected for the temperatures, are shown in Table 15-4.

Table 15-4, Debris Bed Head Loss Corrected for Temperatures for BVPS-1 Test 6

Temperature (°F)	Density (lbm/cu.ft)	Viscosity (lbm/ft/sec)	Head Loss (ft-water)
65	62.33	7.04E-04	3.26
90 (test temperature)	62.14	5.14E-04	2.99
100	62.02	4.59E-04	2.91
150	61.20	2.95E-04	2.66
180	60.58	2.35E-04	2.55
212	59.85	1.90E-04	2.46

The head loss test results for BVPS-2 Test 1A at an approach velocity of 0.0108 ft/sec, corrected for the temperatures, are shown in Table 15-5.

Table 15-5, Debris Bed Head Loss Corrected for Temperatures for BVPS-2 Test 1A

Temperature (°F)	Density (lbm/cu.ft)	Viscosity (lbm/ft/sec)	Head Loss (ft-water)
65	62.33	7.04E-04	7.44
89 (test temperature)	62.15	5.20E-04	6.50
100	62.02	4.59E-04	6.19
150	61.20	2.95E-04	5.32
180	60.58	2.35E-04	4.98
212	59.85	1.90E-04	4.71

The head loss test results for BVPS-2 August 2009 Test 2 at an approach velocity of 0.009813 ft/sec, corrected for the temperatures, are shown in Table 15-6.

Table 15-6, Debris Bed Head Loss Corrected for Temperatures  
for BVPS-2 August 2009 Test 2

Temperature (°F)	Density (lbm/cu.ft)	Viscosity (lbm/ft/sec)	Head Loss (ft-water)
65	62.33	7.04E-04	9.19
100	62.02	4.59E-04	7.63
102 (test temperature)	62.00	4.52E-04	7.58
150	61.20	2.95E-04	6.53
180	60.58	2.35E-04	6.10
212	59.85	1.90E-04	5.76

NOTE: The above tables report head loss values at test termination.

**RAI 16:**

**The flow distribution used for the calculation of the BVPS-1 clean strainer head loss (CSHL) calculation was not provided. Because the strainer is a long train of modules, CSHL will be lower when there is no debris on the strainer. A conservative calculation would assume that the flow is balanced between all modules. For BVPS-2, a conservative assumption of uniform flow through each strainer module was assumed. Please provide the strainer flow distribution assumed for the BVPS-1 CSHL calculation.**

**FENOC Response**

The BVPS-1 strainer consists of two strings of two sided strainer modules. Each string has a central duct into which all of the filtered water flows. The strings of modules form a wye (see Figure 16-1) which ends with a duct that is connected to the suction box, which covers the inlets to the ECCS suction pipe inlets. String 1 contains four modules, numbered 1/1 to 1/4, and String 2 contains nine modules, numbered 2/1 to 2/9. The head loss through the strings of strainer modules is dependent on the flow distribution among the individual modules. The flow distribution is in turn dependent on the head loss through the debris bed. When the strainers are clean, the majority of the flow enters the central duct in the first few modules closest to the wye connection. When the strainers are laden with debris, the flow is much more evenly distributed among the modules.

The head loss through the strainer modules is separated into several parts as shown in Figure 16-1. These head losses are itemized below.

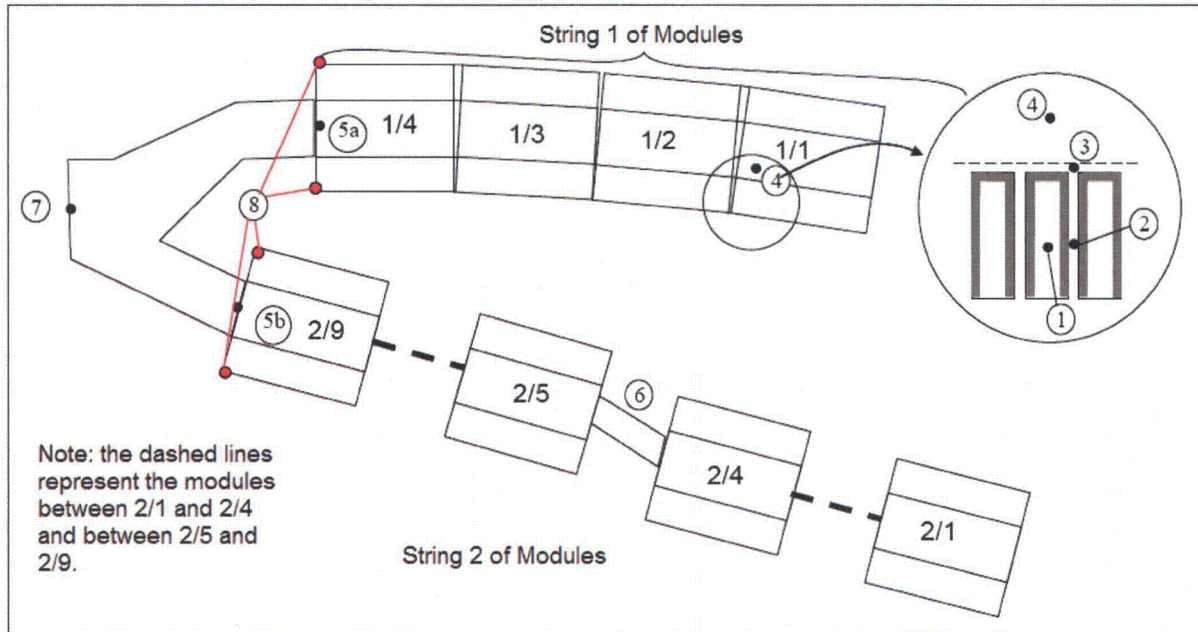


Figure 16-1, Head Losses in Strainer Modules

- a. The head loss between points 1 and 2 is the head loss across the strainer pocket. When the strainer is clean, this head loss is dominated by the hydraulic resistance of the perforated plate. This resistance is determined using correlations for perforated plates from *The Handbook of Hydraulic Resistance* by Idelchik. When the strainer is laden with debris, the head loss between points 1 and 2 is dominated by the hydraulic resistance of the debris bed. The debris bed resistance is determined using the results of the strainer vendor head loss tests.
- b. The head loss between points 2 and 3 occurs in the narrow channels that exist between the strainer pockets. Typically, the flow here is in the transition region between laminar and turbulent flow. The head loss in the narrow channels is determined as equivalent pipe flow with a conservative Moody friction factor of 0.04 based on values in Idelchik.
- c. The head losses between points 3 and 4 and between points 4 and 5a/5b are calculated with two different methodologies. In the first methodology, the central duct of the strainer modules is treated as a series of converging tees with straight flow along the central duct and branch flow entering the side of the duct from each module. Head loss correlations for converging tees from Idelchik are used to determine the hydraulic resistance for the central duct and side entrance of each module.

In the second methodology, the head loss of the central duct is calculated for linearly increasing flow along a square duct. The head loss is determined using pipe flow equations from Idelchik and a conservative Moody friction factor of 0.04. There are also flow restrictions between each module where the central duct temporarily narrows (point 6). The hydraulic resistance of these restrictions is determined using head loss correlations for an orifice found in Idelchik.

These two methodologies are conservatively added together for the total pressure loss in the piping. This is conservative because it increases the losses in the duct, which increases the percentage of the flow that will be drawn from the modules closest to the wye.

- d. The head loss between points 5a and 5b and the junction of the wye, point 7, is calculated as a converging tee using head loss correlations in Idelchik.

The hydraulic resistance correlations outlined in items a through d were determined for each module considered in the strainer strings. These resistance correlations were solved simultaneously to determine the flow distribution among the strainer modules and the head loss of each module.

For the clean strainer head loss (CSHL), when there is no debris bed, it is expected that most of the flow will go through the modules closest to the wye because the head loss will be dominated by losses in the ducts. In the BVPS-1 analysis, the flow was modeled as entering the closest two modules of String 1 and the closest three modules of String 2 (in Figure 16-1, these are modules 1/3, 1/4, 2/7, 2/8, and 2/9). To further refine the analysis, the module closest to the wye in each string was split into three sections. This allows the maximum pocket entrance velocity to be more accurately determined.

At the maximum flow rate of 14,500 gpm (0.9147 m<sup>3</sup>/s), String 1 has roughly 6770 gpm (0.427 m<sup>3</sup>/s) and String 2 has roughly 7720 gpm (0.487 m<sup>3</sup>/s). Of this total flow rate for String 1, ~6480 gpm (0.409 m<sup>3</sup>/s) enters module 1/4, and ~4410 gpm (0.278 m<sup>3</sup>/s) enters the closest third of module 1/4. For String 2, ~7200 gpm (0.455 m<sup>3</sup>/s) enters module 2/9 and ~4610 gpm (0.291 m<sup>3</sup>/s) enters the closest third of module 2/9. Modules 1/4 and 2/9 are adjacent to the wye joining the strings and are, therefore, nearest to the suction box.

The clean side head loss is also determined using the process outlined above. Note, the clean side head loss is different from the clean strainer head loss described above. The clean side head loss is the sum of all of the losses starting at the perforated plate and ending at the suction box, that is, all the losses aside from the debris bed head loss. When there is no debris, the clean side head loss is equal to the clean strainer head loss. Figure 16-2 shows the relationship between the clean side head loss and the debris bed head loss. The BVPS-1 design head loss calculation conservatively uses the maximum clean side head loss. Figure 16-3 shows the relationship between the clean side head loss and the normalized pocket entrance velocity. The normalized velocity is the ratio of the maximum pocket entrance velocity of any module to the

average pocket entrance velocity for all the modules. A normalized velocity of 1 signifies uniform flow across all of the modules. Per Figure 16-3, the maximum clean side head loss occurs at nearly uniform flow among all the modules.

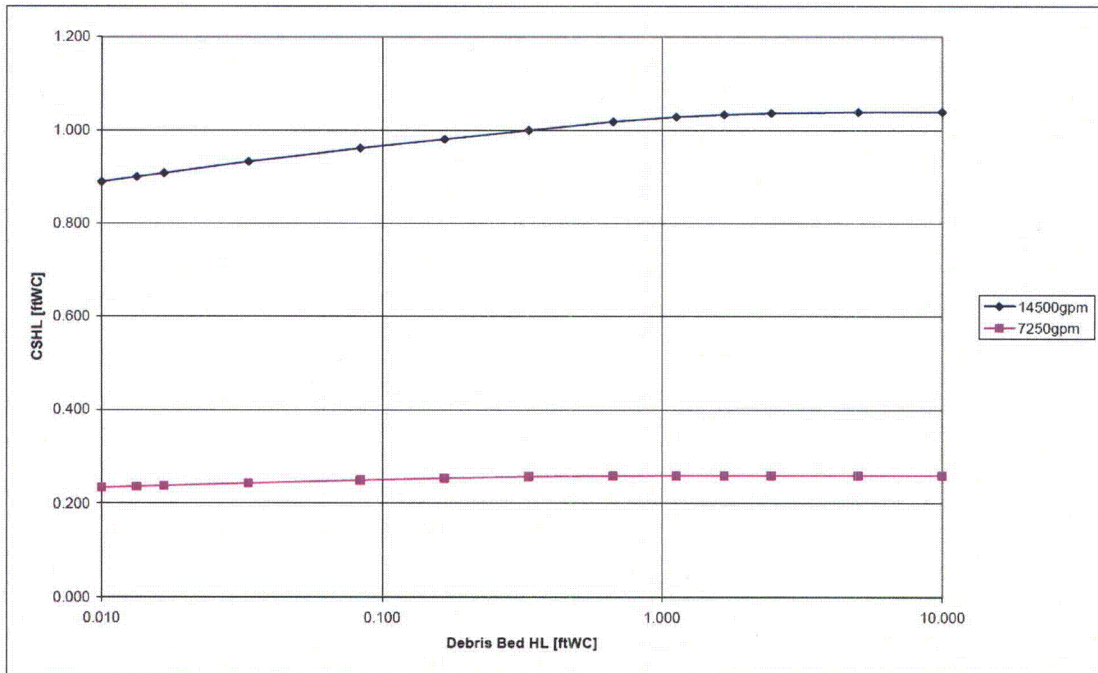


Figure 16-2, Clean Side Head Loss Correlation with Debris Bed Head Loss

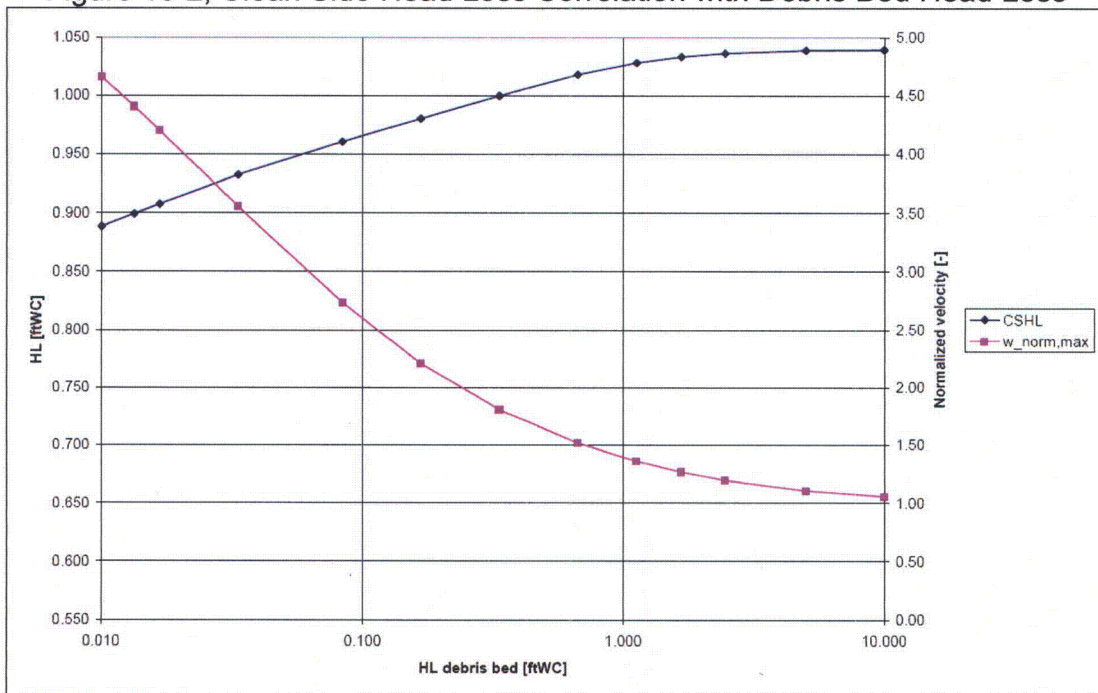


Figure 16-3, Normalized Pocket Entrance Velocity compared to Clean Side Head Loss

**RAI 17:**

**The height of the loop seal for the quench spray piping that penetrates the BVPS-1 strainer boundary was not provided. It was not stated how this loop seal is maintained full of water during all phases of a postulated LOCA response. Please provide additional details on the configuration of the loop seal and how it is ensured that the seal is maintained full of water throughout the mission time of the strainer.**

**Response:**

The configuration of the B train loop seal is shown in Figure 17-1 (A train is similar):

During normal operation, the quench spray (QS) piping is maintained full of water near the top of the loop seal. This ensures the loop seal is present at the beginning of a LOCA. When QS is in operation, the loop seal is maintained full by the flow that comes from the QS pump and supplies the spray ring, and direct injection into the recirculation spray (RSS) pump suction lines (inside the sump strainer waterbox). After the refueling water storage tank (RWST) is depleted and QS flow terminates, the loop seal remains full since it is sized to meet these conditions. After QS flow is terminated, a vacuum is drawn in the pipe downstream of the loop seal. The maximum pressure in the containment following QS termination is 8 psig (22.36 psia) based on the containment analyses. Additionally, emergency operating procedures require the operator to maintain containment pressure less than 8 psig. Therefore, the required height of the loop seal is  $(22.36 - 0 \text{ psia}) \times 144 \text{ sq in/ sq feet} / 62.4 \text{ lbm/ cubic feet} = 51.6 \text{ feet}$ . The actual loop seal piping heights are 55.7 feet on Train A to 54.7 feet on train B. The loop seal heights contain adequate margin to accommodate evaporation over the course of an operating cycle.

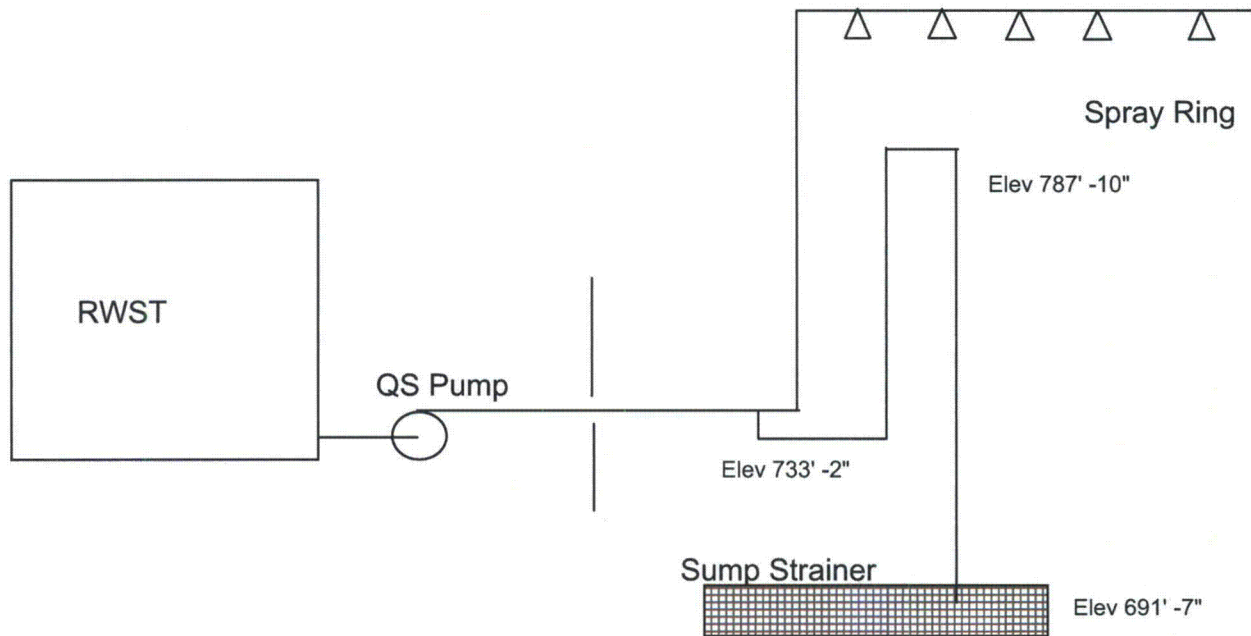


Figure 17-1, BVPS-1 Loop Seal Configuration

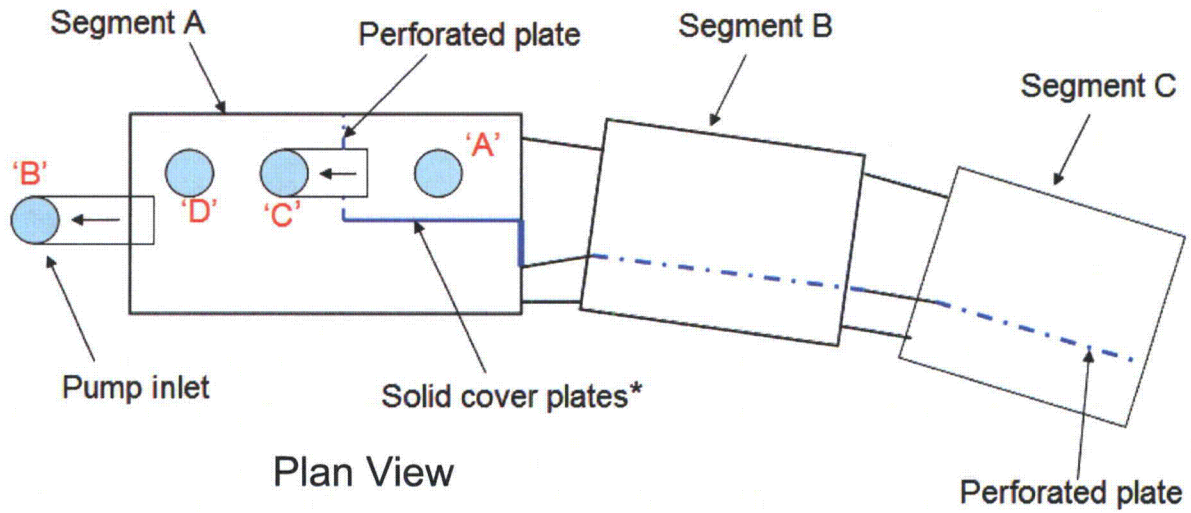
If a QS train fails to start, no flow occurs in the direct injection path to the sump and no vacuum is drawn. Under these no flow conditions, air will still exist downstream of the loop seal at the pressure inside the sump strainer. This pressure will only be a few feet less than the containment general static pressure and therefore this case is bounded by the case discussed above.

**RAI 18:**

**In Reference 1, it is stated that the BVPS-2 strainer is divided into two trains. The purpose for this feature was not provided. Please state the purpose of dividing the BVPS-2 strainer into an A and B train and discuss the effect that dividing the strainer into two trains has on strainer performance.**

**FENOC Response**

The BVPS-2 strainer initially was divided into two sections internally. This feature was carried forward from the original BVPS-2 strainer design into the new strainer. However, the new containment sump strainer is not subject to passive failure. Therefore, two strainer trains are unnecessary. As shown in Figure 18-1, the divider was mostly solid under Segment A of the strainer and had 14 gage perforated plates with 3/32 inch holes under Segments B and C.



\* Note: bolted cover plates were removed [8 total] in 2R14

Figure 18-1, BVPS-2 Strainer Segments

In 2009, when questions were raised during GL 2004-02 reviews at other utilities about possible blockage of the internal divider, it was determined that the divider could negatively affect strainer performance. To address this vulnerability, the solid cover plates in Segment A were removed during the 2009 BVPS-2 refueling outage (2R14).

Segment A of the strainer covers the recirculation pump suction. The divider plate hole covers within strainer Segment A have been removed. Removing these covers opened eight 9.125 inch diameter holes between the formerly separated strainer sections to allow full communication between the two sections of the strainer.

Under strainer Segments B and C, between the first and second rows of top hat strainers, the perforated plates remain. There is no need for water flow through the perforated plates because of the open holes in the A Segment.

**RAI 19:**

**The head loss graph, Figure 3.o.2.17-7 in Reference 1, shows that a flow sweep was conducted prior to the final debris addition and prior to the test reaching a stable value. Please provide the basis for this test sequence. Please provide information that justifies that the flow sweep did not affect the head loss result non-conservatively.**

**FENOC Response**

In the June 30, 2009 supplemental response, Figure 3.o.2.17-7 shows a supplemental debris addition after the flow sweep. The flow sweep was conducted after the total design basis debris load had been added (non-chemical and chemical debris loads) and

the stabilization criteria had been met. When the differential pressure across the debris bed changes by less than or equal to 1 percent over a 1-hour period the head loss is considered stable. The supplemental debris addition after the flow sweep represented an additional 10 percent chemical debris load which was added to the total design basis debris load to allow for increased margin.

Additionally, Figure 3.o.2.17-7 is applicable to BVPS-2 Test 5. At the time of the June 30, 2009 supplemental response, Test 5 represented the head loss for the reactor vessel nozzle break and bounded the maximum allowable Microtherm<sup>®</sup> debris load. However, as discussed in Appendix I of this RAI response attachment, BVPS-2 August 2009 Test 2 now represents the head loss for the reactor vessel nozzle break and bounds the maximum allowable Microtherm<sup>®</sup> debris load. Therefore, BVPS-2 Test 5 is superseded by the BVPS-2 August 2009 Test 2 and is no longer a design basis test.

Figure 19-1 provides the BVPS-2 August 2009 Test 2 Differential Pressure and Velocity Versus Time for the portion of the test when the flow sweep was performed following all debris additions.

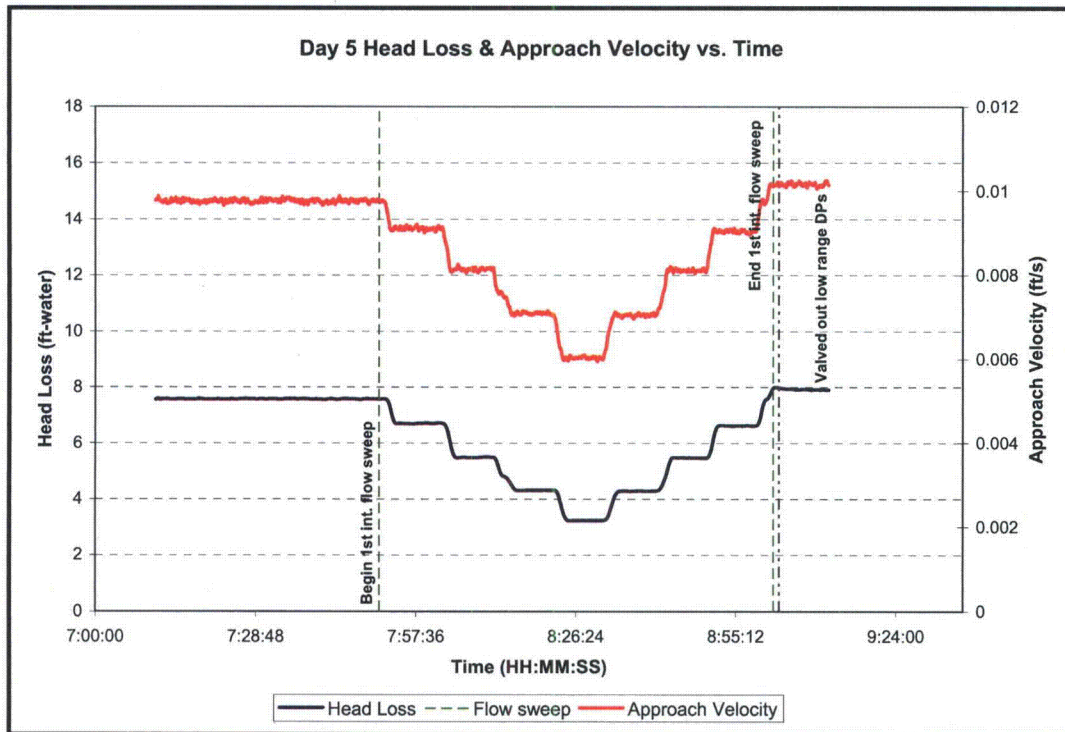


Figure 19-1, BVPS-2 August 2009 Test 2 Differential Pressure and Velocity Versus Time, Flow Sweep Portion

**Net Positive Suction Head (NPSH)**

**RAI 20:**

**Please provide the following additional information concerning water hold up volumes in containment:**

- a. Please clarify and provide the bases for the assumptions on the water hold up (volumes and quantities) at the time that the limiting minimum water level occurs in containment after the initiation of recirculation.**
- b. Please provide the basis for crediting the submerged volumes displaced by hollow components, such as the containment elevator, non-safety-related ductwork, and containment purge vents. Clarify whether these components are leaktight when submerged under post-LOCA conditions, and the difference this makes in the overall evaluation.**
- c. Although the NRC staff agrees that the 0.35-inch net level decrease from three holdup mechanisms not considered by the licensee (see response to item 3.g.10) would be minor for some of the analyzed scenarios, this level change represents over 15% of the 2.2-inch submergence credited for the limiting small-break LOCA for BVPS-1. Accordingly, please provide a basis for neglecting these hold-up volumes or else include them in the minimum water level calculation.**

**FENOC Response**

- a. Please clarify and provide the bases for the assumptions on the water hold up (volumes and quantities) at the time that the limiting minimum water level occurs in containment after the initiation of recirculation.**

The MAAP-DBA code is used to determine the amount of water hold up in the containment nodes and the RCS inventory released for small and intermediate break sizes, which are limiting for sump strainer submergence. An integrated primary system and containment model is used. This model tracks the amount of water contained and released from the RCS including the pressurizer. The accumulators will inject automatically in response to the RCS pressure. If partial or full injection occurs, this water will be available in the RCS and ultimately to the sump.

Water hold up in the containment nodal volumes is determined based on the characteristics of the junctions connecting to adjacent nodes. The junction specifications along with the nodal volume versus height characteristics contain the relevant information to calculate water hold up in each node as appropriate. For example, the refueling cavity must fill to the level of the cavity seal ring before water will flow into the reactor cavity. This is specified as a junction height above the bottom of the cavity. For other nodes where water can collect, the junction specifications characterize curb heights. Some nodes such as those in the upper dome have no means of holding up water, and this is reflected in the results. The model also accounts for the effects of head loss through junctions which may cause an additional increase in the level of water in a node and therefore affect the held up volumes. An example of

this is the junction that transports water from the reactor cavity to the sump area. An increase in the level and hold up mass of water in the reactor cavity occurs after the RSS pumps start due to the increased flow through the junction and resulting higher head loss.

The limiting case for containment sump strainer submergence is the break at the top of the pressurizer. The RSS pumps at BVPS-1 and BVPS-2 start on a level signal from the RWST coincident with a high-high containment pressure signal. The level setpoints for starting the RSS pumps are actuated when the RWST is approximately half empty. The minimum submergence occurs shortly after the Recirculation Spray pumps start as water is drawn from the sump to fill the RSS piping and spray rings. This is characterized as a small decrease in the sump inventory during this period as shown on Figures 20-1 and 20-2.

For BVPS-1, the minimum submergence occurs at approximately 5000 seconds for the 2-inch equivalent break size at the top of the pressurizer. Water is held up in those nodes in the containment where water can collect. As shown in Figure 20-1, the mass of water at this point in the containment sump is approximately 1.28E6 pounds (158,000 gallons). The water mass contained in the RCS at this point in time is approximately 172,000 pounds (21,800 gallons). The accumulators have not injected at this point and contribute nothing to the containment sump or RCS inventory. Of the total water mass held up in the containment, the majority is held up in the refueling and reactor cavities. These volumes contain approximately 260,000 pounds (32,100 gallons) at the point of minimum submergence. The total water held up in all containment nodes other than the sump at the point of minimum submergence is 299,300 pounds (36,900 gallons). As can be seen in Figure 20-1, the minimum submergence occurs before the RWST is empty and therefore, the mass of water in containment along with the sump inventory continues to increase following the point of minimum submergence.

For BVPS-2, the minimum submergence occurs at approximately 7500 seconds. The difference in timing is primarily due to the fact that the volume of the RWST at BVPS-2 is approximately twice that at BVPS-1. As shown in Figure 20-2, the mass of water at this point in the containment sump is approximately 2.62E6 pounds (322,000 gallons). Of the total water mass held up in the containment, the majority is held up in the refueling and reactor cavities. These volumes contain approximately 494,000 pounds (60,600 gallons) at the point of minimum submergence. The water held up in all nodes other than the sump is approximately 649,000 pounds (79,600 gallons) at the time of minimum submergence. The accumulators have injected approximately 17,299 pounds (2100 gallons) at this point in time. As can be seen in Figure 20-2, the minimum submergence occurs before the RWST is empty and therefore, the mass of water in containment along with the sump level continues to increase.

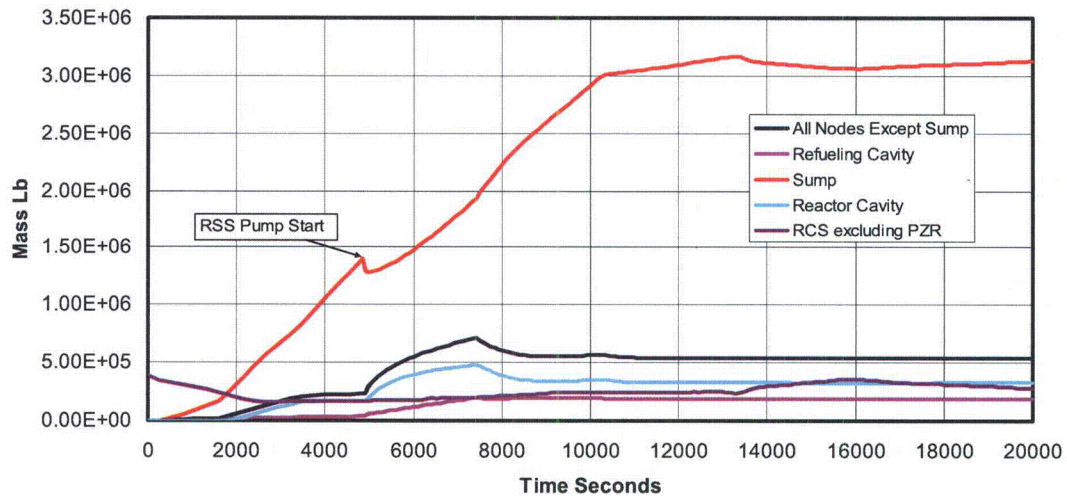


Figure 20-1 BVPS-1 Water Distribution in Containment

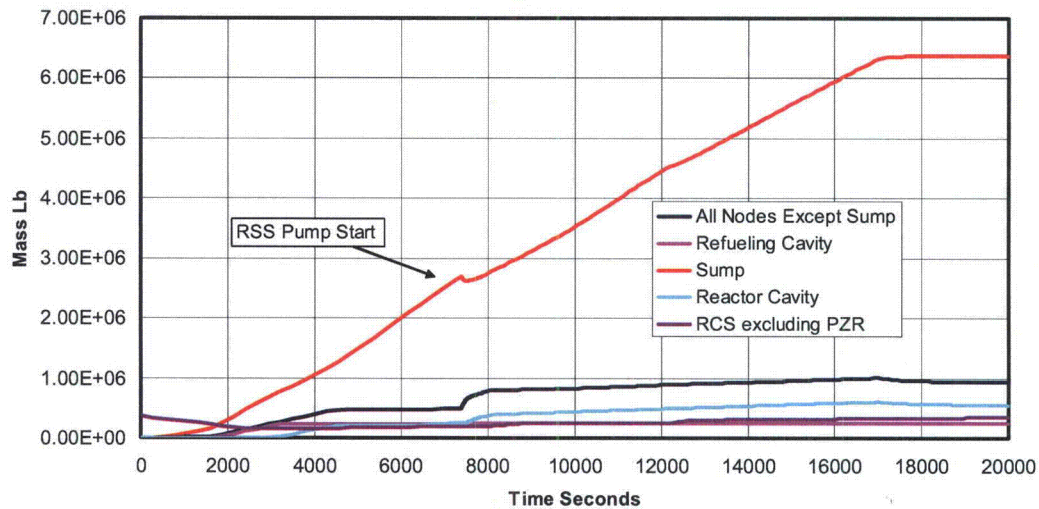


Figure 20-2 BVPS-2 Water Distribution in Containment

**b. Please provide the basis for crediting the submerged volumes displaced by hollow components, such as the containment elevator, non-safety-related ductwork, and containment purge vents. Clarify whether these components are leaktight when submerged under post-LOCA conditions, and the difference this makes in the overall evaluation.**

The response to Item 3.g.11 in the FENOC letter dated June 30, 2009 stated "For the lower containment above the sump, the displacement by the following objects are taken into account in calculating the net free volume at various heights by subtracting these

object volumes from the gross volume: reactor cavity (modeled as a separate node), keyway, keyway wall, cavity wall, floor support columns, crane wall support columns, miscellaneous concrete walls, accumulators, and miscellaneous equipment, Containment Air Recirculation fans and duct work, containment purge vents, containment elevator, structural steel, piping, and supports." Of these, the components which are considered hollow in terms of displacing water under accident conditions are the accumulators, Containment Air Recirculation fans and ductwork, the containment purge vents, the containment elevator, and various piping.

The accumulators are designed to meet ASME III requirements and function to inject water into the RCS following a LOCA. The vessels sit on the containment floor and are qualified to remain intact under accident conditions. Therefore, the volume displaced by these vessels is credited for calculating the level of water in the containment sump.

The Containment Air Recirculation fans and ductwork and the containment purge vents are not credited in the revised analysis to displace water volume for the purpose of calculating sump water level. The components are not considered safety-related. The Containment Air Recirculation cooling coils also sit on the containment floor. These are tube and fin type air cooling units which contain cooling water inside the tubes. The metal volume and internal tube volumes are credited for displacing water in the containment sump.

Portions of the containment elevator are credited for displacing water for the purpose of calculating containment sump level. The elevator structure rests on a base which consists of three concrete walls adjacent to the containment shell. This base extends approximately 4 1/2 feet above the containment floor. The elevator is accessed via a concrete ramp structure. The volumes associated with the concrete base and ramp structures are the only volumes credited for displacing water.

The various piping components are credited for displacing water for the purpose of calculating containment sump level. The piping volume is a relatively insignificant volume representing less than 0.14 percent of the total volume in the containment sump node and less than 0.5 inches of sump level.

Those submerged hollow components, which are not designed to be leak tight under accident conditions, such as non-safety related ducts, were excluded from the inventory of components which displace water in the containment sump area. This resulted in a change to the sump water volume versus height curve used in the MAAP-DBA containment model. This revised curve was utilized in re-analyzing all large and small break LOCA cases. The re-analysis also incorporated changes to the discharge coefficients for junctions connecting the refueling cavity to the reactor cavity, and the reactor cavity to the containment sump as described in the response to RAI 21. The re-analysis also incorporated changes to the limiting break size and location as discussed in the response to RAI 24 and included the net level decrease due to hold up mechanisms not considered as discussed in the response to RAI 20c. The net effect of

these changes on minimum strainer submergence and NPSH for BVPS-1 and BVPS-2 is shown in Tables 20-1 through 20-4.

- c. **Although the NRC staff agrees that the 0.35-inch net level decrease from three holdup mechanisms not considered by the licensee (see response to item 3.g.10) would be minor for some of the analyzed scenarios, this level change represents over 15% of the 2.2-inch submergence credited for the limiting small-break LOCA for BVPS-1. Accordingly, please provide a basis for neglecting these hold-up volumes or else include them in the minimum water level calculation.**

The effect of the net level decrease from three hold-up mechanisms not considered has been included in a re-analysis along with other changes as described in the response to RAI 20b. The results of this re-analysis in terms of containment sump strainer submergence and NPSH margin are shown in Tables 20-1 through 20-4.

Table 20-1, Minimum Sump Strainer Submergence	
Case	Submergence in Inches
BVPS-1 LBLOCA	4.65/6.68*
BVPS-1 SBLOCA	2.17/4.17*
BVPS-2 LBLOCA	10.07
BVPS-2 SBLOCA	8.87

\*The lower submergence value represents the submergence of the highest point of the sump strainer. The higher submergence value represents the submergence of the modules closest to the pump suction inlets which experience the highest initial flow at pump startup prior to debris build up on the strainer.

RSS CASE	Single Failure	Minimum IRS NPSHa <sup>1</sup>	Minimum ORS NPSHa <sup>1</sup>	Strainer HL	NPSHr	Minimum IRS Margin <sup>2</sup>	Minimum ORS Margin <sup>2</sup>
		Feet	Feet	Feet	Feet	Feet	Feet
1L-DEHL MIN SI	DG	24.0	22.2	0.65	12	11.3	9.6
1L1-DEHL MIN SI	LHSI	19.3	17.8	2.30	12	5.0	3.5
2L-DEHL MAX SI	None	19.1	17.7	2.30	12	4.8	3.4
3L-DEHL MIN SI	DG	23.7	22.6	0.64	12	11.1	9.9
4L-DEHL MAX SI	None	18.6	17.5	2.30	12	4.3	3.2
4L1-DEHL MAX SI	QS	21.5	21.3	2.24	12	7.3	7.1
6L-DEPS MIN SI	DG	18.6	19.1	0.63	12	5.9	6.4
6L1-DEPS MIN SI	LHSI	17.2	16.1	2.27	12	3.0	1.9
7L-DEPS MAX SI	CIB	17.1	16.5	0.64	12	4.4	3.9
7L1-DEPS MAX SI	QS	16.8	16.7	2.25	12	2.5	2.5
7L2-DEPS MAX SI	RELAY	19.3	18.0	0.64	12	6.6	5.3
7L3-DEPS MAX SI	None	17.6	16.8	2.25	12	3.3	2.6

LHSI Case	Single Failure	Minimum LHSI NPSHa <sup>1</sup>	Strainer HL	NPSHr <sup>3</sup>	Minimum LHSI Margin <sup>3</sup>
		Feet	Feet	Feet	Feet
6L-DEPS MIN SI	DG	15.8	1.06	12.2	2.5
6L1-DEPS MIN SI	LHSI	15.8	1.07	12.2	2.5
7L-DEPS MAX SI	CIB	20.8	1.50	9.5	9.8
7L1-DEPS MAX SI	QS	17.7	1.48	9.5	6.7
7L2-DEPS MAX SI	RELAY	17.2	1.50	9.5	6.2
7L3-DEPS MAX SI	None	18.0	1.50	9.5	7.0

- Notes: 1. Calculated NPSHa does not include strainer head loss.  
2. NPSH margin = NPSHa – Strainer HL – NPSHr  
3. The NPSHr value is reduced to 9.5 feet when two LHSI pumps are operating in parallel due to a reduced flow of approximately 2500 gpm per pump.

Table 20-4: BVPS-2 Minimum Recirculation Spray Pump Margin					
Case	Single Failure	Minimum NPSHa <sup>1</sup>	Strainer HL	NPSHr	NPSH Margin <sup>2</sup>
		Feet	Feet	Feet	Feet
1L-DEPS MIN SI	DG	21.6	0.97	18.3	2.3
1L1-DEPS MIN SI	SI	24.4	2.09	18.3	4.0
2L-DEPS MAX SI	CIB	26.2	0.99	18.3	6.9
2L1-DEPS-MAX SI	QS	26.1	3.16	18.3	4.6
2L2-DEPS MAX SI	RELAY	25.3	0.99	18.3	6.0
2L3-DEPS MAX SI	NONE	26.1	3.17	18.3	4.6
3L-DEHL	NONE	32.5	3.11	18.3	11.1
3L1-DEHL	QS	28.0	3.15	18.3	6.5
3L2-DEHL	RELAY	30.0	1.00	18.3	10.7
3L3-DEHL	CIB	27.0	0.98	18.3	7.7

Notes: 1. Calculated NPSHa does not include strainer head loss.  
2. NPSH margin = NPSHa – Strainer HL – NPSHr

**RAI 21:**

**Partial and/or total refueling cavity drain blockage could significantly affect the water hold up assumptions described in the supplemental response. Please provide the following information concerning water drainage from upper containment for BVPS-1 and 2:**

- a. The size and quantity of the reactor cavity ventilation openings.
- b. The opening size of the coarse grating over the BVPS-2 reactor cavity ventilation openings.
- c. The opening size of gaps on the side of the shielding below the BVPS-1 permanent reactor cavity seal.
- d. A discussion of the sizes and quantities of debris predicted to transport to the refueling cavity and reactor cavity.
- e. The basis for concluding that blockage of the drainage paths discussed above would not occur following a LOCA, including consideration of the case of a reactor vessel nozzle break potentially leading to significant quantities of debris in the reactor cavity.
- f. A description of whether the potential for partial/total blockage of these drain paths was considered in the dynamic containment water level model incorporated into the MAAP-DBA code.

## **FENOC Response**

Figures 21-1, 21-2, 21-3, 21-4, and 21-5 are provided as a visual depiction of the configuration for the BVPS-1 and BVPS-2 reactor cavities. As an introduction to the response to this RAI, the following flow path discussion is also provided for each unit.

### ***BVPS-1:***

Recirculation sump inventory that accumulates in the BVPS-1 refueling cavity flows through the reactor cavity and to the recirculation pool in the following manner (depicted by Figures 21-1 and 21-2). Flow inventory will first accumulate within the refueling cavity. Once refueling cavity inventory level exceeds the raised permanent refueling cavity seal ring (4.41-inch curb), water will flow into the reactor cavity through seven permanent reactor cavity seal ring ventilation openings. These openings are not obstructed by any cover during normal operation of the plant. Water then flows over the borated concrete supplemental neutron shielding ring and through several gaps that are provided to accommodate air flow and water flow through the reactor cavity. These gaps and the potential for debris to block these flow paths is further discussed in the specific RAI responses below. Water then continues to flow downward through the reactor cavity over the reactor coolant nozzles/piping and the neutron shield tank. The flow path continues between the reactor vessel RMI and the neutron shield tank down to the lower cavity. All accumulated inventory within the reactor cavity then flows through a 12 inch drain hole in the lower cavity wall (centerline of hole is approximately 28 inches above the floor) to the recirculation pool. This 12 inch drain hole in the cavity wall has no cross members or screens that would prohibit flow.

An additional available flow path exists along the reactor coolant piping as it passes through the concrete shield wall to the cubicles, once within the cubicles the inventory then drains to the containment basement and to the recirculation pool.

### ***BVPS-2:***

Recirculation sump inventory that accumulates in the BVPS-2 refueling cavity flows through the reactor cavity and to the recirculation pool in the following manner (depicted by Figures 21-3 and 21-4). Flow inventory will first accumulate within the refueling cavity. Once refueling cavity inventory level exceeds the raised permanent refueling cavity seal ring (4.78-inch curb), water will flow into the reactor cavity through six permanent reactor cavity seal ring ventilation openings. Hatch covers are installed over these ports during operation and consist of grating that allows air flow and water flow to freely pass (details are further discussed in the response to sub-item b). Water then flows past the outside surface of the borated supplemental neutron shielding surrounding the reactor vessel and Microtherm<sup>®</sup> insulation. The flow path continues through the RCS loop penetrations in the concrete shield wall to the cubicles. Once within the cubicles, the inventory then drains to the containment basement and to the recirculation pool.

The following is the response to the specific sub-items of this RAI:

**a. The size and quantity of the reactor cavity ventilation openings.**

Both BVPS-1 and BVPS-2 have openings in the permanent cavity seal ring to provide an air flow path from the lower portions of the reactor cavity as well as to pass water from the refueling cavity. These openings have the following attributes:

BVPS-1 – There are seven openings in the permanent cavity seal ring. Each opening has an approximate diameter of 24 3/4 inches. No cover is utilized during normal operation so blockage is not a concern at these locations.

BVPS-2 – There are six openings in the permanent cavity seal ring. Cavity seal ring safety covers are installed over these openings during normal operation which results in an effective opening of 23 1/4 inches. The covers consist of a coarse grating which allows air and water to readily pass through the grating without introducing any potential for blockage.

**b. The opening size of the coarse grating over the BVPS-2 reactor cavity ventilation openings.**

The coarse grating present over the BVPS-2 reactor ventilation openings is used as a personnel safety cover. This cover is a coarse mesh comprised of bars which are less than or equal to 0.75 inches spaced approximately 6.4 inches to 10 inches apart in one direction, and 2.75 inches in the other direction. Figure 21-6 provides information related to the configuration of these covers.

**c. The opening size of gaps on the side of the shielding below the BVPS-1 permanent reactor cavity seal.**

Approximately 8 inches below the permanent cavity seal ring is an additional ring used for neutron shielding. This is unique to BVPS-1. This ring has openings, which are aligned with some of the openings in the permanent cavity seal ring; however, plugs are installed in these openings during normal operation.

Figure 21-1 provides details on the gaps (in inches) present in the BVPS-1 reactor cavity. The limiting gap along the outer radius of the shield ring is 1.5 inches. The gap along the inner radius is 2 inches in the horizontal plane while there is an additional vertical distance of 1.5 inches (slight elevation difference from the reactor vessel flange), resulting in an approximate angular gap of 2.5 inches.

As shown in Figure 21-1, there are additional gaps in the neutron shield ring which provide additional paths for water to flow through the reactor cavity. These paths include the gap around the concrete plugs that are installed in the six (6) manway access openings as well as the gaps present at the interfaces of the shield ring segments. The total amount of area for these various flow paths around and through the neutron shield ring has been calculated to be approximately 23.5 square feet.

**d. A discussion of the sizes and quantities of debris predicted to transport to the refueling cavity and reactor cavity.**

For both BVPS-1 and BVPS-2, the events that present the greatest potential for debris blocking flow of water through the refueling cavity and subsequently through the reactor cavity include a reactor coolant system loop break and a break at a reactor vessel nozzle.

Blowdown transport fractions for debris blown to upper containment were presented in Table 3.e-1a of the June 30, 2009 supplemental response. Washdown transport fractions for debris which washes down to regions inside the secondary shield wall were presented in Table 3.e-4. However, washdown of debris specifically to the refueling cavity (and subsequently the reactor cavity) is only a portion of this total washdown to regions inside the secondary shield wall. The containment flow split determination concluded that for BVPS-1, 11 percent of containment spray and for BVPS-2, 11.5 percent of containment spray would flow through the refueling cavity.

Tables 21-1 and 21-2 provide the debris sizes and quantities for the materials that the debris generation and debris transport analyses identify as either transporting through the reactor cavity seal and into the reactor cavity (in the case of an RCS loop break) or is generated within the reactor cavity (in the case of a break at the reactor vessel nozzle). Both tables include values from latent and miscellaneous debris as well as dirt and dust that are expected to transport to the refueling cavity during these events.

Miscellaneous debris is comprised of tags, labels, and tape. The presence of miscellaneous debris is not uniform throughout the various elevations of the plant. The quantities of miscellaneous debris are based on a determination of the type and amount of debris that is present in the upper regions of containment and have the potential to transport to the refueling cavity. Washdown of the miscellaneous debris from upper containment to the reactor cavity is then subjected to the containment spray flow split between the refueling cavity and the rest of upper containment as discussed earlier.

Considering the washdown of debris from the refueling cavity to the reactor cavity for both units, the permanent cavity seal ring is at a slightly higher elevation than the cavity floor and introduces a curb which will reduce the amount of small and large debris that transports from the refueling cavity into the reactor cavity. However, to maximize the amount of debris at the strainer, the transport analysis accounted for all of the debris being transported into the reactor cavity. Therefore, all debris is conservatively assumed to transport over the curb. The values in Tables 21-1 and 21-2 reflect this information.

Table 21-1, BVPS-1 Debris in Refueling and Reactor Cavities

Reactor Loop Break		
Debris Type	Debris Size	Amount in Refueling Cavity
RMI	1/4"	14.74 ft <sup>2</sup>
	1/2"	69.27 ft <sup>2</sup>
	1"	71.67 ft <sup>2</sup>
	2"	87.61 ft <sup>2</sup>
	4"	6.24 ft <sup>2</sup>
	6"	4.53 ft <sup>2</sup>
	TOTAL	254.06 ft <sup>2</sup>
Cal-Sil	Fines	2.62 lbm
Coatings (Inside ZOI)	Fines	14.14 lbm
Coatings (Outside ZOI)	Fines	3.95 lbm
Dirt/Dust	Fines	9.04 lbm
Latent Fiber	Fines	0.66 ft <sup>3</sup>
Misc Debris		6.79 ft <sup>2</sup>
Reactor Vessel Nozzle Break *		
Debris Type	Debris Size	Amount in Reactor Cavity
RMI	1/4"	136.2 ft <sup>2</sup>
	1/2"	639.9 ft <sup>2</sup>
	1"	662.1 ft <sup>2</sup>
	2"	811.0 ft <sup>2</sup>
	4"	532.2 ft <sup>2</sup>
	6"	386.5 ft <sup>2</sup>
	TOTAL	3168.0 ft <sup>2</sup>
Coatings (Inside ZOI)	Fines	112.9 lbm
Coatings (Outside ZOI)	Fines	3.95 lbm
Dirt/Dust	Fines	9.04 lbm
Latent Fiber	Fines	0.66 ft <sup>3</sup>
Misc Debris		6.79 ft <sup>2</sup>

\* As discussed in RAI 2 for BVPS-1, fibrous material (Temp-Mat™) was previously identified on the reactor nozzles that had not been accounted for. This is not reflected in this table as the material is to be removed and replaced with RMI.

Table 21-2, BVPS-2 Debris in Refueling and Reactor Cavities

Reactor Loop Break		
Debris Type	Debris Size	Amount in Refueling Cavity
RMI	1/4"	23.8 ft <sup>2</sup>
	1/2"	112.1 ft <sup>2</sup>
	1"	115.9 ft <sup>2</sup>
	2"	142.0 ft <sup>2</sup>
	4"	12.3 ft <sup>2</sup>
	6"	8.9 ft <sup>2</sup>
	TOTAL	415.0 ft <sup>2</sup>
Temp-Mat™	Fines	0.10 ft <sup>3</sup>
	Small	0.22 ft <sup>3</sup>
Thermal Wrap	Fines	0.02 ft <sup>3</sup>
	Small	0.05 ft <sup>3</sup>
Damming Material	Fines	0.01 ft <sup>3</sup>
Cal-Sil	Fines	3.89 lbm
Coatings (Inside ZOI)	Fines	22.57 lbm
Coatings (Outside ZOI)	Fines	12.47 lbm
Dirt/Dust	Fines	10.97 lbm
Latent Fiber	Fines	0.81 ft <sup>3</sup>
Misc Debris		7.96 ft <sup>2</sup>
Reactor Vessel Nozzle Break		
Debris Type	Debris Size	Amount in Reactor Cavity
Microtherm®	Fines	303.0 lbm
Coatings (Inside ZOI)	Fines	84.4 lbm
Coatings (Outside ZOI)	Fines	12.47 lbm
Dirt/Dust	Fines	10.97 lbm
Latent Fiber	Fines	0.81 ft <sup>3</sup>
Misc. Debris		7.96 ft <sup>2</sup>

- e. **The basis for concluding that blockage of the drainage paths discussed above would not occur following a LOCA, including consideration of the case of a reactor vessel nozzle break potentially leading to significant quantities of debris in the reactor cavity.**

### **BVPS-1**

Blockage at the top region of the upper reactor cavity was evaluated because all containment spray water that sprays into the refueling cavity flows through the annular region between the reactor vessel and the refueling cavity floor. There is a seal flange over that annulus, but, as already stated, it has several large openings that will allow water to drain from the refueling cavity into the reactor cavity and on to the recirculation pool. Located several inches below the permanent cavity seal ring is a neutron shield ring that prevents radiation streaming through the annulus. As identified in Figure 21-1, the shield ring has a continuous gap around its inner and outer circumferences as well as intermittent gaps due to the segmented configuration of the shield ring itself. These gaps provide pathways for the flow of water in this region.

Although there is sufficient area for the flow of water, the size of the gaps are small enough that larger pieces of debris (2 inches and larger) have the potential to become trapped and reduce flow through the reactor cavity. Therefore, the potential for blockage of debris in the vicinity of the neutron shield ring was further evaluated.

### ***RCS Loop Pipe Break***

Table 21-1 provides a summary of the debris which transports through the refueling cavity and into the reactor cavity from a break of RCS loop piping. RMI and miscellaneous debris are the only types of debris that are larger than fines while the rest of the debris is fine sized and will readily transport through the cavity without holdup.

Because the miscellaneous debris is comprised of tags, labels, and tape, the size and shape of these items is such that most of the debris will readily pass through the gaps around the neutron shield ring. Approximately 2.5 square feet of miscellaneous debris, comprised of tape, paper tags and small plastic tags/labels have dimensions where there is a very low probability that the material could orient itself in a manner that would block flow through the gaps. Because there are free openings of 1.5 and 2.5 inches at the neutron shield ring outer and inner radii, it is very likely that the larger pieces of tape and paper label debris would not have sufficient strength to bridge the gap. However, conservatively assuming that the entire surface area of the remaining miscellaneous debris could obstruct the openings, the 4.35 square feet of plastic and metal debris would block only a very small amount of the approximately 23.5 square feet of gap area and does not present a flow blockage concern.

The RCS loop break analysis does account for debris reduction during blowdown and washdown resulting from holdup at various levels of grating. As previously stated, the values of RMI in Table 21-1 are those amounts of RMI debris, at the stated distribution of sizes, for transport to the refueling cavity. The permanent cavity seal ring is

configured in a way that water, and associated debris, must first rise over a curb prior to flowing into the reactor cavity. The velocities in the vicinity of the seal ring are not expected to be enough to provide for the transport of all debris deposited in the refueling cavity to the reactor cavity.

Though transport from the refueling cavity to the reactor cavity is expected to be reduced by the raised surface of the permanent cavity seal ring, the debris transport analysis still evaluates the impact if all the debris were to transport into the reactor cavity.

Because the smallest gap is 1.5 inches (the gap associated with the outer radius of the neutron shield ring), all 2-inch, 4-inch and 6-inch pieces of RMI are conservatively expected to remain in the region between the neutron shield ring and the permanent cavity seal ring. All other debris less than 2 inches passes through the gap and washes through the reactor cavity. As indicated by the debris amounts in Table 21-1, the 2-inch, 4-inch and 6-inch debris in the reactor cavity is 98.38 square feet. This amount of RMI equates to a volume of 1.48 cubic feet. The total volume of the region between the neutron shield ring and the permanent cavity seal ring is approximately 106.7 cubic feet. Given the large size and irregular shape of the remaining RMI debris, this small amount of debris could not collect in a manner that would provide significant resistance to water flow through the region and thus does not present a concern for flow blockage.

#### ***Break at Reactor Vessel Nozzle***

A break at a reactor vessel nozzle can blow RMI debris throughout the cavity, including the gaps attributed to the neutron shield ring configuration. Other openings in the reactor cavity region include all six RCS loop piping penetrations in the cavity wall as well as flow down through the lower cavity region past the inner radius of the neutron shield tank (refer to Figures 21-1 and 21-2 for more information).

Here again, the debris types from Table 21-1 that are larger than fines are RMI and miscellaneous debris. Though the miscellaneous debris is not generated from the break, washdown of some of the debris is a potential. As discussed in the RCS loop break discussion, if an RMI debris bed is not formed, the miscellaneous debris will not cause a blockage concern. However, in the presence of an RMI debris bed, it could collect on the debris, thus its contribution to the total quantity of debris is discussed further with the analysis of RMI. With regard to RMI, not all RMI debris will be blown to the upper portion of the cavity and directly to the neutron shield ring gaps. The area attributed to the neutron shield ring gaps was determined to be less than 37 percent of the total area where debris can be distributed. Therefore, as is applied during a break blowdown analysis, this same percentage of RMI is expected to blow toward the upper region of the cavity and potentially block the flow paths around and through the neutron shield ring. This results in an RMI debris load of approximately 1170 square feet of the 3168 square feet of RMI within the break ZOI potentially being deposited in the cavity region around and above the neutron shield ring.

The blockage analysis reduces the debris load by eliminating the 6-inch debris sizes as they are significantly larger than the largest gap (2.5 inches) along the inner circumference of the neutron shield ring. The blockage analysis continues to account for the load from the 4-inch pieces for conservatism and accounts for the smaller debris pieces by assuming they remain in the region even though these pieces can fall back out through the gaps. Eliminating the loading from the 6-inch RMI further reduces the load to approximately 1026 square feet.

This is a very conservative approach because the large majority of small pieces of RMI debris that might transport upwards during the initial blowdown would tend to wash back down into the RV nozzle region, leaving only the small amount of RMI foils that could wedge at "pinch points" in the annular gaps around the neutron shield ring. However, to evaluate the worst case potential for water holdup in the region above the neutron shield ring, the evaluation assumes that the debris trapped at the pinch points between the neutron shield ring and the reactor vessel and reactor cavity allows for the buildup of an RMI debris bed in the cavity region above the neutron shield ring. The pinch points that could allow the RMI debris bed to build up (See figure 21-1) are the 2.5 inch angular opening along the top inner radius of the neutron shield ring and the 1.5 inch opening along the top outer radius of the neutron shield ring.

A comparison of the equivalent volume of the RMI debris blown into the region between the neutron shield ring and the permanent cavity seal ring shows that the volume of the destroyed RMI (less than 16 ft<sup>3</sup>) is much smaller than the total volume of the region (107 ft<sup>3</sup>). This indicates that approximately 15 percent of the volume in this region is taken by the presence of the RMI, resulting in a loose RMI debris bed distributed across the surface of the neutron shield ring. Although this quantity of RMI is not expected to have much of an effect on the flow of water from the refueling cavity into the reactor cavity, further evaluation of the impact was performed.

The presence of RMI in a flowpath has the potential to produce a head loss (though industry experience has shown that the amount of RMI must be fairly high before head loss becomes a concern). One acceptable method of determining head loss comes from Equation 3.7.2-9 in NEI 04-07, "Pressurized Water Reactor Sump Performance Evaluation Methodology."

$$H_L = 0.108 * U^2 * (A_{RMI} / A_{Strainer})$$

Where:

$U$  = Approach Velocity

$A_{RMI}$  = Area of the RMI

$A_{Strainer}$  = Area of the strainer

For application of this equation to the determination of head loss in this region, it is necessary to determine an acceptable approach velocity. Given the flow path configuration where the water flows into the reactor cavity through the openings in the permanent cavity shield ring and then spreads throughout the subject region, an approach velocity was determined based on averaging the flow across the largest and

smallest flow paths, that is, across the area represented by the neutron shield ring or the area represented by just the gaps through and around the shield ring. Maximum accident condition spray flows into the refueling cavity were also integrated into the blockage analysis. This resulted in an average approach velocity of 0.343 ft/sec for use in the head loss analysis.

The head loss correlation is influenced by the area of the strainer (that is, the smaller the area, the higher the head loss). The strainer area for this analysis is represented by the minimum area which flow in this region can pass through. This area is the area of the gaps around and through the neutron shield ring (approximately 23.5 square feet).

The miscellaneous debris is introduced in a different manner than the RMI. The debris enters the region between the neutron shield ring and the cavity seal ring during washdown by the containment spray after the RMI has already been deposited in this region. The presence of the irregular surface of the RMI debris bed would prevent the miscellaneous debris from accumulating in direct proximity to the gaps between the neutron shield ring, reactor vessel and reactor cavity. Therefore, blockage of these gaps by miscellaneous debris is not credible. However, the miscellaneous debris has the potential to collect on top of the RMI debris bed distributed over the neutron shield ring. This results in the potential to increase the head loss across the RMI debris bed by increasing the approach velocity of the water flowing through the RMI debris bed. As discussed earlier, the approach velocity for the RMI debris bed is calculated based in part on the area of the RMI debris bed distributed over the surface of the neutron shield ring. The miscellaneous debris reduces the 164.24 square feet total area of the RMI debris bed exposed to water flow by 6.79 square feet. The average approach velocity calculation accounts for the reduced flow area of the RMI debris bed.

When the average approach velocity is applied to the equation, along with an RMI debris foil surface area of 1026 square feet and a strainer area of 23.5 square feet, the resultant head loss is approximately 6.6 inches at the maximum expected flow rate. The total height of the region between the permanent cavity seal ring and the neutron shield ring is approximately 8 inches. Therefore, the head loss resulting from the deposit of RMI in this region will not cause any additional hold up of water back into the refueling cavity nor will it preclude the adequate flow of water through the cavity during maximum accident condition spray flow conditions.

The other openings in the reactor cavity were also evaluated for blockage.

Gaps around the cavity wall penetrations: As shown by Figure 21-1, debris from a nozzle break can be blown through the reactor cavity wall penetrations for the reactor coolant loop piping. The insulation on the broken line, as well as on the piping on each side of the break, is expected to be blown out of the cavity area. The total gap area around the piping, with and without insulation, is more than adequate to pass debris and flow water from the reactor cavity to the recirculation pool.

Gap on the inner neutron shield tank surface: The gaps on the inner neutron shield tank surface are slightly larger than the gaps around the neutron shield ring but are small enough to preclude the flow of some larger pieces of debris. The impact from blockage of this flow path was evaluated in a similar manner as the gaps associated with the neutron shield ring, and it was also determined that the potential head loss from debris being blown into this gap (plus the additional pile up of debris washed down from the upper gaps to the top surface of the neutron shield tank) did not result in an unacceptable head loss or inventory hold-up. If the level of water held up above the top of the neutron shield tank reaches the openings in the cavity wall which contain the RCS piping, flow will exit the cavity through these openings and drain to the sump. This situation is more favorable for sump inventory considerations since less water is held up in the lower reactor cavity.

As evident from the BVPS-1 blockage analyses previously described, the potential for blockage is small and where blockage occurs, the resultant head loss does not result in water holdup beyond that already assumed in the containment analysis for minimum strainer submergence. The analysis was approached in a conservative manner whereby RMI debris was assumed to deposit in the pinch points at the neutron shield ring inner and outer radii, forming a debris bed above the shield ring, without crediting the likelihood that the smaller debris sizes would transport down through the gaps. Even when approached in this manner, that is, maximizing the potential for debris loading and associated blockage, the ability to flow water through the reactor cavity and to the recirculation pool is maintained.

### **BVPS-2**

The physical configuration of BVPS-2 differs from BVPS-1 as a result of BVPS-2 not having a neutron shield ring in the upper reactor cavity just below the permanent cavity seal ring (see Figures 21-3, 21-4). Therefore, the potential for blockage of this flow path is greatly reduced.

The blowdown of RMI from an RCS loop pipe break results in RMI debris being transported to the refueling cavity and into the reactor cavity. As was the case for BVPS-1, a curb is also present in the BVPS-2 permanent seal ring configuration that will also greatly reduce the potential for RMI debris to transport into the reactor cavity. The lower cavity above the neutron shield tank then becomes the primary point at which debris may collect.

The quantity of RMI, plus the quantity of miscellaneous debris washed down by containment spray, determined to transport to the reactor cavity and potentially be held up above the neutron shield tank is identified in Table 21-2. The quantity of debris is not enough to preclude the flow of water through the cavity wall openings where the RCS piping penetrates the cavity.

A break in a BVPS-2 reactor vessel nozzle does not present a potential for blockage as it did in BVPS-1. As shown in Figure 21-3, the configuration of the neutron shield is different in that it is installed in a cylindrical shape around the vessel rather than below

the permanent cavity seal. As presented in Table 21-2, the only materials within the ZOI for a nozzle break are Microtherm<sup>®</sup> and other fine debris. The Microtherm<sup>®</sup> is installed along the upper reactor vessel behind the supplemental neutron shield. Failure of this Microtherm<sup>®</sup> is not expected to interfere with flow through the cavity wall openings where the RCS piping penetrates the cavity. Therefore, the cavity wall openings provide the necessary flow path from the refueling cavity through the reactor cavity and to the recirculation pool. Additionally, a breach of the neutron shielding would allow water to flow through the gap between the neutron shield tank and the reactor vessel insulation to the lower reactor cavity. Water in this area will drain to the containment sump through the drain hole shown in Figure 21-5.

**f. A description of whether the potential for partial/total blockage of these drain paths was considered in the dynamic containment water level model incorporated into the MAAP-DBA code.**

As described in the response to RAI 21e, there is a potential for debris to partially block the drainage gaps in the reactor cavity for BVPS-1. As discussed, the primary debris of concern is RMI from the reactor vessel due to a nozzle break. The calculated head loss as stated in the response to RAI 21e is expected to be small, that is, approximately 6.6 inches at the maximum expected flow. The effects of this blockage have been considered in a re-analysis along with other changes as noted in the response to RAIs 20 and 24. The following discussion provides the details of the methodology for evaluating the effects of the potential blockage of the reactor cavity flow paths.

The MAAP-DBA model for BVPS-1 characterizes the containment as 18 nodal volumes. Connecting the nodal volumes are junctions that are defined by a flow area, orientation, elevations relative to the adjacent nodes, and a discharge coefficient that characterizes the pressure drop in response to liquid or vapor flow. The flow paths which are involved in this discussion are the junction connecting the refueling cavity to the reactor cavity primarily and the junction connecting the reactor cavity to the lower compartment or sump area.

In order to evaluate the effects of blockage through the junction connecting the refueling cavity to the reactor cavity for BVPS-1, a discharge coefficient was calculated that includes the effects of head loss due to form losses through the seal ring openings, the RMI debris head loss and the form losses associated with the gaps surrounding the neutron shield ring. These three head loss terms were determined individually and grouped in series represented by one junction loss term. This is conservative since it was determined that the head loss associated with the gaps around the neutron shield ring and the RMI debris above the shield ring are not high enough to raise the water level in this area above the openings in the shield ring. By grouping these loss terms together in one coefficient, the water is forced to hold up in the refueling cavity above the seal ring. Since this node has a much higher cross sectional area than below the seal ring, the volume of water held up is overstated relative to what can be held up in the volume between the seal ring and the shield ring. Figures 21-1 and 21-2 contain a representation of this concept.

The effect of the increased loss coefficient for this junction is to increase the amount of water held up in the refueling cavity, which decreases the amount of water available to the sump. Additionally, the loss coefficient associated with the junction between the reactor cavity and the sump area was recalculated based on the removal of personnel barriers from the 12-inch drain hole located in the lower cavity wall, which were in the form of coarse grating. This change lowered the head loss associated with this junction, which has the effect of lowering the amount of water held up in the reactor cavity and results in an increase in sump level. The net effect of these changes along with the other changes incorporated can be seen in Tables 20-1 through 20-3, which provide the minimum submergence and NPSH results.

Once the water drains from the refueling cavity into the upper reactor cavity, two flow paths are available to reach the containment sump. The first flow path is through the gap between the neutron shield tank and the reactor vessel insulation. The second flow path is through the openings in the reactor cavity wall which contain the RCS piping. If the neutron shield tank gap becomes partially or fully blocked by debris, the water will flow out of the RCS loop piping penetrations through the cavity wall. The limiting minimum sump inventory analysis for those breaks where debris may be present in the reactor cavity assumes limited or no blockage of the neutron shield tank gap such that all flow goes to the lower reactor cavity via this path. This case is more limiting due to the additional water held up in the lower reactor cavity, which is caused by the relatively small size of the drain hole in this area.

For BVPS-2, no additional head loss in the reactor cavity flow paths was considered since the potential for blockage is minimized by the configuration as described in the response to RAI 21e. Similar to BVPS-1, the limiting case for minimum sump inventory for those breaks where debris may be present in the reactor cavity assumes all flow passes through the gap between the neutron shield tank and the reactor vessel insulation. At BVPS-2, for this to occur, a breach of the neutron shielding must also occur. Again, this is more conservative than a case where all flow exits the reactor cavity through the RCS loop piping penetrations due to water hold-up in the lower reactor cavity. An adjustment was made to the loss coefficient for the junction connecting the reactor cavity to the sump area based on the removal of the coarse grating from the 12-inch drain hole located in the lower cavity keyway wall, similar to BVPS-1.

The limiting sump strainer submergence case for both BVPS-1 and BVPS-2 is a 2-inch equivalent break on the top of the pressurizer. For this break, no debris blockage of the reactor cavity flow paths is postulated since the break is relatively small and the pressurizer cubicle is a contained volume with limited paths available for flow to the reactor cavity. The debris loss term described above for BVPS-1 is based on the debris generation associated with a large nozzle break and has been conservatively applied to nozzle and loop breaks of all sizes considered.

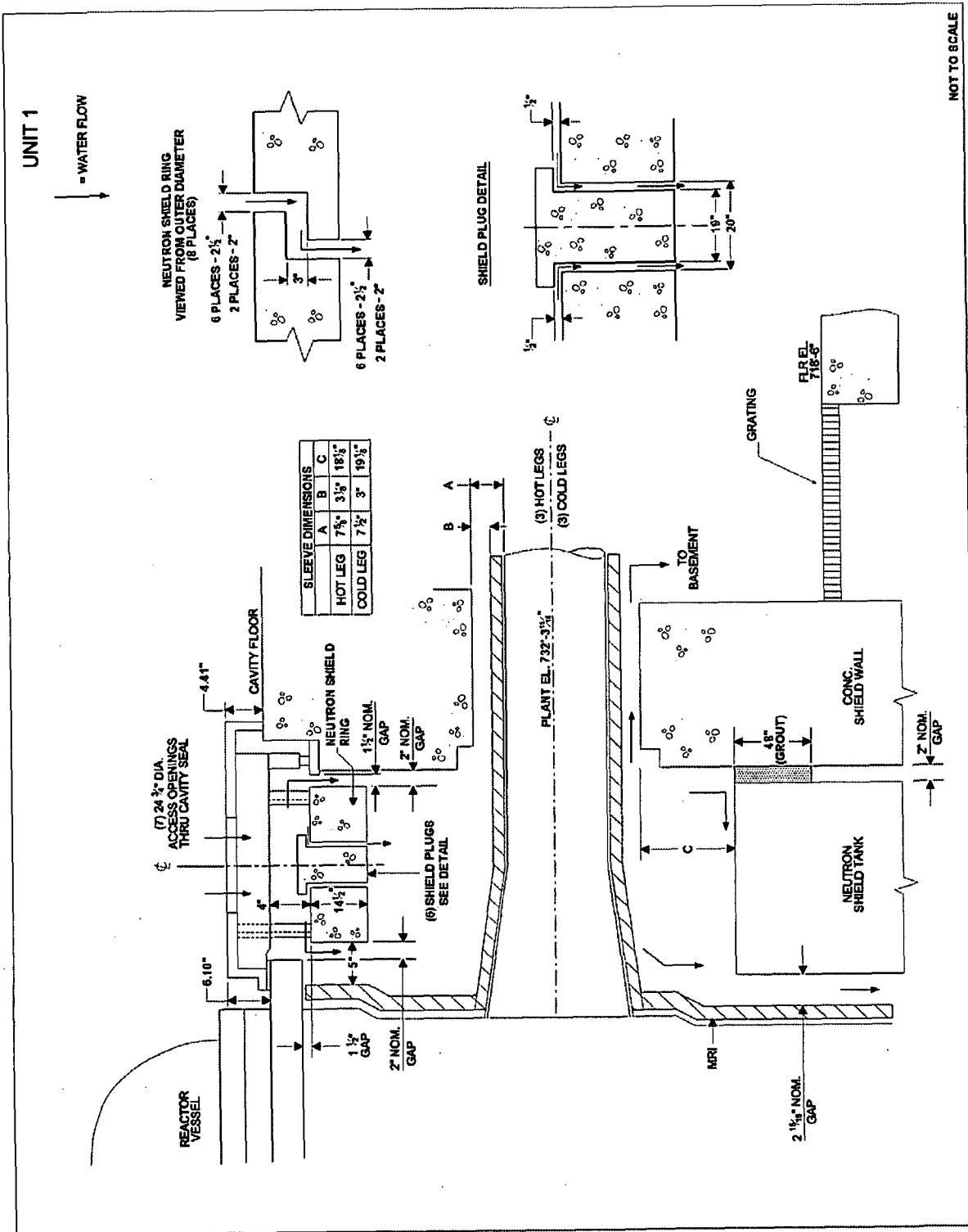


Figure 21-1, BVPS-1 Reactor Cavity Configuration

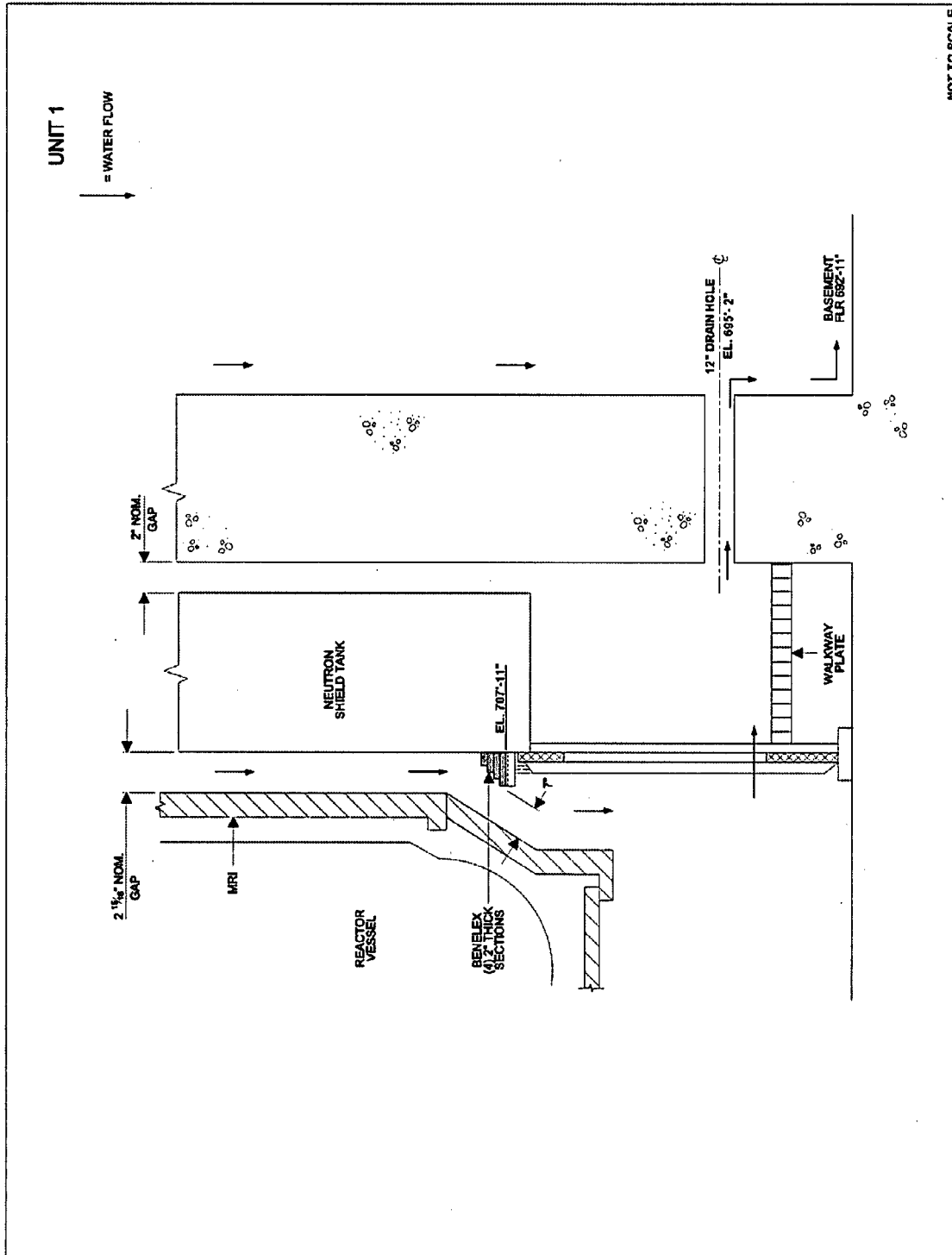


Figure 21-2, BVPS-1 Reactor Cavity Configuration (Lower Cavity)

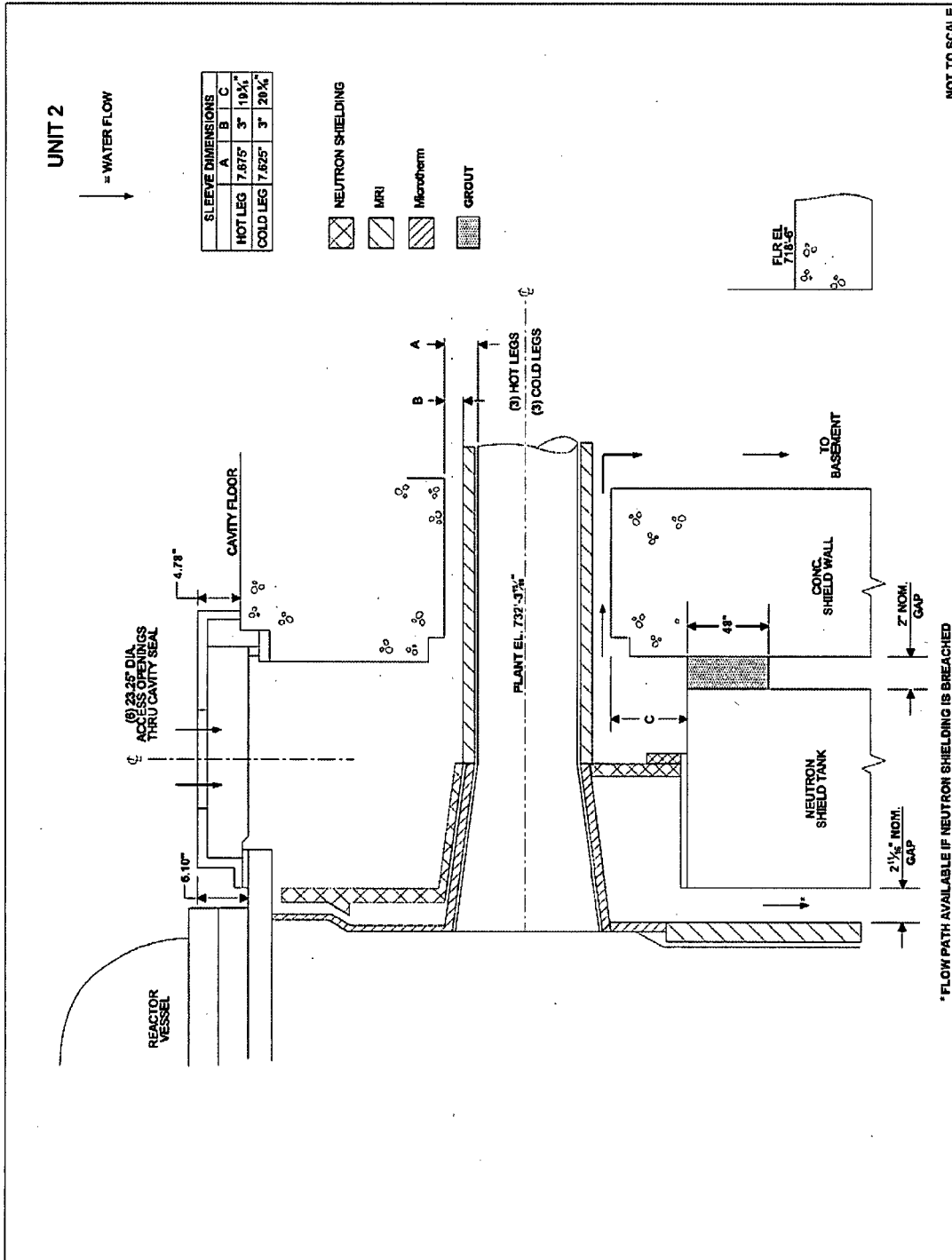


Figure 21-3, BVPS-2 Reactor Cavity Configuration

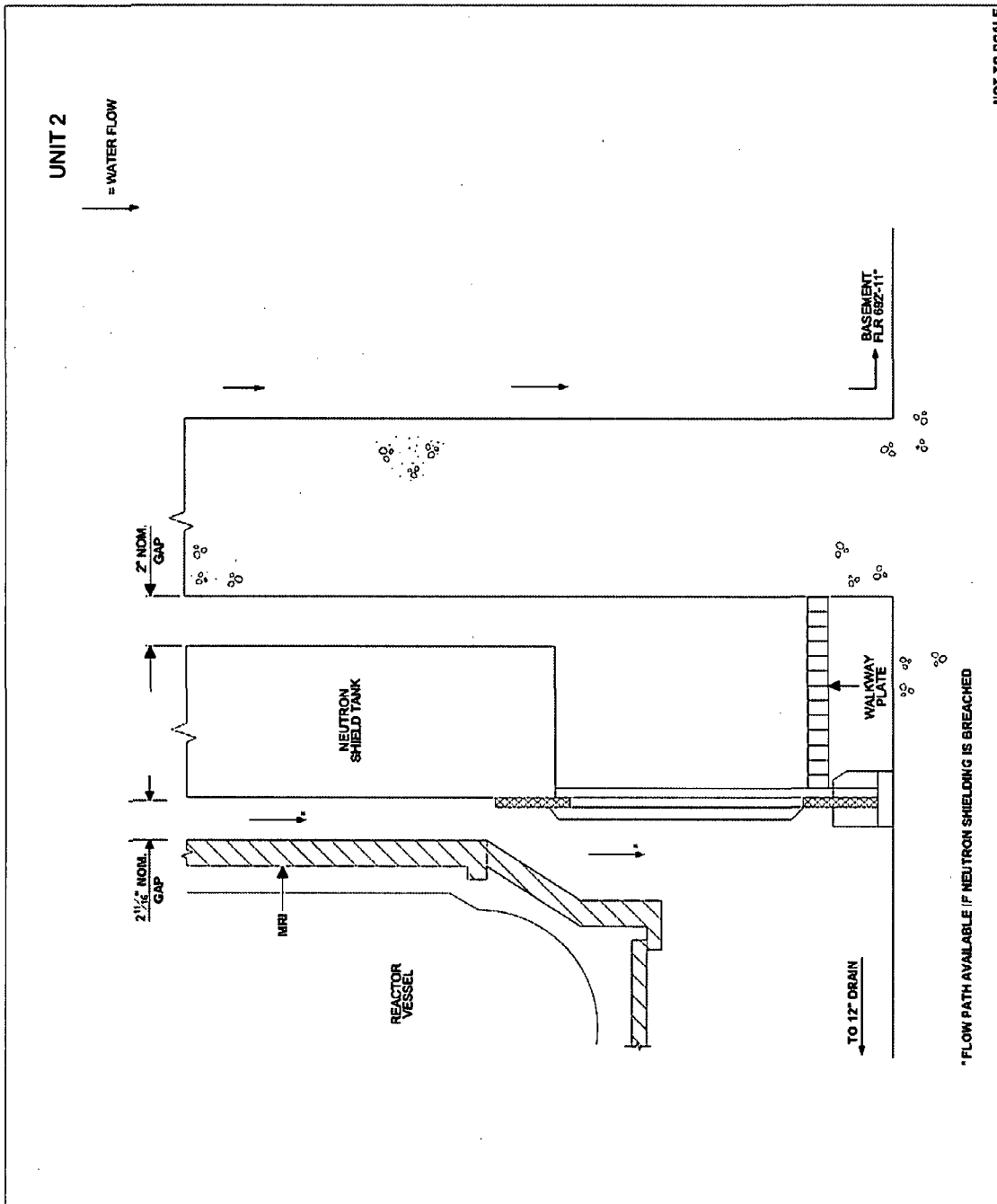


Figure 21-4, BVPS-2 Reactor Cavity Configuration (Lower Cavity)

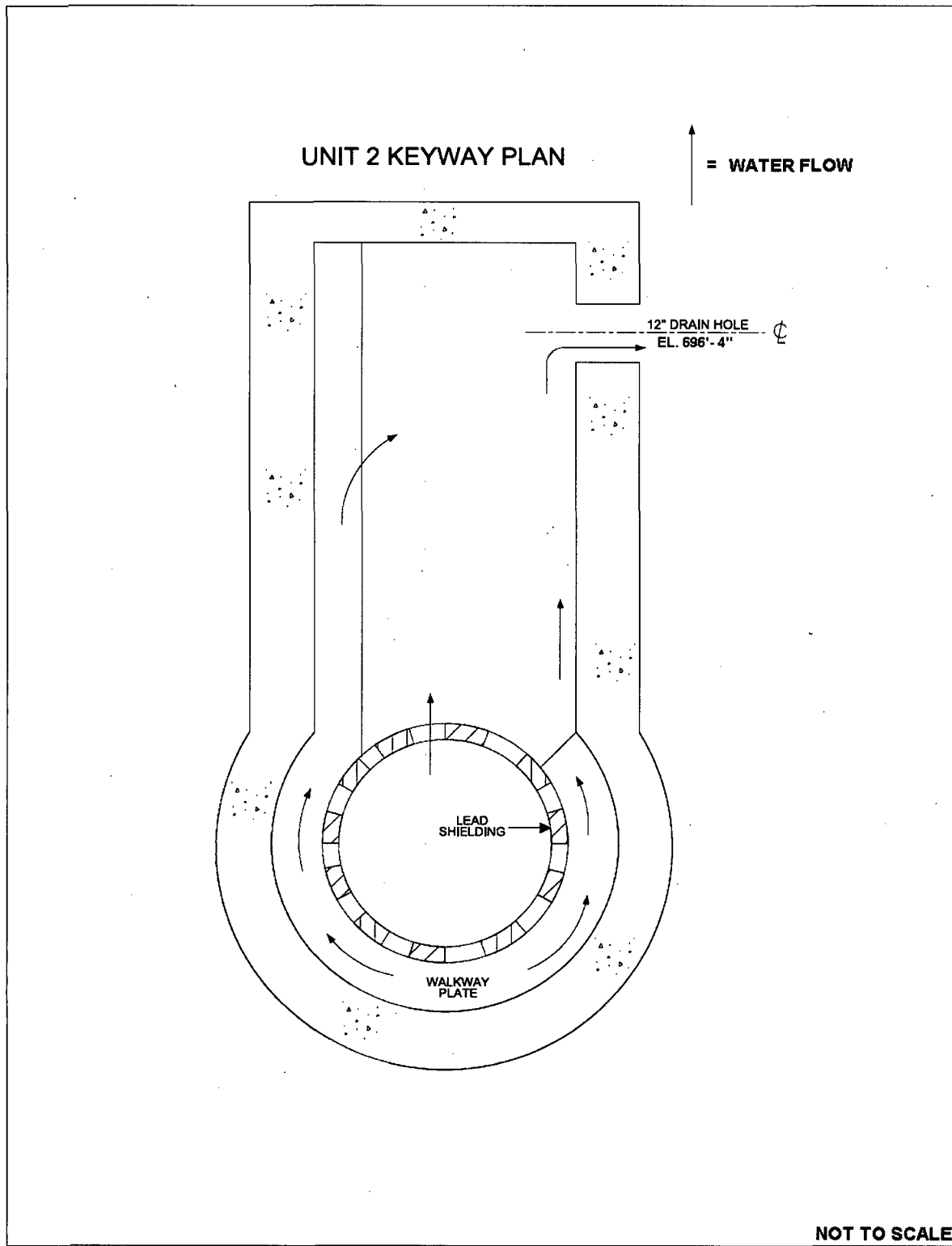


Figure 21-5, BVPS-2 Reactor Cavity Keyway Plan

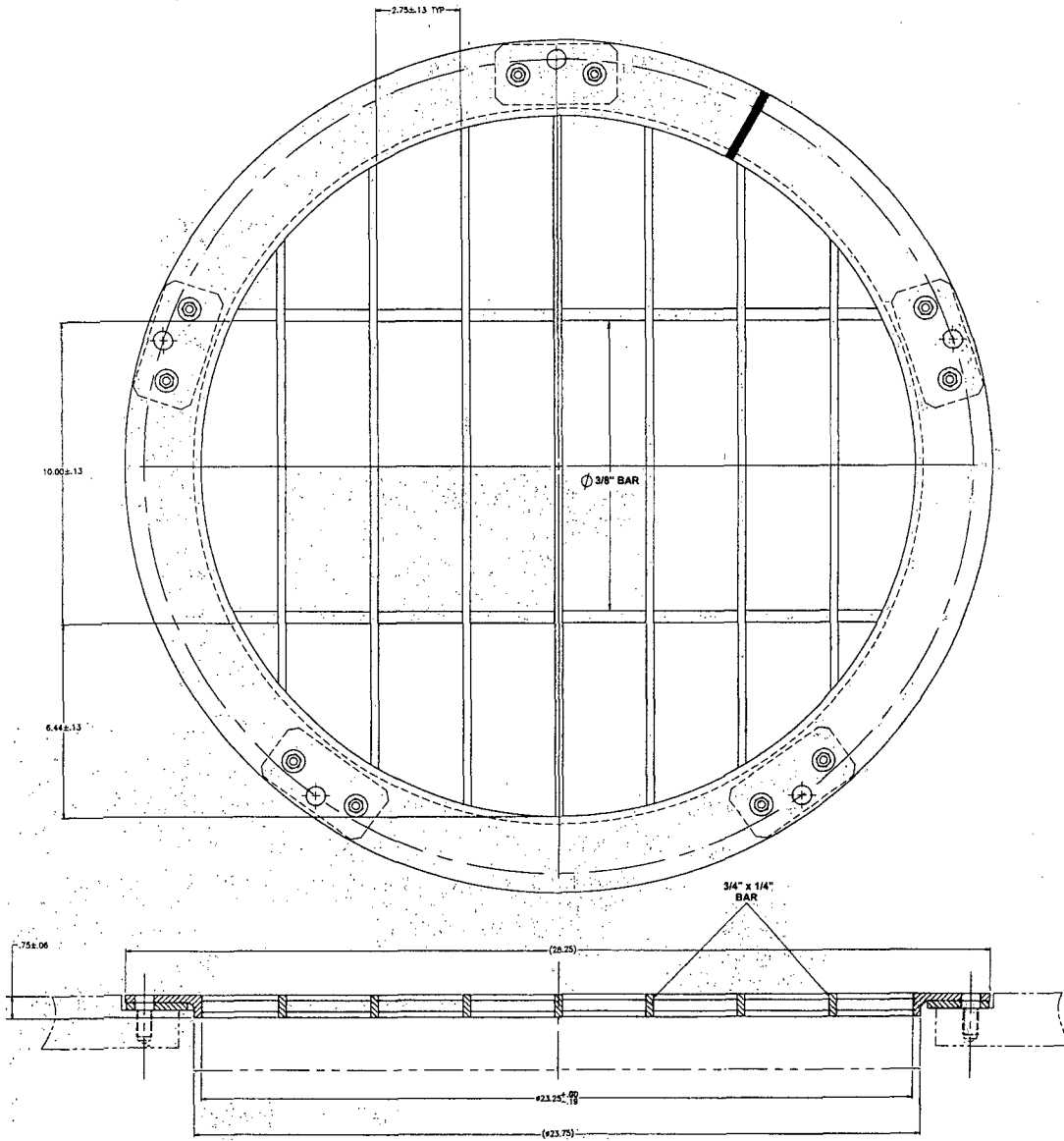


Figure 21-6, BVPS-2 Cavity Seal Opening Safety Cover

**RAI 22:**

**For BVPS-2, please provide additional detail to confirm that the cold leg recirculation NPSH results are bounding with respect to all potential hot leg recirculation flow lineups. Based on the information provided in the supplemental response dated June 30, 2009, and the NRC staff's review of the BVPS-2 Updated Final Safety Analysis Report, the NRC staff accepted that the cold leg recirculation lineup NPSH margin results are limiting with respect to the hot leg recirculation lineup wherein the recirculation spray system (RSS) pumps feed the hot legs via the high-head safety injection/charging pumps. However, it was not clear that the cold leg recirculation lineup was bounding with respect to the configuration in which the RSS pumps recirculate sump fluid through low-head safety injection system piping and into the hot legs. Please clarify whether this latter flow configuration is permissible per emergency operating procedures, and, if so, provide a more detailed basis for concluding that the flows and NPSH margin results for this case are bounded.**

**FENOC Response:**

The latter flow condition wherein the RSS pumps recirculate sump fluid through low-head safety injection system piping and into the hot legs is permissible and required by the emergency operating procedures. However it is bounded by the cold leg recirculation alignment based on the following discussion.

The BVPS-2 hot and cold leg recirculation alignments are as follows:

In cold leg recirculation, two of the four RSS pumps (2RSS-P21C, D) provide flow to the suction of the high head safety injection (HHSI) pumps and in parallel, directly to the cold legs through three 6-inch diameter injection paths. The HHSI pumps provide flow to the cold legs through six 2-inch diameter injection paths.

After 6 hours, the system is transferred to hot leg recirculation. In this alignment, two of the four RSS pumps (2RSS-P21C,D) provide flow to the suction of the HHSI pumps and in parallel, directly to the hot legs through two 6-inch diameter flow paths. Hot leg connections from the LHSI system are provided on the "B" and "C" reactor coolant loops. The HHSI pumps provide flow to the hot legs through six 2-inch diameter injection paths.

Since there is approximately 33 percent less flow area available in the LHSI piping to the hot legs than the cold legs, and the HHSI piping is essentially equivalent, the flows in the hot leg recirculation alignment are lower than those which occur during cold leg recirculation. Additionally, since this hot leg recirculation alignment is not put into service until after 6 hours have elapsed, the sump level is higher (and the sump temperature is lower), which provides additional NPSH margin with respect to the limiting conditions.

**RAI 23:**

**The supplemental response dated June 30, 2009, describes an internal divider plate installed between the two channels of the BVPS-2 strainer. Please describe the location of the internal divider plate and its function, provide the size of the perforations in the divider plate and its total surface area, and provide the basis for the determination that blockage will not occur at the divider plate based on the sizes and quantities of debris in the flow stream downstream of the strainer surface. Please provide similar information for BVPS-1 if a divider plate internal to the BVPS-1 replacement strainer exists.**

**FENOC Response**

As stated in the response to RAI 18, the BVPS-2 containment sump strainer divider has been removed. Information on the divider is provided in response to RAI 18. BVPS-1 does not have divided strainers.

**RAI 24:**

**In its response to Item 3.g.12 in Reference 1, the licensee provided a table showing the post-LOCA distribution of water for various LOCA sizes. It is not clear what break elevations were assumed in the analysis. If a break occurred in the top of the pressurizer, the entire RCS volume (e.g., including the pressurizer) would be susceptible to refill. Please clarify what break elevations were assumed for the small-break LOCA cases and discuss whether a small-break LOCA at an elevation allowing complete refill of the RCS would be bounded by the assumptions.**

**FENOC Response**

Break elevations for small break LOCA cases were assumed to occur at the elevation corresponding to the center of the RCS hot or cold leg. This is based on the elevation of the safety injection piping penetrations. If a break occurred at the top of the pressurizer, the break is not bounded by the center of loop elevation assumption. Additional hold up of water in the RCS will occur for this break location. The containment/NPSH analyses were revised to include this break location. The results confirm that the break at the top of the pressurizer is more limiting for minimum sump strainer submergence. A minimum break size of 2 inches equivalent diameter was analyzed in accordance with NEI 04-07. When compared to a 2-inch break postulated to occur at the middle elevation of the hot or cold legs, the minimum submergence decreased by approximately 0.8 inches for BVPS-1 and BVPS-2. Since the pressurizer break location was determined to be more limiting, it will be used as the limiting case for containment sump strainer submergence and the results have been reflected in Table 20-1 in the response to question 20c. This change has no impact on NPSH margins since the small breaks in general are much less limiting for NPSH results.

**RAI 25:**

Table 3.g.1-2 of Reference 1 indicated that the maximum sump flow during safety injection recirculation for BVPS-2 is 13,640 gpm. In response to Item 3.g.6, the licensee stated that emergency operating procedures will be modified to ensure that one of the BVPS-2 RSS pumps supplying the containment spray headers will be shut down when the containment pressure is reduced below a predetermined value to prevent head losses from exceeding the structural limit at low temperatures. Please clarify the following information:

- a. The total sump flow rate before and after the securing of one of the RSS pumps used for spraying containment.
- b. The calculated time and containment pressure when one RSS pump can be terminated.
- c. The calculated time and sump pool temperature when the strainer head loss could exceed its structural limit.

**FENOC Response**

- a. The total sump flow rate before and after the securing of one of the RSS pumps used for spraying containment

The total sump flow rate before securing one of the RSS pumps is approximately 13640 gpm. This flow rate is reduced to approximately 9930 gpm after one RSS pump is secured.

- b. The calculated time and containment pressure when one RSS pump can be terminated.

The procedures direct the operator to shut down one of two operating RSS pumps supplying the spray headers when the containment pressure reaches a value of 13.5 psia. The time required to reach this point is dependent primarily on the capacity of the heat removal system. For maximum safeguards operation (all containment spray pumps operating) with the minimum service water temperature (32 °F), this pressure could be reached in approximately 40 minutes. However, as discussed in the response to question 25c, operator response under these conditions is not critical for protecting the strainer from exceeding structural limits.

- c. The calculated time and sump pool temperature when the strainer head loss could exceed its structural limit.

Since the issuance of the June 30, 2009 supplemental response, BVPS has performed additional testing for BVPS-2 based on taking credit for the revised buffering agent. The latest head loss results also reflect a reduction in tags and labels present in the containment which was implemented in the most recent refueling outage. The results of this testing indicate that in order to challenge the containment sump strainer structural limit of 5 psid, the sump temperature would have to drop to approximately 37.5 °F.

Containment analyses run with maximum heat removal capacity and all RSS pumps operating predict that a temperature this low would not be reached for approximately 18 days assuming no operator actions are taken. Based on this timing and low temperature, RSS flow reduction as described in the June 30, 2009 supplemental response to prevent head losses from exceeding the strainer structural limit are not considered critical operator actions.

### **Chemical Effects**

#### **RAI 26:**

**The evaluation of the chemical effects was discussed in Reference 1. Although the NRC staff has no additional questions about the current chemical effects evaluation, there are open commitments to address additional Temp-Mat and fibrous insulation in the reactor vessel annulus that is not bounded by the current analyses. If the re-evaluation results in additional chemical and non-chemical debris loading of the strainer, changes should be evaluated to determine if the existing testing and analysis adequately address the revised debris amounts. Please describe your evaluation of the impact of any additional Temp-Mat and fiber.**

#### **FENOC Response**

The existing chemical effects evaluation provided within the FENOC June 30, 2009 supplemental response to Generic Letter 2004-02 will not change due to the additional amounts of Temp-Mat™ insulation that were identified on the BVPS-1 Reactor Vessel Nozzles. This additional Temp-Mat™ insulation was recognized during the BVPS-1, 1R19 Refueling Outage and identified to the NRC via FENOC letter dated April 30, 2009 (ADAMS Accession No. ML091250180). This Temp-Mat™ insulation on the hot and cold leg reactor vessel nozzles will be removed and replaced with RMI during the BVPS-1, 1R20 Refueling Outage scheduled for fall 2010. Since the basis for the chemical effects evaluation does not include this additional amount of Temp-Mat™ and the Temp-Mat™ will be removed and replaced with RMI consistent with the evaluation assumption, the outcome of the evaluation does not change. (See also RAI 2.)

**Appendix I, BVPS-2 August 2009 Test 2 Summary**

The June 30, 2009 supplemental response included Test 5, a test that represented the head loss for the reactor vessel nozzle break and bounded the maximum allowable Microtherm® debris load. However, the BVPS-2 August 2009 Test 2 now represents the head loss for the reactor vessel nozzle break, bounds the maximum allowable Microtherm® debris load, and supersedes the BVPS-2 Test 5 as the design basis test.

The Test 5 information provided in the June 30, 2009 supplemental response is also superseded by the following BVPS-2 August 2009 Test 2 data and information. Where appropriate, the affected June 30, 2009 supplemental response section is referenced in the discussion.

BVPS-2 August 2009 Test Summary - Reactor Nozzle Break Test

The BVPS-2 August 2009 Test 2 determined the head loss for the Reactor Vessel Nozzle Break debris loads (including maximum fiber loading, Microtherm®, latent debris, and coatings) plus WCAP predicted chemical precipitants. Table AI-1 below provides a summary of the BVPS-2 August 2009 Test 2.

Table AI-1

Test No.	Test Description	Break
BV2 Aug 2009 Test 2	Scaled Load Test Debris 37.1 percent Microtherm® (with Bypass Eliminator)	BVPS-2 Reactor Vessel Nozzle Break

The debris type and scaled quantity used for this case are listed in Table AI-2. The materials used were the same as the materials discussed in Section 3.f.4 of the June 30, 2009 supplemental response (Reference 1).

Table AI-2

Test No.	Nukon™ (lbm)	Micro- therm (lbm)	Ground Silica (lbm)	Paint Chips Surrogate (lbm)	Dirt/ Dust (lbm)
BV2 Aug 2009 Test 2	1.57	17.8	22.6	8.3	8.9

The head loss test results for the BVPS-2 August 2009 Test 2 at an approach velocity of 0.009813 ft/sec, corrected for the temperature, are shown in Table AI-3. The test

configuration for the BVPS-2 August 2009 Test 2 is the same as the BVPS-2 configuration described in Section 3.f.4 of the June 30, 2009 supplemental response.

Table AI-3

Temperature (°F)	Head Loss (ft-water)
65	9.19
100	7.63
150	6.53
180	6.10
212	5.76

Note: The above table reports head loss values at test termination. No extrapolation was required to 30 days since the head loss was stable or decreasing at test termination.

This test represents the head loss for the BVPS-2 reactor vessel nozzle break and bounded the maximum allowable Microtherm<sup>®</sup> debris load. Similar to the other bounding BVPS-2 test, Test 1A, the resultant head loss values indicate that a partial thin bed was potentially formed, resulting from the additional contribution of the particulates and chemical precipitates. As with Test 1A, the BVPS-2 August 2009 Test 2 head loss values were low enough to accommodate this potential partial thin bed formation.

The discussion in Sections 3.f.8, 3.f.12 and 3.f.13 of the June 30, 2009 supplemental response are also applicable to the BVPS-2 August 2009 Test 2. The same margins and conservatisms were used in the calculations. There was no near-field settling effects credited, and the same temperature corrections were performed.

Table AI-4 represents the composite maximum head loss from both the loop break (Test 1A) and the nozzle break (August 2009 Test 2). The head loss for a specific case is adjusted on a transient basis for the actual sump strainer flow and temperature in the MAAP-DBA code for use in calculating available NPSH.

Table AI-4, BVPS-2 Total Debris and Strainer Head Loss

Temperature (°F)	Head Loss (ft.)
65	10.13
100	8.56
150	7.45
180	7.03
212	6.68

Note: The above table includes a flow correction and the clean screen head loss.

The theoretical equivalent bed thickness of the fibrous debris in BVPS-2 was found to be 0.05 inches for the BVPS-2 August 2009 Test 2. Visual observation of the debris beds indicated that this theoretical equivalent bed thickness is not enough to completely coat the strainer with fibrous debris. Given the small amount of fibrous debris used in testing, a lack of complete debris bed coverage is a reasonable conclusion.

Similar to BVPS-1, integrated chemical effects testing for BVPS-2 also used WCAP-16530-NP chemical precipitates. Test 1A and the BVPS-2 August 2009 Test 2 were determined to be the bounding tests for BVPS-2. Test 1A bounds the debris and chemical quantities for BVPS-2 loop break and surge line break. The BVPS-2 August 2009 Test 2 bounds the debris and chemical quantities for the BVPS-2 reactor vessel nozzle break, and identifies the maximum allowable Microtherm<sup>®</sup> load. The discussion in Section 3.o.2.2.i of the June 30, 2009 supplemental response is also applicable to the BVPS-2 August 2009 Test 2. Sections 3.o.2.3.i, 3.o.2.4.i, 3.o.2.10.i, 3.o.2.12.i, 3.o.2.13.i, 3.o.15 and 3.o.2.16.i of the June 30, 2009 supplemental response are all applicable to the BVPS-2 August 2009 Test 2 test proceedings. The single exception is that for 3.o.2.3.i, only the sodium tetraborate buffer pH ranges were considered. The type and amount of predicted WCAP-16530-NP plant specific precipitates for the bounding BVPS-2 tests are shown (before scaling amounts) in Table AI-5 below.

Table AI-5, BVPS-2 August 2009 Test 2

Precipitate	Pounds
Sodium Aluminum Silicate	106
Aluminum Oxyhydroxide	0

The curves in Figures AI-1 through AI-5 below illustrate the pressure drop as a function of time (uncorrected for temperature) for the BVPS-2 August 2009 Test 2. These figures depict the results of the BVPS-2 August 2009 Test 2 by plotting the differential pressure across the debris bed and fluid average theoretical approach velocity versus time, with subtest debris additions and flow adjustments indicated by vertical lines. Other test control operations and observations are marked with arrows at the time of execution/occurrence.

The methodology described in Section 3.o.2.17 of the June 30, 2009 supplemental response is applicable to the BVPS-2 August 2009 Test 2. Temperature corrections were applied to the head loss data analysis. Additionally, for the BVPS-2 August 2009 Test 2 the head loss was decreasing at the end of the test, therefore no extrapolation was performed.

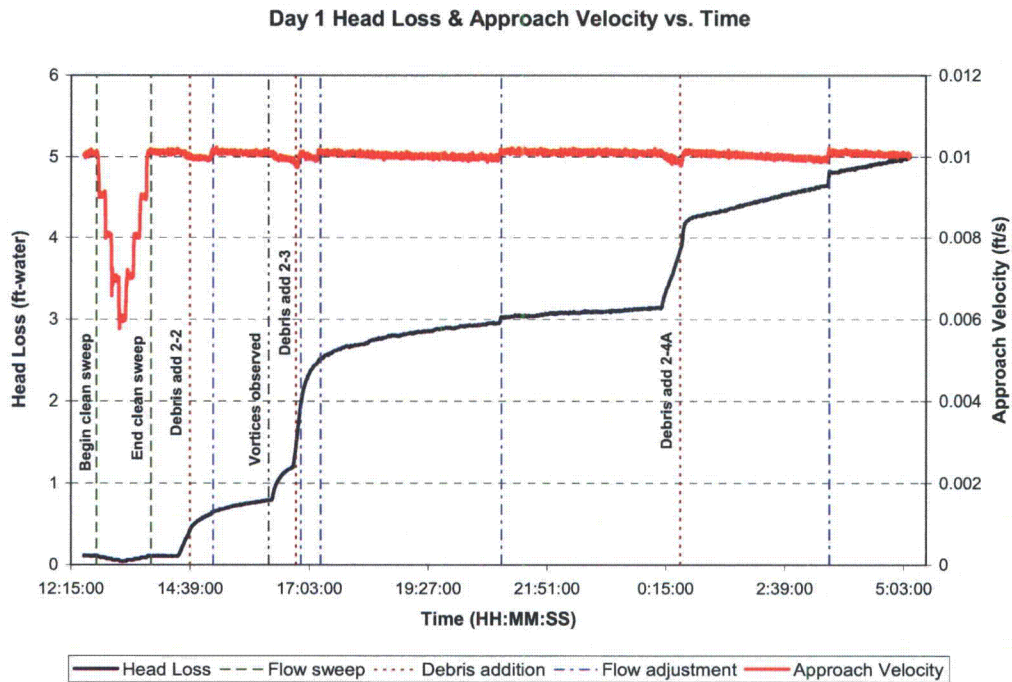


Figure AI-1

BVPS-2 August 2009 Test 2 Differential Pressure and Velocity vs. Time - Day 1

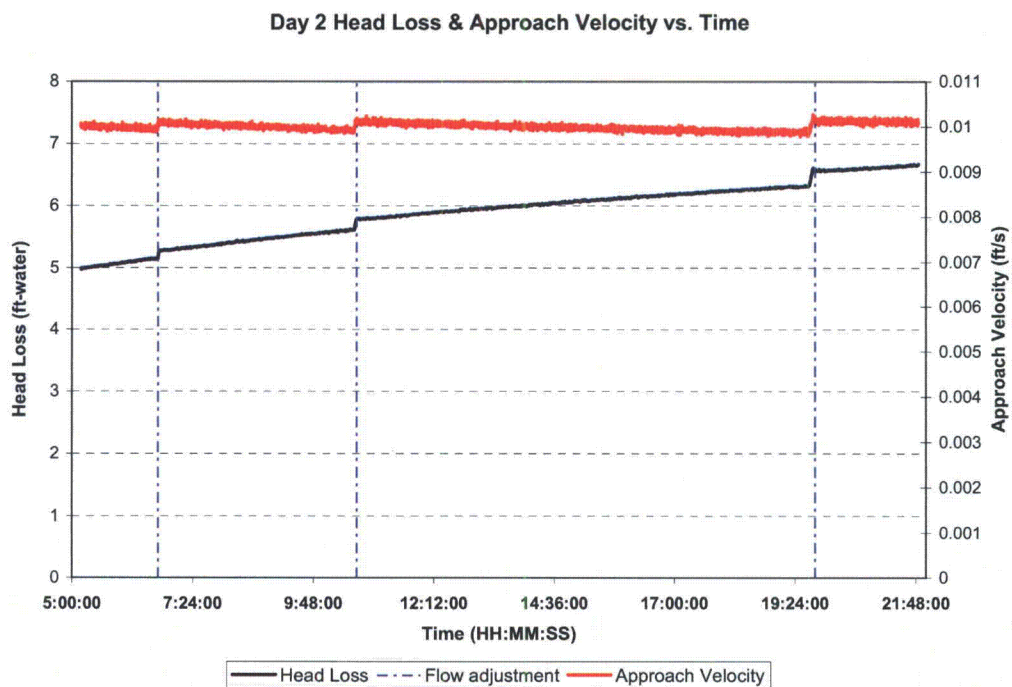


Figure AI-2

BVPS-2 August 2009 Test 2 Differential Pressure and Velocity vs. Time - Day 2

Day 3 Head Loss & Approach Velocity vs. Time

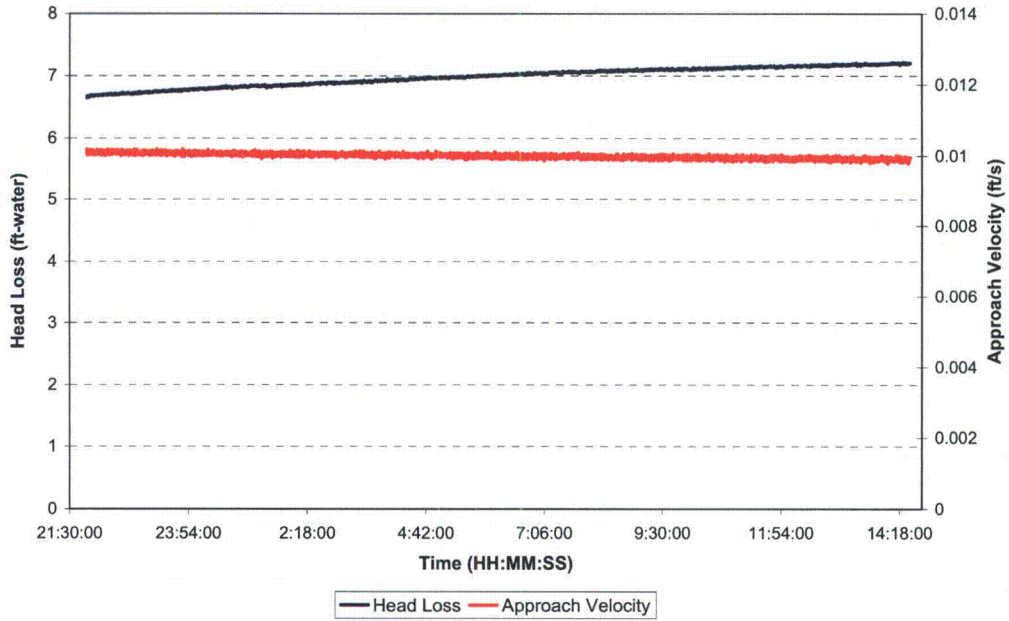


Figure AI-3,  
BVPS-2 August 2009 Test 2 Differential Pressure and Velocity vs. Time - Day 3

Day 4 Head Loss & Approach Velocity vs. Time

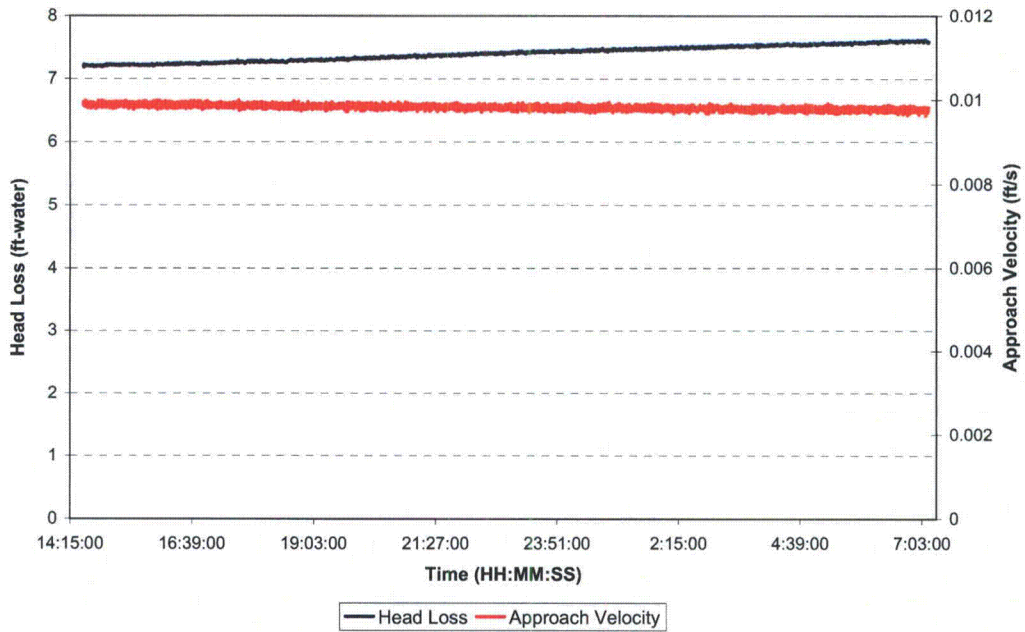


Figure AI-4  
BVPS-2 August 2009 Test 2 Differential Pressure and Velocity vs. Time - Day 4

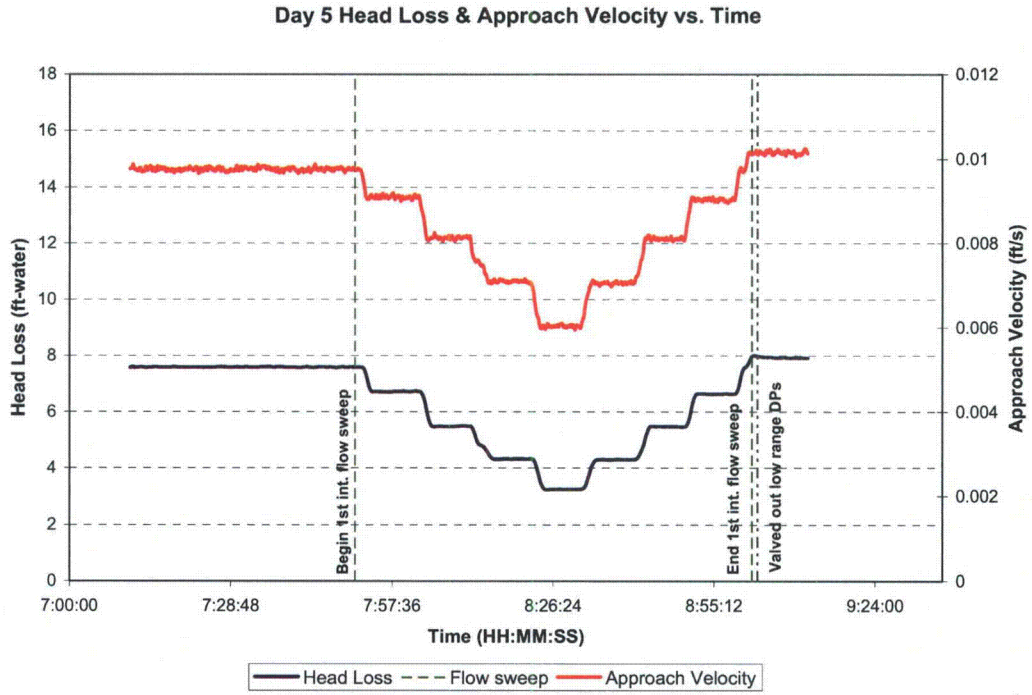


Figure AI-5  
BVPS-2 August 2009 Test 2 Differential Pressure and Velocity vs. Time – Day 5

## **Appendix II, BVPS Chemical Effects Resolution**

The June 30, 2009 supplemental response included a response to item 3.o.2.2.3 regarding plant specific materials and buffers and their impact on chemical effects loads. In particular, the response included any assumptions used to determine chemical effects loading. The following Argonne National Laboratory (ANL) correlation approach to delaying the onset of chemical effects should be added to supplement the response. The reason for delaying the onset of chemical effects at both Beaver Valley Power Station units is to provide a more realistic application of the strainer head loss test results. Also note that the basis for the delay in the onset of chemical effects at both Beaver Valley Power Station units is temperature based only; references to the post-LOCA timing are made to simplify the post-accident timeline of events, and are based on the plant specific maximum temperature, minimum cooling scenario for each unit.

### BVPS-2 ANL Correlation

The following discussion and methodology is from the BVPS-2 Recirculation Sump Strainer Hydraulic Head Loss Calculation and provides a justification for the delay of application of chemical effect head loss until 16.7 hours post-LOCA. At that time post-LOCA, the temperature has fallen to 140 degrees Fahrenheit (°F) in the maximum temperature, minimum cooling scenario.

After 16.7 hours post-LOCA at BVPS-2 approximately 1.1 kilograms (kg) (0.38 parts per million [ppm]) of aluminum could be released, assuming that the aluminum release rate predicted using WCAP-16530, "Evaluation of Post-Accident Chemical Effects in Containment Sump Fluids to Support GSI-191," is doubled (in accordance with guidance provided in the NRC SE of WCAP-16530) and the worst case temperature profile is used. During the same period, a maximum of 50.7 kg (18.1 ppm) of silicon could be released into the sump fluid per WCAP-16530.

With regard to sodium aluminum silicate (NAS) formation, dissolved aluminum is the limiting reactant at BVPS-2, and only 10.4 kg of NAS can form in the first 16.7 hours post-LOCA. This corresponds to approximately 0.38 ppm aluminum-equivalent of sodium aluminum silicate in the sump, which is less than 10 percent of the full chemical precipitate debris load. Small amounts of sodium aluminum silicate (less than 4 ppm aluminum-equivalent) have been shown in Alion testing for Vogtle (observed by the NRC as documented in trip report ADAMS Accession number ML092670458) to have no effect on debris head loss at temperatures above 140°F. The Vogtle testing is relevant to BVPS-2 because the two plants have similar containment sump pH values and aluminum concentrations.

If no NAS forms at 140°F, the maximum possible aluminum concentration at 140°F is 0.38 ppm, and all aluminum is predicted to remain in solution by the ANL correlation below.

At 140°F and the minimum sump pH of 7.0, the aluminum solubility limit per the ANL aluminum solubility correlation is as follows:

$$[\text{Aluminum (ppm)}] = 26980 \times 10^{7.0 - 14.4 + 0.0243 \times 140^\circ\text{F}}$$

Aluminum solubility limit at 140°F and pH 7.0 = 2.7 ppm

The maximum dissolved aluminum concentration at BVPS-2 is 1.8 ppm after 30 days. Even if the maximum 30-day dissolved aluminum concentration is conservatively assumed to be present in the sump after 16.7 hours at a sump temperature of 140°F, no aluminum is predicted to precipitate as aluminum oxyhydroxide.

Based on the application of the ANL correlation to the BVPS-2 sump conditions 16.7 hours post-LOCA at a temperature of 140°F, and the insignificant quantity of sodium aluminum silicate that can form at this time and temperature, the application of head loss due to chemical effects at BVPS-2 can be conservatively delayed up to 16.7 hours after the initiation of a LOCA when the sump temperature at BVPS-2 has fallen to 140°F. This analysis is for the maximum temperature, minimum cooling scenario. For other breaks that result in more rapid cooling, use of 140°F for the application of chemical effect head loss is conservative since other breaks will result in the sump temperature falling to 140°F in less than 16.7 hours, which will result in less dissolved aluminum and silicon than in the maximum temperature case.

#### BVPS-1 ANL Correlation

The response to item 3.f.14 of the June 30, 2009 supplemental response indicates that the BVPS-1 analyses predicted a potential for some minor flashing to occur across the strainer for a brief period of time shortly after the RSS pumps start. However, those analyses conservatively use the strainer head loss considering the full debris bed and the effect of chemical precipitates. The dissolution of precipitate forming chemicals into the containment sump inventory is a relatively slow process, and will delay the formation of precipitates and their effect on strainer head loss until well after the start of the RSS pumps. Therefore, no flashing is expected to occur.

The following discussion and methodology is from the BVPS-1 Recirculation Sump Strainer Hydraulic Head Loss Calculation and provides a justification for the delay of application of chemical effect head loss until 8.6 hours post-LOCA. At that time post-LOCA, the temperature has fallen to 150°F in the maximum temperature, minimum cooling scenario.

After 8.6 hours post-LOCA at BVPS-1, approximately 24.6 kg (20.6 ppm) of aluminum could be released, assuming that the aluminum release rate predicted using WCAP-16530 is doubled (in accordance with guidance provided in the NRC SE of WCAP-16530) and the worst case temperature profile is used. During the same period, a maximum of 2.0 kg (1.7 ppm) of silicon could be released into the sump fluid per WCAP-16530.

With regard to sodium aluminum silicate (NAS) formation, dissolved silicon is the limiting reactant at BVPS-1, and only 6.3 kg of NAS can form in the first 8.6 hours post-LOCA. This corresponds to approximately 0.54 ppm aluminum-equivalent of sodium aluminum silicate in the sump, which is less than 6 percent of the full chemical precipitate debris load. Small amounts of sodium aluminum silicate (less than 4 ppm aluminum-equivalent) have been shown in Alion testing for Vogtle (observed by the NRC as documented in trip report ADAMS Accession number ML092670458) to have no effect on debris head loss at temperatures above 140°F. The Vogtle testing is relevant to BVPS-1 because the two plants have similar containment sump pH values and aluminum concentrations.

If 0.54 ppm aluminum forms NAS, the remaining aluminum in solution after 8.6 hours, 24 kg (20.0 ppm), is predicted to remain in solution at a temperature of 150°F by the ANL aluminum solubility correlation below. If no NAS forms, the maximum possible aluminum concentration at 150°F is 20.6 ppm, and all aluminum is predicted to remain in solution by the ANL correlation below.

At 150°F and the minimum sump pH of 7.8, the aluminum solubility limit per the ANL aluminum solubility correlation is as follows:

$$[\text{Aluminum (ppm)}] = 26980 \times 10^{7.8 - 14.4 + 0.0243 \times 150^\circ\text{F}}$$

Aluminum solubility limit at 150°F and pH 7.8 = 29.9 ppm

The maximum dissolved aluminum concentration at BVPS-1 is 29.3 ppm after 30 days. Even if the maximum 30-day dissolved aluminum concentration is conservatively assumed to be present in the sump after 8.6 hours at a sump temperature of 150°F, no aluminum is predicted to precipitate as aluminum oxyhydroxide, and the quantity of sodium aluminum silicate is predicted to be only 6.3 kg, or 0.54 ppm aluminum-equivalent.

Based on the application of the ANL correlation to the BVPS-1 sump conditions 8.6 hours post-LOCA at a temperature of 150°F, as well as the insignificant quantity of sodium aluminum silicate that can form at this time and temperature, the application of head loss due to chemical effects at BVPS-1 can be conservatively delayed up to 8.6 hours after the initiation of a LOCA when the sump temperature at BVPS-1 has fallen to 150°F. This analysis is for the maximum temperature, minimum cooling scenario. For other breaks that result in more rapid cooling, use of 150°F for the application of chemical effect head loss is conservative since other breaks will result in the sump temperature falling to 150°F in less than 8.6 hours, which will result in less dissolved aluminum and silicon than in the maximum temperature case.

### **Appendix III, Evaluation of the Susceptibility of Benelex<sup>®</sup> 401 to Erosion or Dissolution in the Post-LOCA Environment**

#### **1. Introduction**

Polymer Consultants, Inc. was requested by FENOC and Alion Science and Technology to evaluate the material characteristics for Benelex<sup>®</sup> 401 (hereafter referred to simply as Benelex<sup>®</sup>), manufactured by the Masonite Corporation. Specifically, Polymer Consultants was requested to evaluate how Benelex<sup>®</sup> would react when exposed to the post-loss of coolant accident (LOCA) environment at BVPS-1.

Polymer Consultants, Inc. is a consulting firm with many years of experience specializing in the fields of polymer formulation, manufacturing techniques and marketing of polymer based products. The principals of the corporation have designed and built polymer depolymerization facilities, operated polyester bottle recycling plants, developed polymer blends of olefinic polymers and high percentage content thermoset rubbers, and invented green technology for the removal of polychlorinated biphenyls (PCBs) from automobile shredder residue. The corporate website at [www.polymerconsultants.net](http://www.polymerconsultants.net) has further details.

Benelex<sup>®</sup> is a dense, lignin-resin/cellulose, laminated hardwood product that is used as a supplemental neutron shield near the bottom of the reactor vessel at BVPS-1. The shield is comprised of four layers of 2-inch thick Benelex<sup>®</sup> material shaped in the form of a large ring. The material is bolted together and supported by structural steel. This ring does not perform any structural function; it is provided strictly for neutron shielding.

The location of the Benelex<sup>®</sup> ring could result in exposure to mildly alkaline steam/water spray/cascade, with a short term (less than 2 hour) temperature of as high as 255°F and longer term temperatures ranging from 170°F at two hours to a minimum of 65°F over the 30 day mission time. The Benelex<sup>®</sup> ring is not expected to be immersed but effects from immersion are considered for completeness. Given that the Benelex<sup>®</sup> is a wood-based product, a question exists as to whether the material may deteriorate in this environment. Benelex<sup>®</sup> is no longer produced by the Masonite Corporation, and technical documentation such as exact chemical composition or test results are no longer available from the manufacturer. However, information is available from a number of secondary sources, such as patent applications, product specification sheets and interviews with current and former Masonite employees (including the former technical manager for the Masonite Manufacturing Facility in Laurel, Mississippi during the time period when the Benelex<sup>®</sup> in question was manufactured), such that a solid understanding of the physical and chemical properties of the material was obtained and is presented in this evaluation.

## 2. Purpose

The purpose of this study is to determine the material properties of Benelex<sup>®</sup>, and compare them with other materials for which published data is available with respect to the potential for deterioration in the post-LOCA environment. Specifically, the material will be evaluated for the potential to dissolve or erode due to immersion or spray exposure over a 30 day period.

## 3. Characteristics of Benelex<sup>®1</sup>

Benelex<sup>®</sup> was developed and patented by Mr. Charles F. Story under two separate patents, Patent No. 2459851 "Ligno-Cellulose die-Stock and Process of Making Same," dated January 25, 1949 and Patent No. 2550730, "Diestock and Process of Making Same," dated May 1, 1951. Both patents were assigned to Masonite Corporation of Laurel, Mississippi, which manufactured Benelex<sup>®</sup> 30, Benelex<sup>®</sup> 70, Benelex<sup>®</sup> 100, Benelex<sup>®</sup> 401 and Benelex<sup>®</sup> 402 until 1993.

Benelex<sup>®</sup> is composed of pure cellulose fully encapsulated in lignin. Both the cellulose and the lignin were derived from the typical hardwood trees found in Southern Mississippi and included oak, sweet gum, birch, beech, ash and poplar. Masonite received their hardwood feedstocks as bulk truckloads of chipped wood.

Hardwood lignocellulosic biomass contains cellulose, hemicelluloses, lignin and extractives in the ratio of 5:2:2:1. The desired water insoluble cellulose and lignin is extracted from the hardwood biomass by steam explosion, which destroys the gross structure of the wood separating the insoluble cellulose and lignin from the soluble hemicelluloses and extractives. The resultant mixture is dumped into water stock tanks maintained at 180°F and the solid cellulose and lignins are filtered out.

Ten pounds of wood chip yields 6 pounds of pure cellulose and lignin with a ratio of 2 to 1 cellulose to lignin. This mixture is dried to a moisture content of 8 to 10 percent and formed into mats, which are pressed into 0.5-inch thick low density lifts of 0.5 specific gravity. These low density mats are then interleaved with paper sheets that have been saturated with phenol formaldehyde (PF) to attain an ultimate PF content in the finished laminate of 1 to 2 percent by weight. The stack of low density mats were then loaded into a vertical press and brought to 10,000 pounds per square inch (psi) and held until the core temperature of the laminate reached 400 to 450°F as determined by thermocouple readings.

Press times varied with the thickness of the end product being manufactured and ranged from 1.5 hours for a 1/8 inch sheet of Benelex<sup>®</sup> to as much as 7 to 8 hours for a 2-inch thick piece of Benelex<sup>®</sup>. During pressing the lignin begins to flow at 340°F and fully encapsulates the cellulose fibers creating a uniform composite matrix (further

---

<sup>1</sup> Source: Tom Ruffin, retired Technical Manager for Masonite 1995 – 2008, Masonite Process Engineer in Benelex<sup>®</sup> manufacturing 1973 – 1995.

discussion is in similarity section concerning polymer matrices). The fully encapsulated cellulose fibers range in length from micron size up to a maximum of 1/8 inch in length. Manufacturing specifications for Benelex<sup>®</sup> call for a minimum of 19 percent fines. Finished Benelex<sup>®</sup> product densities range from 1.37 to 1.45 specific gravity.

The Benelex<sup>®</sup> installed at the BVPS-1 facility is Benelex<sup>®</sup> 401. This differs slightly from Benelex<sup>®</sup> 402 because in the Benelex<sup>®</sup> 401 product, the individual 1/8 inch lifts of lignin/cellulose laminate are adhered to each other utilizing phenol formaldehyde impregnated paper leafing from Kimberly Clark (part number K2021). In the Benelex<sup>®</sup> 402 product, the individual lifts were adhered together by spraying uncured liquid phenol formaldehyde resin between each lift prior to compressing the lifts together to create the final desired product thickness. The material characteristics of Benelex<sup>®</sup> 401 are provided in the product literature (Reference 4, Attachment E) and shown in Appendix III, Table 1.

### 3.1. Similarity to Other Materials

The first thermosetting plastic resins developed were phenol-formaldehyde resins (phenolic or PF resins). The PF resins were modeled on the naturally occurring phenol based lignin resins and contain identical ether linkages. Cellulose filled PF resins have very similar properties to Benelex<sup>®</sup> with 24 hour water absorption of 0.05 to 0.90 percent and specific gravity of 1.37 to 1.46, in addition to being resistant to weak alkalis. Both lignin and PF resins contain similar phenolic moieties with ether linkages, and therefore they perform in a similar manner. Thus, for the purpose of evaluating the performance of Benelex<sup>®</sup>, data associated with lignin and PF resins is considered equivalent.

Microscopic studies of filled polymers reveals that the fillers, whether they are wood, glass fiber or various minerals, are typically dispersed as discrete filler particulates fully encapsulated by resin. It is reasonable to expect that the lignin flows in a manner similar to PF resins due to their comparable chemical nature and that the lignin fully encapsulates the cellulose as PF resins fully encapsulate fillers compounded into them. Although no pictures are available, Masonite personnel maintain that the lignin does indeed fully encapsulate the cellulose filler used in Benelex<sup>®</sup>.

It is not unusual for a filled polymeric compound to contain various compatibilizers designed to chemically link the filler to the resin that serves as the continuous matrix. The use of these compatibilizers typically improves the physical properties of the finished compound. Benelex<sup>®</sup> demonstrates similar linkage in the hydrogen bonding that occurs between the wood particulates and the encapsulating lignin resin.

## 4. Design Considerations

4.1. The Benelex<sup>®</sup> material will not be subject to direct blowdown jet impingement (Reference 4). It may be exposed to a short term saturated steam environment with a maximum temperature of approximately 255°F (Reference 5).

- 4.2. The material will be exposed to a cascade or spray of a steam/water solution containing a maximum of 2600 ppm boron, buffered by sodium hydroxide (NaOH) (Reference 6). During the blowdown phase of the event, the Benelex<sup>®</sup> may be briefly exposed to an unbuffered steam/water mixture. However, the time period will be extremely short and Benelex<sup>®</sup> is resistant to mild acids. Therefore, the pH effects of the initial blowdown are considered negligible for the purpose of this evaluation.
- 4.3. The Benelex<sup>®</sup> will be exposed to water with a pH ranging from 10.1 to 7.8. Maximum pH will decrease over 2 hours from 10.1 to 8.7 (Reference 7).
- 4.4. The maximum temperature water to which the Benelex<sup>®</sup> will be exposed will be 250°F. Within 2.06 hours, the water temperature will be less than 170°F. Minimum water temperature will be 65°F. This range of temperatures bounds the various case configurations described in Reference 5.
- 4.5. Mission time is 30 days (Reference 5).
- 4.6. Although the Benelex<sup>®</sup> is not expected to be immersed in water (Reference 7), this evaluation will address the potential effects from immersion.

## 5. Evaluation

This evaluation will utilize published manufacturing and test data to determine the potential for Benelex<sup>®</sup> material to dissolve, erode or otherwise degrade from its as-manufactured state as a result of exposure to the post-LOCA environmental conditions described in Section 4.

### 5.1. Potential for Benelex<sup>®</sup> degradation due to water cascade/spray/immersion.

As characterized in Section 4, the Benelex<sup>®</sup> material will be exposed to a steam/water spray or immersion in water with a maximum pH of 10.1 and a maximum temperature of 255°F (124 degrees Celsius [°C]). Insoluble lignin and cellulose (the constituent components of Benelex<sup>®</sup>) were evaluated to determine whether they would be expected to degrade under the specified conditions. Based on the following discussions, Benelex<sup>®</sup> is not expected to degrade as a result of spray or immersion in the water generated in the BVPS-1 post-LOCA environment.

#### 5.1.1. Cellulose

Cellulose is a high molecular weight, crystalline linear polymer consisting of D-anhydroglucopyranose units joined together in long chains by beta-1,4 glycoside bonds.

Cellulose is insoluble in either cold or boiling water.

Cellulose is resistant to alkaline hydrolysis.

- Studies conducted by The Laboratory for Waste Management of the Nuclear Energy and Safety Research Department at the Paul Scherrer Institute at 25°C in the absence of air at a pH of 13.3 indicate that the alkaline degradation of cellulose

will occur in a time period ranging from 100 years to in excess of 10,000 years (Reference 8).

- Alkaline treatment of crushed, steam exploded beech and cedar woods yielded no saccharification (breakdown) of cellulose (Reference 9).
- Alkaline hydrolysis equipment/processes sold by corporations such as BioSafe Engineering (Reference 10), specifically describe the alkaline hydrolysis of biological materials to break the materials down and render them harmless. This equipment and/or process is typically conducted at elevated temperatures of 300°F under alkaline conditions. BioSafe states that while large carbohydrate molecules such as cellulose are sterilized by the process, cellulose is not digested by alkaline hydrolysis. See website Chapter 6 “Alkaline Hydrolysis”, Section 3.1 – Principles of Operation, “Carbohydrate Degradation” page 5.

#### 5.1.2. Lignin

Lignin is a thermoplastic, macromolecular polyol comprised of varying percentages of three different phenolic based monomers – (1) paracoumaryl alcohol, (2) coniferyl alcohol and (3) sinapyl alcohol. These three alcohols are linked through ether linkages.

Lignin is both aromatic and hydrophobic in character making it naturally resistant to aqueous attack. It is insoluble in either cold or boiling water.

Lignin is also resistant to alkaline hydrolysis except under extreme conditions. A series of experiments were run by Monlin Kuo, and others at The Division of Forestry, at Iowa State University (Reference 11). Kuo ran a series of lignin alkaline hydrolysis experiments on lignin derived from southern pine wood feedstock. The experimental conditions were much more aggressive than those anticipated that might occur in the BVPS-1 facility in the event of a hot alkaline water loss.

Lignin was exposed to both 15 percent and 20 percent aqueous sodium hydroxide (pH equal to 12.2 initial) at temperatures of 170°C and 200°C for time periods of 0.5, 1.0 and 2.0 hours. The experimental pH exceeds the anticipated event pH by a factor in excess of 10 and the experimental temperature ranges were from 90°F to 140°F higher than the maximum anticipated event temperature.

Solids lignin losses ranged from 0 percent to 1 percent by weight. See Reference 11, Table 1. The conclusions of Kuo were that:

- The methoxyl contents of lignin samples hydrolyzed at 170 and 200°C are nearly the same as that of the unhydrolyzed kraft lignin. This result indicates that little demethylation occurred when the kraft lignin was hydrolyzed with 15 and 20 percent NaOH at or below 200°C. See Reference 11, Table 2.
- The aliphatic hydroxyl content of lignin samples hydrolyzed at 170 and 200°C is about the same as that of the unhydrolyzed kraft lignin. This implies that very little

or no change in aliphatic hydroxyl content occurred during alkaline hydrolysis at or below 200°C. See Reference 11, Table 2.

Further lignin depolymerization experiments were conducted by James Miller and others at Sandia National Laboratories in 2002. Miller's work (Reference 12) looked at temperature effects, concentration effects, sodium to lignin ratios and co-base effects on Alcell lignin derived from hardwoods. The time of reaction ranged from 1.0 to 1.25 hours. Reaction temperatures were 290°C to 330°C, well in excess of the expected LOCA event maximum temperature of 255°F (124°C). Alkali concentrations ranged from 1 percent up to 30 percent versus the maximum of 0.1 percent expected in a LOCA event. Effectiveness of reaction was determined by measuring residual solids in the reaction mixture.

Miller was able to prove the following: 1) increased reaction temperatures drove the depolymerization further to completion, 2) increased reaction temperature increased the reaction rate, 3) lower sodium to lignin ratios decreased the conversion percentage, 4) the reaction is stoichiometrically tied to sodium concentration versus catalyzed by the presence of sodium, and 5) the presence of co-bases can have a synergistic dissolution effect.

Miller did not run any experiments at temperatures lower than 290°C but his curves detailing the extent of reaction rise asymptotically towards minimal reaction occurring at the lower temperature range of his experiments. Also, a LOCA event will expose the Benelex<sup>®</sup> to sodium concentrations significantly below the stoichiometric ratios necessary to drive lignin depolymerization to levels that would adversely affect the physical properties of the Benelex<sup>®</sup>.

Loss in weight of lignin when subjected to alkaline hydrolysis is critical to whether the lignin retains the ability to serve as an encapsulating agent for the cellulose. As lignin decomposes, the length of the polymer chain diminishes from that of a high molecular weight polymer all the way down to individual monomeric sections. It is only at the point that the lignin has decomposed to its individual monomeric sections, paracoumaryl alcohol, coniferyl alcohol and sinapyl alcohol, that the individual components of the polymer become soluble in alkaline water and can be removed from the matrix.

Following loss in weight as a measure of the extent of the reaction is further validated by Miller. "Because smaller molecular weight compounds tend to have greater solubility, the extent of depolymerization can be characterized by the amount of water and ether insoluble material remaining after the reaction." (Reference 12, Page 5)

In the absence of alkali, the monomeric alcohols comprising lignin are only slightly soluble in boiling water. Dimers and higher oligomers of the lignin alcohols are not soluble in water and therefore they would be retained in the Benelex<sup>®</sup> matrix explaining the minimal loss in weight in the Kou experiments.

As long as the lignin retains some semblance of polymeric nature, (two or more alcohol units linked together), the lignin will serve as an encapsulating matrix for the cellulose in the Benelex<sup>®</sup>. If the lignin does diminish in molecular weight, the physical properties of the Benelex<sup>®</sup> will decrease very slowly over time but the Benelex<sup>®</sup> in question is not a structural part. Any decrease in physical properties will occur first on the surface of the Benelex<sup>®</sup> and proceed inward to the center of any particular piece of Benelex<sup>®</sup> exposed to the attacking agent.

A real life example of resistance to decomposition exists for Benelex<sup>®</sup> 401. A section of the Benelex<sup>®</sup> 401 was fabricated into a basketball backboard and vertically mounted in southern Mississippi where it has been exposed to the weather since 1980. The Benelex<sup>®</sup> has been exposed to repeated hot/cold cycles, wet/dry cycles and full sun exposure during this time period. Close inspection of this piece of Benelex<sup>®</sup> shows no delamination of the materials comprising the board.

### 5.1.3. Applications

- PF resin based strand board is used extensively in exterior and structural applications where it is repeatedly exposed to high moisture, fluctuating temperature conditions without degradation. (Reference 13)
- Paper and cotton fiber laminates impregnated with PF resins are commonly used in applications that require high heat resistance, an excellent moisture barrier and very good resistance to weak alkalis. (Reference 13)

### 5.2 Potential for Benelex<sup>®</sup> degradation due to erosion over 30-day mission time

As discussed in section 3.1, the Benelex<sup>®</sup> material will retain the structural characteristics of lignin and PF resins as long as the cellulose does not break down under the anticipated temperature and pH conditions. Thus, Benelex<sup>®</sup> can be expected to behave in the same manner as pure lignin or PF resins.

Benelex<sup>®</sup> has a Rockwell Hardness of 90 (M scale) and wood filled PF resins exhibit a Rockwell Hardness of 64 to 95 (M). Although limited test data has been found on erosion of lignin or phenol-formaldehyde resins, their hardness makes them very resistant to erosion. This conclusion is supported by the applications where PF resin and lignin-based Benelex<sup>®</sup> products have historically been used.

#### 5.2.1 Applications

PF resin has historically been used to mold 100 percent PF resin under the hood automotive parts such as thermostat housings, throttle bodies, water pumps, rocker arm covers and water pump impellers. The housings, water pumps and impellers are items that are continuously exposed to elevated temperature water (170 to 225°F) for years at a time. (Reference 13)

PF resins are also routinely used as the binding agent for abrasives due to their thermal, water and mechanical resistance. (Reference 13)

Benelex<sup>®</sup> 401 has historically been used in a wide range of applications requiring high abrasion resistant materials. Typical examples are drawn from Masonite literature (Reference 14) and are as follows:

- Benelex<sup>®</sup> 401 used to replace steelclad plywood trays used to carry parts on a conveyor. The steel suffered heavy wear. New trays were fabricated out of Benelex<sup>®</sup>. The abrasion resistant Benelex<sup>®</sup> significantly increased the lifespan of the trays, outlasting the steel cladding.
- Benelex<sup>®</sup> 401 was used to replace bronze elevator shoe guides which outlasted the bronze and had the added benefit of low moisture absorption ensuring high dimensional stability.
- Benelex<sup>®</sup> 401 used as bounce plates in bowling pinspotters. It is installed in 86,000 pinspotters and has withstood 10 years of being hit by a 16-pound bowling ball traveling at up to 35 miles per hour. In addition, it must resist the wear caused by the endless return belt constantly rubbing against the Benelex<sup>®</sup>.
- Benelex<sup>®</sup> 401 used as the support surface for a flat-flex stainless steel conveyor belt which routinely drags loads up to 10 pounds per square foot at 75 ft/min across the support surface. "Despite the extreme abrasion experienced, the Masonite brand Benelex<sup>®</sup> surfaces show little wear and provide years of trouble-free service."

### 5.3 Chemical Effects

Because the post-LOCA conditions are not adequate to cause decomposition of the material, the debris would not react with other substances in the water pool with the following characteristics: 2600 ppm boron, buffered with NaOH to pH = 10.1 to 7.8, temperature 250°F to 65°F.

Phenolic resins will form boron complexes under carefully controlled high temperature (270°C to 400°C) experimental conditions that typically require reacting the neat resins together such as is found in US Patent No. 4,271,311 "Esterification of Phenol Catalyzed With a Strong Base Plus Boron" by William W. Knickmeyer. These reactions typically require the removal of water from the reaction mixture. The conditions that would be found in the environment of a post-LOCA event are contrary to the formation of a phenol-boron compound.

Boron can catalyze the polymerization of phenolic compounds at very high temperatures (300°C) and alkaline conditions. This implies that if the Benelex<sup>®</sup> were to be left to dry, heated to 300°C, and boron and sodium hydroxide residues left on the surface of the Benelex<sup>®</sup>; that any remaining low molecular weight phenolic moieties,

would tend to increase in molecular weight countering any reductions in molecular weight that might arise from alkaline depolymerization.

No chemical compounds would be expected to form in the pool as a result of Benelex<sup>®</sup> in the post LOCA environment.

## 6. Conclusion

Based on the evaluation provided above, Benelex<sup>®</sup> 401 is a hard, stable material that will withstand the post-LOCA environment at BVPS-1 with virtually no degradation over 30 days. No chemical compounds would be expected to form as the result of the destruction of Benelex<sup>®</sup> into fines.

APPENDIX III  
TABLE 1

### Physical Properties of Benelex<sup>®</sup>

Property	Units	Test Method	Value
Density	gm/cc	D972-Method A	1.37
Specific Volume	in <sup>3</sup> /lbm		19.89
Tensile Strength (Lengthwise/Crosswise)	psi	D638	7,600/7,600
Compressive Strength (Flatwise)	psi	D695	29,000
Flexural Strength Crosswise (Flatwise/Edgewise)	psi	D790	12,000/13,500
Flexural Strength Lengthwise (Flatwise/Edgewise)	psi	D790	11,300/13,000
Modulus of Elasticity Flexure Lengthwise (Flatwise/Edgewise)	psi	D790	1,265,000/ 1,340,000
Modulus of Elasticity Flexure Crosswise (Flatwise/Edgewise)	psi	D790	1,315,000/ 1,410,000
Izod Impact Strength (Lengthwise/Crosswise/Edgewise)	ft lb/in	D256	1.68/1.61/0.53
Rockwell Hardness	M Scale	D785	90.2
Bond Strength	psi	D952	868
Thermal Expansion Coefficient (Lengthwise/Crosswise)	in/in/°F		0.907 x 10 <sup>-5</sup> / 0.499 x 10 <sup>-5</sup>
Maximum Operating Temperature (Continuous/48 Hrs)	°F		170/190
Coefficient of Friction (Static/Kinetic)		D2534	0.314/0.236

## **Appendix IV, Coatings Evaluation**

### Change in Coatings Zone of Influence

The NRC, in reviewing the testing completed by the PWR Owner's Group to support GL 2004-02, expressed concern about the testing done to revise the zone of influence for qualified coatings in containment. WCAP-16568-P, Jet Impingement Testing to Determine the Zone of Influence (ZOI) for DBA-Qualified/Acceptable Coatings was specifically addressed in the conference call between the NRC and the PWR licensees on January 13, 2010. During that call, the NRC announced that they were considering raising the acceptable ZOI for qualified untopcoated inorganic zinc coatings from 5D to 10D (10 pipe diameters). Subsequently, the NRC has issued revised guidance regarding coatings zone of influence for review of final licensee responses to GL 2004-02. This guidance was issued via NRC letter dated April 6, 2010 addressed to the Nuclear Energy Institute. Based on the staff's review, it no longer finds a 5D ZOI acceptable for untopcoated inorganic zinc. Instead, licensees may rely on the staff's prior acceptance of a 10D ZOI for untopcoated inorganic zinc as documented in its SE for NEI.04-07.

Following the industry notification of this issue, the impact of this change on BVPS was evaluated. In the containment areas potentially affected by a loss of coolant accident, BVPS has qualified untopcoated inorganic zinc on the neutron shield tanks. Therefore, the revised ZOI for the qualified untopcoated inorganic zinc affected the coating load for the nozzle breaks. The new ZOI for inorganic zinc values are bounded by the coatings load included in the head loss tests for the nozzle breaks. Therefore, the change in ZOI for qualified inorganic zinc within the revised ZOI of 10D has no effect on the BVPS containment sump head loss.

The ex-vessel component downstream wear analysis was done with the limiting coating debris load from the RCS loop break. This remains the bounding break for coatings debris generation. Therefore, the downstream wear analysis is not impacted by the change in ZOI for untopcoated inorganic zinc.

Consequently, the change in the destruction radius (10D ZOI) for inorganic zinc from the values formerly issued in WCAP-16568-P has no impact on the BVPS sump performance.

## **Appendix V, BVPS-1 June 2010 Test 7 Summary**

As discussed in RAI 1, a recent re-evaluation identified a location at BVPS-1 where the fibrous debris load, which had previously been bounded by the limiting breaks, could potentially exceed the fibrous debris load for the limiting breaks following insulation replacement efforts. The pressurizer code safety relief valve (SRV) insulation boxes contain a volume of Temp-Mat™ insulation that exceeds the fibrous debris quantity associated with the limiting RCS loop break. A calculation was performed to determine the bounding quantity of debris that would be generated from a break in a 6-inch line leading to one of the SRVs. The calculation determined the quantity of Temp-Mat™ and coatings debris that would be generated from the subject break. Based on existing insulation configuration plus the planned Cal-Sil reduction efforts to address RAI 5, Temp-Mat™ and coatings are the only break-specific debris sources other than RMI. The calculation showed that the worst case Temp-Mat™ debris load at the sump strainer would be less than 9 cubic feet. Strainer testing was then performed using the break specific debris load, combined with unqualified coatings and miscellaneous debris loads, and accounting for chemical effects. This appendix provides details of the analytical process used to determine the maximum debris quantities used in testing and the overall testing methodology.

### **BVPS-1 Top of Pressurizer Debris Generation Analysis Summary**

There are three SRV pipe lines coming from the upper pressurizer in BVPS-1. Each of these lines is enclosed in an insulation box. These insulation boxes are comprised of several individual cassettes constructed of 1.5 inch thick Temp-Mat™ insulation encapsulated in 22-gauge stainless steel sheet metal enclosures. The cassettes are then connected to each other and to the pressurizer using fasteners and mechanical latches. Computer Aided Design (CAD) models of these boxes were constructed using Inventor® computer software based on engineering drawings. CAD models of these boxes are shown in Figure AV-1, with the entire pressurizer shown in Figure AV-2. Figure AV-3 and Figure AV-4 show the construction of one of the insulation boxes. The open sides of the insulation boxes butt up against the pressurizer.

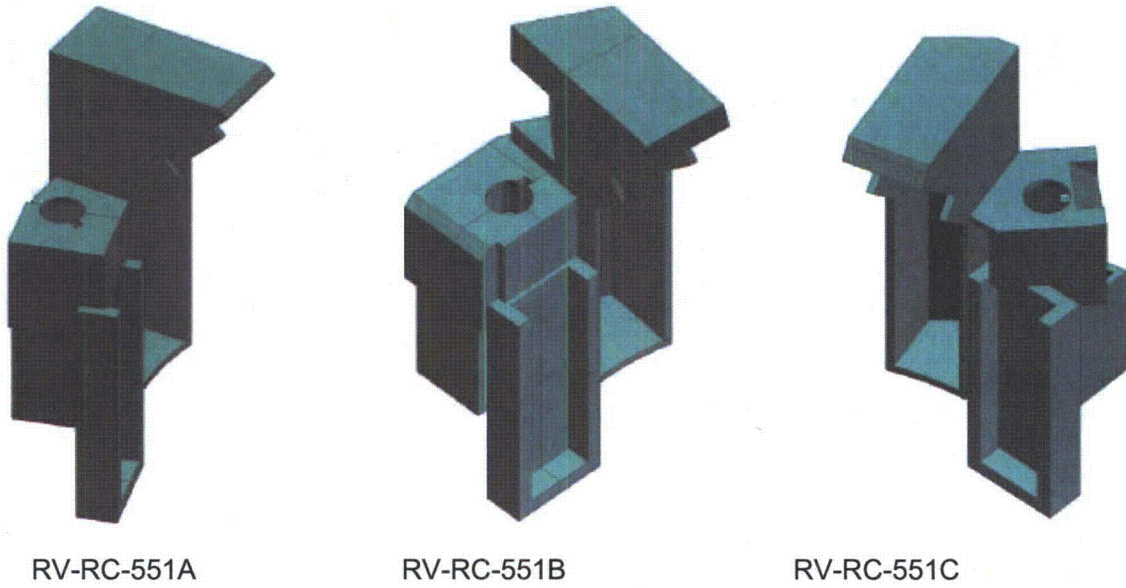


Figure AV-1, Temp-Mat™ Insulation Boxes on the SRV Pipe Lines in BVPS-1

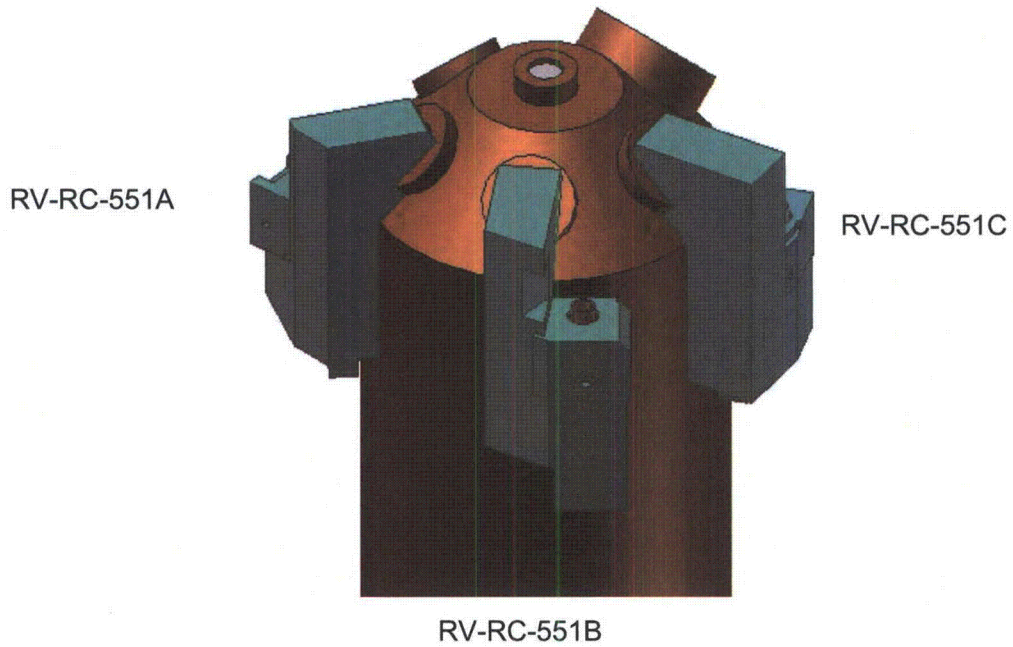


Figure AV-2, Pressurizer Showing SRV Pipe Lines and Insulation Boxes

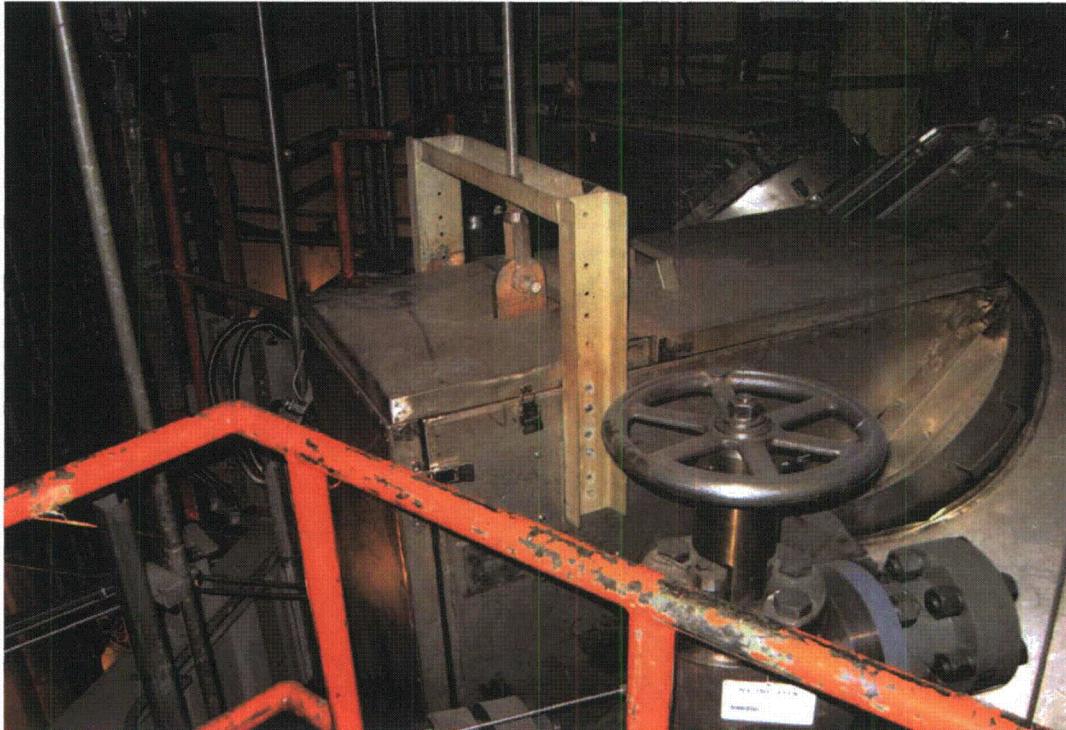


Figure AV-3, "A" Pressurizer Safety Insulation Box Assembly



Figure AV-4, "A" Pressurizer Safety Insulation Box Assembly Interior

CAD models of each box were used to determine the amount of Temp-Mat™ insulation in each box. These boxes have 8.82 cubic feet (A), 8.94 cubic feet (B), and 8.89 cubic feet (C) of total Temp-Mat™ insulation.

The SRV pipe lines are 6-inch schedule 160 stainless steel piping and are only pressurized up to the closed SRVs located adjacent to pressurizer. Because of this arrangement, in the event of a line break, there is no pressure source to propagate a steam/water jet from the SRV side of the pipe section where the break occurs. Therefore, any complete break will result in a one-sided jet. This arrangement also eliminates the need to consider a limited axial offset break.

To determine the total Temp-Mat™ destruction, the BVPS-1 Debris Generation calculation conservatively assumes that the entire insulation box associated with the broken pipe is destroyed by a complete pipe break, resulting in, at most, 8.94 cubic feet of Temp-Mat™ debris. As a further conservatism, the Temp-Mat™ is assumed to be destroyed completely as fines, with 100 percent of these fines transported to the sump strainer. FENOC validated this assumption by performing a series of evaluations considering various break jet configurations to ensure that this assumed debris volume was conservative. The results of those evaluations are summarized below:

Per the NRC Safety Evaluation (Reference 3, Table 3-2), the destruction pressure of Temp-Mat™ enclosed in fiberglass cloth with stainless steel wire mesh retainer is 10.2 pounds per square inch (psi), corresponding to an 11.7D (11.7 pipe diameters) zone of influence (ZOI). The Temp-Mat™ insulation under consideration here is not held in place with wire retainers but encapsulated in 22-gauge stainless steel sheet metal cassettes, with individual cassettes constructed by overlapping the sheet metal ends and fastening the ends with pop-rivets or sheet metal screws. This construction is considered more robust than Temp-Mat™ enclosed in fiberglass cloth with wire mesh. Therefore, FENOC has concluded that the use of the Temp-Mat™ nominal destruction pressure of 10.2 psi provided in the Safety Evaluation (Reference 3) is appropriate for this application:

The pressure profile from a fully offset axial (guillotine) SRV line break was determined using ANSI/ANS 58.2 and saturated vapor conditions (2250 pounds per square inch absolute – psia, and 652.8 degrees Fahrenheit) that exist at the top of the pressurizer. The application of the ANSI model at BVPS is discussed in detail in FENOC's response to RAI 3. The ZOI for Temp-Mat™ destruction is conservatively determined from the isobar at the Temp-Mat™ destruction pressure (10.2 pounds per square inch gauge - psig). This isobar is shown in red in Figure AV-5. For simplicity, the ZOI calculated using this isobar is represented as a cylinder with the maximum jet radius as the cylinder radius and maximum jet length as the cylinder length – shown in black on Figure AV-5. The representative cylindrical ZOI increases the level of conservatism for this jet.

Zones of influence were analyzed by super-imposing the ZOI cylinder on the pressurizer CAD model in the break flow direction at various locations (as shown in Figure AV-6) to determine if any adjacent insulation boxes are impacted. Thrust forces resulting from a complete pipe break at any pipe location would tend to direct the jet further away from any adjacent insulation box. All three SRV legs were evaluated, and it was concluded that no portion of an adjacent insulation box would be damaged by a steam/water jet from a completely offset axial break of any piping leg, thus validating the assumption of total destruction of one complete insulation box as being conservative for this case.

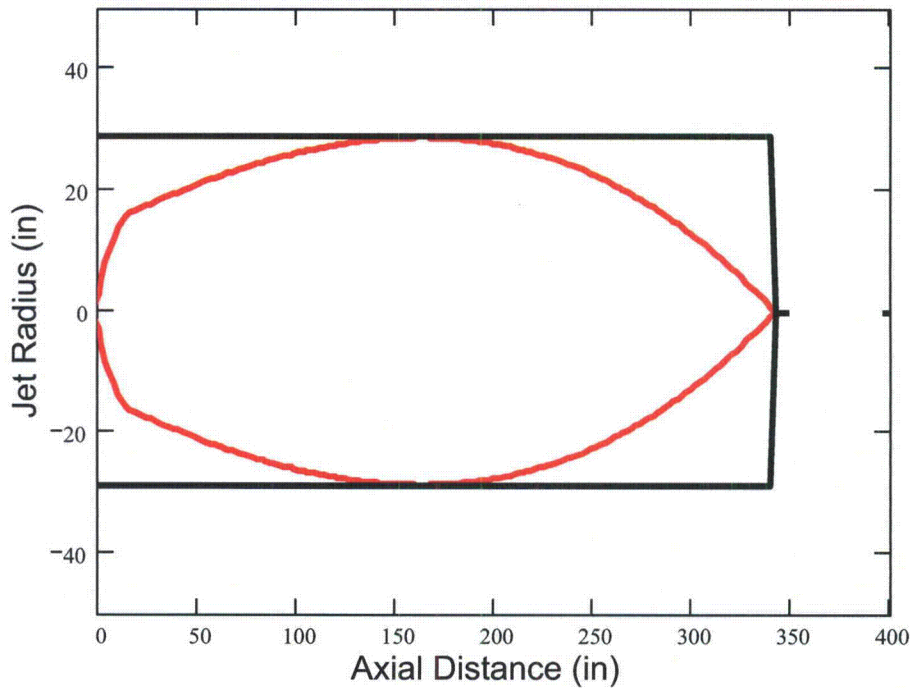


Figure AV-5, Actual ZOI (red) and Simplified ZOI (black) for Temp-Mat™ Destruction

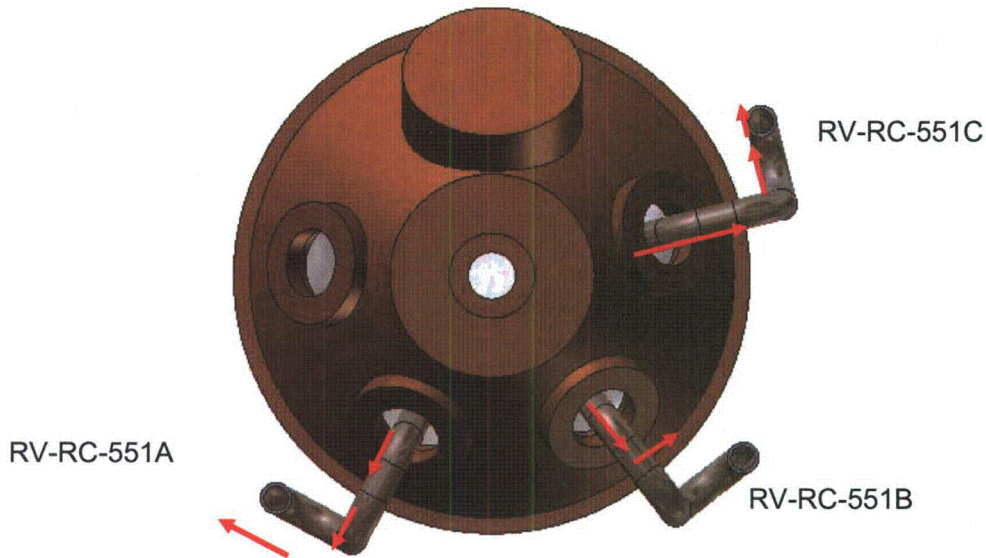


Figure AV-6, BVPS-1 Upper Pressurizer showing SRV Lines and Jet Directions

To account for pipe whip effects and non-axial breaks, evaluations were also performed using a spherical ZOI representing the 10.2 psi destruction pressure for Temp-Mat™. These evaluations were performed to ensure that the assumption of the destruction of one complete box is conservative.

Using the ANSI steam jet model described earlier, destruction is conservatively determined from the isobar at the Temp-Mat™ destruction pressure (10.2 psig). Since the break jet will only emanate from the pressurizer side of the break, the ZOI of this jet is represented using a sphere with the same volume as half of an 11.7D sphere. This results in a 9.29D equivalent spherical ZOI as shown in Equation 1.

$$V_{ZOI} = \frac{\frac{4}{3}\pi(11.7D)^3}{2} = \frac{4}{3}\pi(9.29D)^3 \quad \text{Equation 1}$$

Figure AV-7 illustrates the application of a spherical ZOI for the worst-case break location. The dimensions and configurations of the boxes are such that a 9.29D ZOI will encompass one complete box and a portion of the adjacent box. Conservatively assuming that any cassette that falls within the ZOI is completely destroyed, the maximum volume of debris generated would be 12.29 cubic feet. A debris size distribution of 60 percent small fines and 40 percent large pieces is then applied as specified in NEI 04-07 (Reference 3), Section 3.4.3.3.1. Due to the location of the postulated break, it is highly unlikely that large pieces of Temp-Mat™ will wash down from the upper pressurizer cubicle. However, for conservatism, it is assumed the large pieces will wash down to the recirculation pool.

The BVPS-1 Debris Transport calculation shows that large pieces of Temp-Mat™ located in the recirculation pool will not transport to the sump strainer. However, erosion of 10 percent of the large piece material to small fines is also considered, resulting in a total transportable quantity of Temp-Mat™ debris of 64 percent. Applying this fraction to the 12.29 cubic feet debris load results in 7.87 cubic feet of Temp-Mat™ debris transported to the sump strainer.

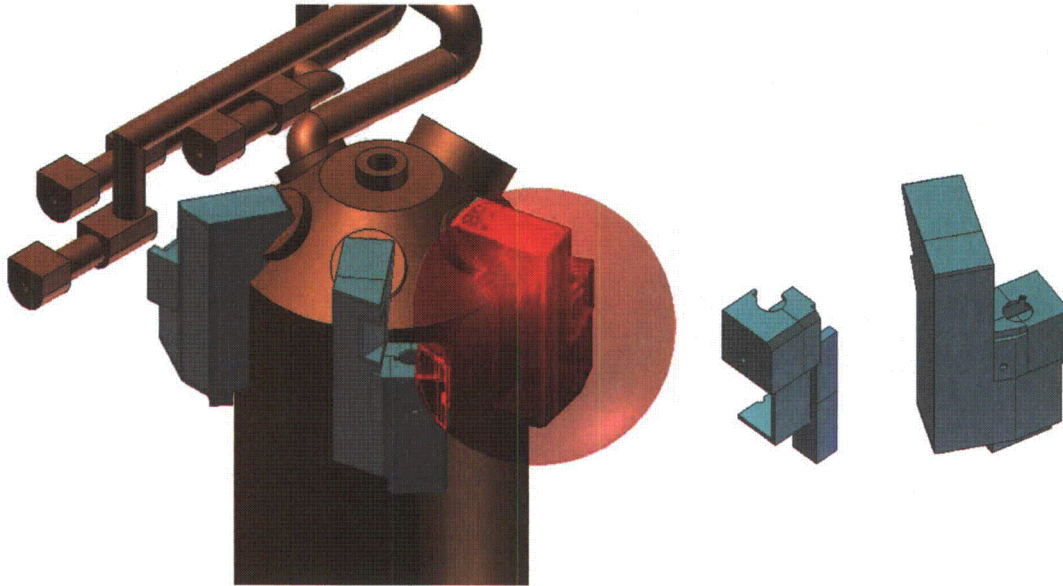


Figure AV-7, Spherical ZOI Area of Effect

To address the potential for a through-wall break in the SRV piping, a hemispherical ZOI at  $11.7D$  was also considered. Per ANSI/ANS 58.2, the maximum equivalent diameter of a through-wall break is half of the inner diameter. This ZOI is bounded by the  $9.29D$  spherical ZOI.

Therefore, the maximum amount of Temp-Mat™ insulation destroyed and transported to the sump strainer in the event of a complete pipe break is conservatively bounded by the assumed 8.94 cubic feet, which represents the maximum insulation from one complete insulation box and its support column.

#### BVPS-1 June 2010 Test 7 Summary – Top of Pressurizer Break Test

The BVPS-1 June 2010 Test 7 was performed for the purpose of determining the head loss of the maximum fiber test that bounded the debris quantities for the BVPS-1 Top of Pressurizer Break debris loads (Temp-Mat™, latent debris, coatings) plus WCAP predicted chemical precipitates. Table AV-1 provides a summary of the BVPS-1 June 2010 Test 7.

Table AV- 1

Test No.	Test Description	Break
BV1 June 2010 Test 7	Scaled Temp-Mat™ Test	BVPS-1 Top of Pressurizer Break

In general, BVPS-1 June 2010 Test 7 was conducted in the same manner as the previous BVPS-1 testing. Any exceptions are described in this appendix. The test load of 9.1 cubic feet of Temp-Mat™ was conservatively based on one insulation box of Temp-Mat™ debris destroyed and transported entirely as fines and 100 percent transport for all remaining debris loads (latent debris, coatings).

The debris types and scaled quantities used for this case are listed in Table AV-2. The materials used were the same as the materials discussed in Section 3.f.4 of the June 30, 2009 supplemental response, except the surrogate for the qualified and unqualified coatings fine particulate. BVPS-1 June 2010 Test 7 used silicon carbide at an average size of 10 microns spherical particle diameter.

Table AV- 2

Test No.	NUKON® Fines (lbm)	Temp-Mat™ Fines (lbm)	Silicon Carbide (lbm)	Dirt/Dust (lbm)	Paint Chips (lbm)
BV1 June 2010 Test 7	0.72	2.58	3.59	4.08	0.87

BVPS-1 June 2010 Test 7 used 100 percent NUKON® fines and 100 percent Temp-Mat™ fines. The fine debris preparation was enhanced from the previous BVPS-1 testing where the fine fibrous debris was prepared using a blender. For BVPS-1 June 2010 Test 7, the NUKON® and Temp-Mat™ fine fibrous debris was prepared using the Alion fine fibrous debris preparation protocol that was witnessed by the NRC staff and documented in a February 23, 2009, trip report (ADAMS Accession No. ML090500230). The NUKON® and Temp-Mat™ fiberglass sheets are double shredded and then beaten in ¼ pound fiber batches (with approximately 4 gallons of water) with a paint mixer attached to an electric drill for 4 minutes. Consistent with staff guidance, fiber fines are defined as Classes 1-3 (defined in the NUREG/CR-6808 Table 3-2) in the debris preparation procedure, and inspected to ensure that they are representative as Classes 1-3. The photographs of the NUKON® and Temp-Mat™ fines are provided in Figure AV-8 through Figure AV-11.



Figure AV-8, NUKON® Fines

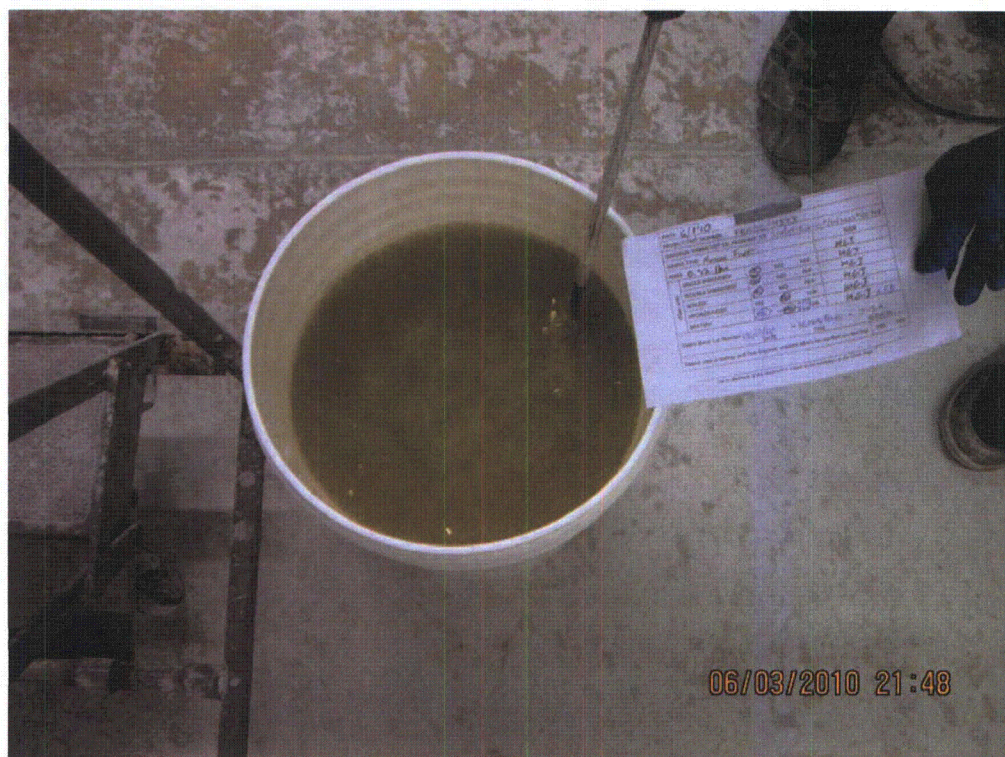


Figure AV-9, NUKON® Fines



Figure AV-10, Temp-Mat™ Fines



Figure AV-11, Temp-Mat™ Fines

The same test set-up and protocol, described in RAI 13 for the previous BVPS-1 testing, was used for BVPS-1 June 2010 Test 7 in order to ensure that the debris was properly suspended, and diluted sufficiently to avoid agglomeration. Additionally, debris was added slowly and directly above the return line sparger, to further ensure that agglomeration did not occur. Based on NRC staff guidance regarding RAI 14, for BVPS-1 June 2010 Test 7, paint chips were added after all fibrous debris was added.

The head loss test results for the BVPS-1 June 2010 Test 7 at an approach velocity of 0.0100 ft/sec, corrected for the temperature, are shown in Table AV-3. The test configuration for the BVPS-1 June 2010 Test 7 is the same as the BVPS-1 configuration described in Section 3.f.4 of the June 30, 2009 supplemental response.

Table AV- 3

Temperature (°F)	Head Loss (ft-H2O)
65	0.66
89	0.64
100	0.64
150	0.61
180	0.60
212	0.59

Note: The above table reports head loss values at test termination. No extrapolation was required to 30 days since the head loss was stable or decreasing at test termination.

The measured head loss was corrected for changes in temperature using the laminar and turbulent ratios provided below in Table AV-4. The laminar/turbulent ratios were determined consistent with the methodology described in RAI 15.

Table AV-4

Approach Velocity (ft/s)	Laminar	Turbulent	Laminar Ratio	Turbulent Ratio
0.0100	0.0366	0.5573	6.2%	93.8%
0.0088	0.0322	0.4315	6.9%	93.1%
0.0075	0.0275	0.3135	8.1%	91.9%
0.0063	0.0231	0.2212	9.4%	90.6%
0.0050	0.0183	0.1393	11.6%	88.4%

This test represents the strainer head loss for the BVPS-1 top of pressurizer break and is bounded by the existing design basis BVPS-1 Test 6. Similar to BVPS-1 Test 6, the

resultant head loss indicated that the amount of material was not enough to completely coat the strainer. This open screen area was also demonstrated by visual evidence of the debris bed prior to the addition of WCAP predicted chemical precipitants. The photographs in Figure AV-12 and Figure AV-13 show the open screen area. As with Test 6, testing demonstrated that the debris loads from this configuration (BVPS-1 June 2010 Test 7) are small enough that a thin bed will not form.



Figure AV-12, BVPS-1 June 2010 Test 7 Non-Chemical Debris Bed



Figure AV-13, BVPS-1 June 2010 Test 7 Non-Chemical Debris Bed

The discussion in Sections 3.f.8, 3.f.12 and 3.f.13 of the June 30, 2009 supplemental response are also applicable to the BVPS-1 June 2010 Test 7. Consistent margins and conservatism were used in the calculations, there was no near-field settling effects credited, and the same temperature corrections were performed.

As BVPS-1 June 2010 Test 7 is bounded by the existing design basis BVPS-1 Test 6, it is not necessary to calculate the available NPSH.

Consistent with the previous BVPS-1 testing, BVPS-1 June 2010 Test 7 used WCAP-16530-NP chemical precipitates. The discussion in Section 3.o.2.2.i of the June 30, 2009 supplemental response is also applicable to the BVPS-1 June 2010 Test 7. Sections 3.o.2.3.i, 3.o.2.4.i, 3.o.2.10.i, 3.o.2.12.i, 3.o.2.13.i, 3.o.2.15 and 3.o.2.16.i of the June 30, 2009 supplemental response are all applicable to the BVPS-1 June 2010 Test 7 test proceedings. The type and amount of predicted WCAP-16530-NP plant specific precipitates for BVPS-1 June 2010 Test 7 are shown (before scaling amounts) in Table AV-5.

Table AV-5, BVPS-1 June 2010 Test 7

Precipitate	Lbs
Sodium Aluminum Silicate	121
Aluminum Oxyhydroxide	148

As with the previous BVPS-1 testing, there was no insulation or chemical precipitate observed to have settled on the tank/flume floor. The only materials evidenced to have settled to the floor were some paint chips and dirt/dust. Due to the high average approach velocity utilized in the testing, and the sparger system, the insulation and chemical debris remained suspended and deposited on the strainer array. The photographs in Figure AV-14 through Figure AV-17 show the lack of settled debris.



Figure AV-14, BVPS-1 June 2010 Test 7 Settled Debris



Figure AV-15, BVPS-1 June 2010 Test 7 Settled Debris



Figure AV-16, BVPS-1 June 2010 Test 7 Settled Debris



Figure AV-17, BVPS-1 June 2010 Test 7 Settled Debris

The curves in Figure AV-18 through Figure AV-20 illustrate the pressure drop as a function of time (uncorrected for temperature) for the BVPS-1 June 2010 Test 7. These figures depict the results of the BVPS-1 June 2010 Test 7 by plotting the differential pressure across the debris bed and fluid average theoretical approach velocity versus time, with subtest debris additions and flow adjustments indicated by vertical lines. Other test control operations and observations are marked at the time of execution/occurrence.

The methodology described in Section 3.o.2.17 of the June 30, 2009 supplemental response is applicable to the BVPS-1 June 2010 Test 7. Temperature corrections were applied to the head loss data analysis. Additionally, for the BVPS-1 June 2010 Test 7 the head loss was no longer increasing/decreasing at the end of the test, therefore no extrapolation was performed.

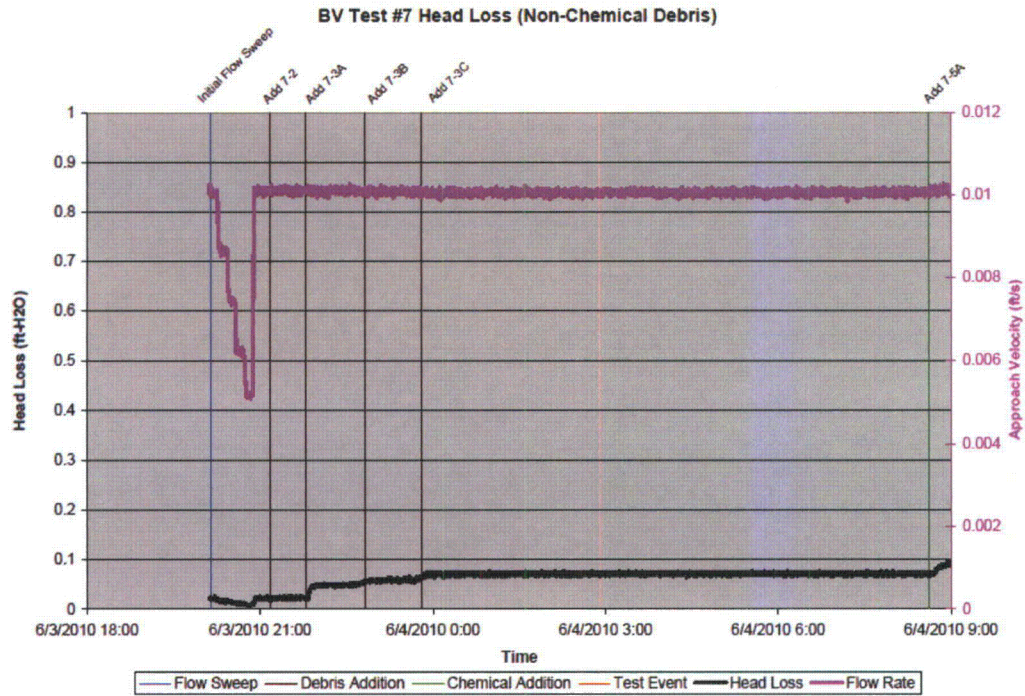


Figure AV-18, BVPS-1 June 2010 Test 7 Differential Pressure and Velocity vs. Time – Non-Chemical Debris Additions

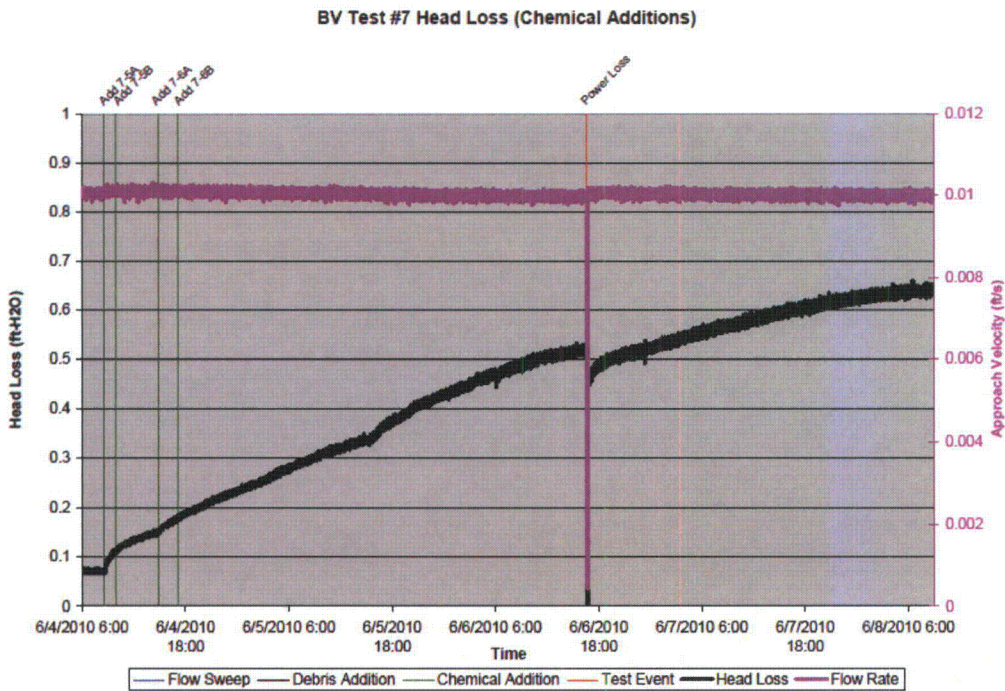


Figure AV-19, BVPS-1 June 2010 Test 7 Differential Pressure and Velocity vs. Time – Chemical Debris Additions

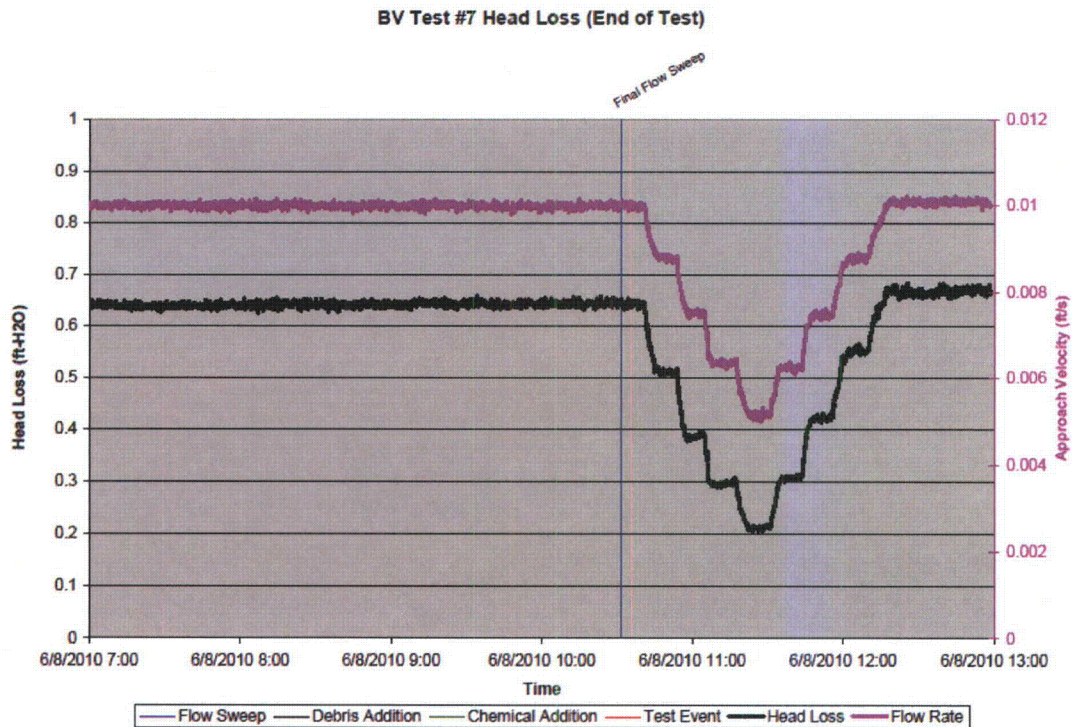


Figure AV-20, BVPS-1 June 2010 Test 7 Differential Pressure and Velocity vs. Time – Final Flow Sweep

The BVPS-1 Top of the Pressurizer Debris Generation Analysis and Test have been developed considering the following conservatisms:

1. Three evaluation methodologies were used to account for all potential break scenarios and verify that the total Temp-Mat™ insulation debris quantity developed in the debris generation and transport calculations is approximately 15 percent less than the volume used for head loss testing.
2. The Temp-Mat boxes enclosing the pressurizer SRV lines are constructed of 22 gauge stainless steel cassettes, which would be more robust than the wire mesh and cloth jacketing used in the Safety Evaluation (Reference 3, Table 3-2) to establish the Temp-Mat™ destruction pressure.
3. For all zones of influence, an entire insulation cassette has been considered to be destroyed if any portion of the cassette is contacted by the ZOI (referred to as full cassette destruction).
4. A washdown transport fraction of 100 percent was assumed for all debris types. This is conservative, as it is expected that some fibrous debris will deposit in

locations that are not exposed to washdown flow, or will be retained on gratings and structures as they migrate towards the ECCS recirculation sump.

5. As recommended by NRC staff review guidance for testing, all particulate debris (coatings surrogates, dirt/dust) was added first.
6. All failed coatings were assumed to be in the form of fine particulate debris. Additionally, due to the very low fibrous debris load, all failed coatings were assumed to be in the form of paint chips. Therefore, the unqualified/chips coatings load was added as both silicon carbide and paint chips.
7. Extra quantities of inorganic zinc and epoxy coatings were added to allow for increased margin.
8. Extra quantities of latent dirt/dust (approximately 35 pounds, un-scaled) and latent fiber (approximately 6 pounds, un-scaled), were added to allow for increased margin.

### List of References

1. FirstEnergy Nuclear Operating Company (FENOC) Letter L-09-152, Beaver Valley Power Station, Unit Nos. 1 and 2, "Supplemental Response to Generic Letter 2004-02 (TAC Nos. MC4665 and MC4666)," ADAMS Accession No. ML091830390, dated June 30, 2009.
2. FENOC letter L-09-131, "Generic Letter 2004-02, 'Potential Impact of Debris Blockage on Emergency Recirculation During Design Basis Accidents at Pressurized-Water Reactors' - Request for Extension of Completion Date for Additional Corrective Actions (TAC Nos. MC4665)," ADAMS Accession No. ML091250180, dated April 30, 2009.
3. NEI 04-07 Pressurized Water Reactor Sump Performance Evaluation Methodology (Volume 1– "Pressurized Water Reactor Sump Performance Evaluation Methodology," and Volume 2 – "Safety Evaluation by the Office of Nuclear Reactor Regulation Related to NRC Generic Letter 2004-02, Revision 0, December 6, 2004"), Revision 0 of both volumes, dated December 2004.
4. ALION-CAL-FENOC-2937-004, Revision 2, "Beaver Valley Power Station - Unit 1 HELB Debris Generation Calculation."
5. ALION-REP-FENOC-4373-12, Revision 0, "Beaver Valley Unit 1 WCAP Chemical Product Formation Report."
6. ALION-REP-FENOC-4373-003, Revision 0, "Summary Report for Impact of Chemical Effects on ESF Sump Screen Head Loss – BVPS-1 & 2."
7. DIT-SUMP-0027-00, BVPS-1 Design Input Transmittal for Evaluation of Benelex<sup>®</sup> Material.
8. "Cellulose degradation at alkaline conditions: Long-term experiments at elevated temperatures," Nuclear Energy and Safety Research Department, Laboratory for Waste Management, by M. A. Glaus and L. R. Van Loon, PSI Bericht 04-01.
9. "Renewable Biological Systems for Alternative Sustainable Energy Production," by the Food and Agricultural Organization of the United Nations, Chap 3.3.1, Ed. Kazuhisa Miyamoto, 1997.
10. "Carcass Disposal: A Comprehensive Review" by the National Agricultural Biosecurity Center Consortium, Chapter 6, "Alkaline Hydrolysis," H. Leon Thacker, August 2004.
11. Kuo, Monlin and others, "Alkali Treated Kraft Lignin as a Component in Flakeboard Resins," *Holzforschung*, Volume 45 (1991) pages 47 to 54.
12. James E. Miller and others, "Batch Microreactor Studies of Lignin Depolymerization by Bases. 2. Aqueous Solvents," Sandia National Laboratories, SAND2002-1318, May 2002.
13. Goodman, Sidney, "Handbook of Thermoset Plastics," Second Edition, Chapter 2, Noyes Publications, NJ, 1998, pages 23 to 71.
14. Benelex<sup>®</sup> Product Manual, Masonite Corp.

Attachment 2  
L-10-115

Regulatory Commitment List  
Page 1 of 1

The following list identifies those actions committed to by FirstEnergy Nuclear Operating Company (FENOC) for Beaver Valley Power Station Unit No. 1 (BVPS-1) and Unit No. 2 (BVPS-2) in this document. Any other actions discussed in the submittal represent intended or planned actions by FENOC. They are described only as information and are not Regulatory Commitments. Please notify Mr. Thomas A. Lentz, Manager - Fleet Licensing, at (330) 761-6071 of any questions regarding this document or associated Regulatory Commitments.

Regulatory Commitment	Due Date
1. Plant modifications will be completed for BVPS-1 associated with Cal-Sil insulation removal that ensures that the requirements of FENOC's revised methodology of assuming 100 percent destruction of Cal-Sil to fines is met.	1. Prior to startup from the next refueling outage (1R20, Fall 2010)
2. Plant modifications will be completed for BVPS-2 associated with Cal-Sil insulation removal that ensures that the requirements of FENOC's revised methodology of assuming 100 percent destruction of Cal-Sil to fines is met.	2. Prior to startup from the next refueling outage (2R15, Spring 2011)
3. Plant modifications, repairing and/or replacing NUKON <sup>®</sup> insulation will be completed on the 3-inch and 6-inch BVPS-2 PORV supply piping with appropriately applied stainless steel jacketing and sure-hold bands.	3. Prior to startup from the next refueling outage (2R15, Spring 2011)